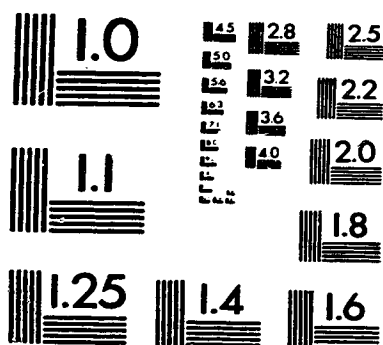


1

PM-1 3½"x4" PHOTOGRAPHIC MICROCOPY TARGET  
NBS 1010a ANSI/ISO #2 EQUIVALENT



PRECISION<sup>SM</sup> RESOLUTION TARGETS



National Library  
of Canada

Acquisitions and  
Bibliographic Services Branch

395 Wellington Street  
Ottawa, Ontario  
K1A 0N4

Bibliothèque nationale  
du Canada

Direction des acquisitions et  
des services bibliographiques

395, rue Wellington  
Ottawa (Ontario)  
K1A 0N4

*Your file    Votre référence*

*Our file    Notre référence*

## NOTICE

The quality of this microform is heavily dependent upon the quality of the original thesis submitted for microfilming. Every effort has been made to ensure the highest quality of reproduction possible.

If pages are missing, contact the university which granted the degree.

Some pages may have indistinct print especially if the original pages were typed with a poor typewriter ribbon or if the university sent us an inferior photocopy.

Reproduction in full or in part of this microform is governed by the Canadian Copyright Act, R.S.C. 1970, c. C-30, and subsequent amendments.

## AVIS

La qualité de cette microforme dépend grandement de la qualité de la thèse soumise au microfilmage. Nous avons tout fait pour assurer une qualité supérieure de reproduction.

S'il manque des pages, veuillez communiquer avec l'université qui a conféré le grade.

La qualité d'impression de certaines pages peut laisser à désirer, surtout si les pages originales ont été dactylographiées à l'aide d'un ruban usé ou si l'université nous a fait parvenir une photocopie de qualité inférieure.

La reproduction, même partielle, de cette microforme est soumise à la Loi canadienne sur le droit d'auteur, SRC 1970, c. C-30, et ses amendements subséquents.

THE DEVON OBSERVATORY CCD IMAGING SYSTEM AND ITS APPLICATION TO  
PHOTOMETRY OF THE ELLIPSOIDAL VARIABLE HR 4646

BY

ERIC STEINBRING



A THESIS

SUBMITTED TO THE FACULTY OF GRADUATE STUDIES AND RESEARCH  
IN PARTIAL FULFILLMENT OF THE REQUIREMENTS FOR THE DEGREE OF  
MASTER OF SCIENCE

DEPARTMENT OF PHYSICS  
UNIVERSITY OF ALBERTA

EDMONTON, ALBERTA

FALL, 1995



**National Library  
of Canada**

**Acquisitions and  
Bibliographic Services Branch**

**395 Wellington Street  
Ottawa, Ontario  
K1A 0N4**

**Bibliothèque nationale  
du Canada**

**Direction des acquisitions et  
des services bibliographiques**

**395, rue Wellington  
Ottawa (Ontario)  
K1A 0N4**

*Your file    Votre référence*

*Our file    Notre référence*

**THE AUTHOR HAS GRANTED AN  
IRREVOCABLE NON-EXCLUSIVE  
LICENCE ALLOWING THE NATIONAL  
LIBRARY OF CANADA TO  
REPRODUCE, LOAN, DISTRIBUTE OR  
SELL COPIES OF HIS/HER THESIS BY  
ANY MEANS AND IN ANY FORM OR  
FORMAT, MAKING THIS THESIS  
AVAILABLE TO INTERESTED  
PERSONS.**

**L'AUTEUR A ACCORDE UNE LICENCE  
IRREVOCABLE ET NON EXCLUSIVE  
PERMETTANT A LA BIBLIOTHEQUE  
NATIONALE DU CANADA DE  
REPRODUIRE, PRETER, DISTRIBUER  
OU VENDRE DES COPIES DE SA  
THESE DE QUELQUE MANIERE ET  
SOUS QUELQUE FORME QUE CE SOIT  
POUR METTRE DES EXEMPLAIRES DE  
CETTE THESE A LA DISPOSITION DES  
PERSONNE INTERESSEES.**

**THE AUTHOR RETAINS OWNERSHIP  
OF THE COPYRIGHT IN HIS/HER  
THESIS. NEITHER THE THESIS NOR  
SUBSTANTIAL EXTRACTS FROM IT  
MAY BE PRINTED OR OTHERWISE  
REPRODUCED WITHOUT HIS/HER  
PERMISSION.**

**L'AUTEUR CONSERVE LA PROPRIETE  
DU DROIT D'AUTEUR QUI PROTEGE  
SA THESE. NI LA THESE NI DES  
EXTRAITS SUBSTANTIELS DE CELLE-  
CI NE DOIVENT ETRE IMPRIMES OU  
AUTREMENT REPRODUITS SANS SON  
AUTORISATION.**

**ISBN    0-612-06543-X**

**Canada**

UNIVERSITY OF ALBERTA  
RELEASE FORM

NAME OF AUTHOR: ERIC STEINBRING

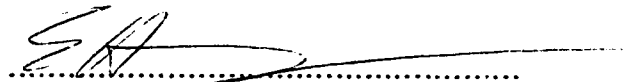
TITLE OF THESIS: THE DEVON OBSERVATORY CDD IMAGING SYSTEM AND ITS APPLICATION TO PHOTOMETRY OF THE ELLIPSOIDAL VARIABLE HR 4646

DEGREE: MASTER OF SCIENCE

YEAR THIS DEGREE GRANTED: 1995

Permission is hereby granted to the University of Alberta Library to reproduce single copies of this thesis and to lend or sell such copies for private, scholarly or scientific research purposes only.

The author reserves all other publication and other rights in association with the copyright in the thesis, and except as hereinbefore provided neither the thesis nor any substantial portion thereof may be printed or otherwise reproduced in any material form whatever without the author's prior written permission.

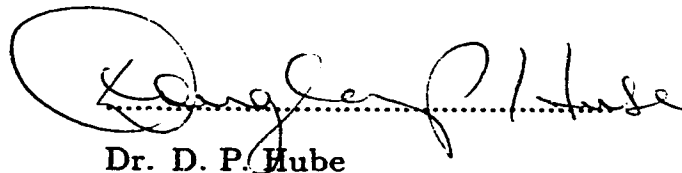
A handwritten signature in dark ink, appearing to read 'Eric Steinbring', is written over a horizontal dotted line.

Eric Steinbring

Date: August 31, 1995

UNIVERSITY OF ALBERTA  
FACULTY OF GRADUATE STUDIES AND RESEARCH

The undersigned certify that they have read, and recommend to the Faculty of Graduate Studies and Research for acceptance, a thesis entitled THE DEVON OBSERVATORY CCD IMAGING SYSTEM AND ITS APPLICATION TO PHOTOMETRY OF THE ELLIPSOIDAL VARIABLE HR 4646 in partial fulfillment of the requirements for the degree of MASTER OF SCIENCE.

  
.....

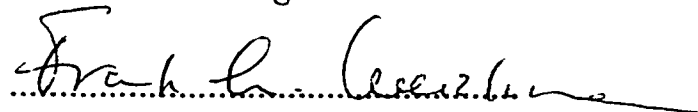
Dr. D. P. Hube

  
.....

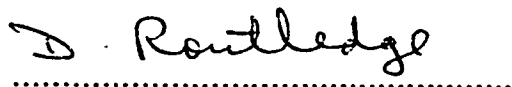
Dr. B. E. Martin

  
.....

Dr. E. H. Pinnington

  
.....

Dr. F. L. Weichman

  
.....

Dr. D. Routledge

Date: *August 31, 1995*

## ABSTRACT

The Devon Astronomical Observatory 0.5 m Cassegrain reflecting telescope has recently been equipped with a SpectraSource Instruments CCD camera. The system uses a back illuminated Tektronix TK512 512×512 pixel chip. This corresponds to a  $1.38 \text{ pix arcsec}^{-1}$  image scale at a focal ratio of  $f/8$ . The operation of the CCD imaging system is discussed with an emphasis on stellar photometry. Observing as well as data transfer and reduction procedures for this system at its present early stage of development are discussed. A straightforward observing method enabling the operator to acquire and process potentially hundreds of observations per night is developed. A complete manual of the procedures is presented as an Appendix. The first application of these procedures, a program of observations of ellipsoidal variables, is discussed. Specifically, the first results, observations of the star HR 4646, are analyzed. The CCD photometry of the close binary HR 4646 is presented and analyzed in combination with previously published spectroscopic data and suggests that HR 4646 is an ellipsoidal binary system.

## ACKNOWLEDGMENTS

In writing this thesis, the author would like to acknowledge the support and advice of Dr. Douglas P. Hube and Dr. Brian E. Martin. This work was funded through a scholarship from the Natural Sciences and Engineering Research Council.



## TABLE OF CONTENTS

<b>1. INTRODUCTION</b>	<b>1</b>
<b>1.1 The Devon Observatory CCD Stellar Photometer</b>	<b>1</b>
<b>1.2 Ellipsoidal Variables</b>	<b>1</b>
1.2.1 General Properties of Ellipsoidal Variables	1
1.2.2 The Ellipsoidal Variable Program	3
<b>1.3 HR 4646</b>	<b>4</b>
<b>2. CCD PHOTOMETRY</b>	<b>5</b>
<b>2.1 The Application of CCDs to Stellar Photometry</b>	<b>5</b>
2.1.1 General Characteristics of CCDs	5
2.1.2 Stellar Photometry	6
2.1.3 CCD Observations	8
2.1.3.a <i>Image Processing for CCD Observations</i>	8
2.1.3.b <i>CCD Aperture Photometry</i>	13
<b>2.2 The Devon Observatory CCD System</b>	<b>16</b>
2.2.1 Introduction	16
2.2.2 System Hardware	19
2.2.2.a <i>Focal Ratio</i>	19
2.2.2.b <i>Telescope Tracking</i>	19
2.2.2.c <i>Vignetting</i>	19
2.2.2.d <i>Equipment Setup</i>	19
2.2.2.e <i>The Cooling System</i>	19
2.2.3 CCD Characteristics	21
2.2.3.a <i>Gain and Readout Noise</i>	21
2.2.3.b <i>Thermal Characteristics</i>	23
2.2.3.c <i>Flat-Fields</i>	26
2.2.3.d <i>Other Effects</i>	32

2.2.4 Images . . . . .	35
2.2.4.a Image Quality and Sampling . . . . .	35
2.2.4.b Maintenance of Telescope Focus . . . . .	35
2.2.4.c General Observing Procedures . . . . .	35
2.2.4.d General Reduction Procedures . . . . .	37
<b>3. OBSERVATIONS / REDUCTIONS . . . . .</b>	<b>39</b>
3.1 Observations of HR 4646 . . . . .	39
3.2 Data Reductions . . . . .	39
3.2.1 Image Processing . . . . .	39
3.2.2 Differential Aperture Photometry . . . . .	45
3.3 Noise Analysis . . . . .	57
3.4 The Light Curve for HR 4646 . . . . .	59
<b>4. MODELING OF HR 4646 . . . . .</b>	<b>65</b>
4.1 A Simple Model . . . . .	65
4.1.1 Purely Ellipsoidal Variability . . . . .	65
4.1.2 Analysis of the Model . . . . .	65
4.2 Spectroscopic Data . . . . .	66
4.3 A More Sophisticated Model . . . . .	66
4.3.1 Estimation of System Parameters . . . . .	67
4.3.2 Wilson-Devinney Code Applied to HR 4646 . . . . .	72
4.3.2.a The Operation of LC . . . . .	72
4.3.2.b The Operation of DC . . . . .	73
4.3.3 WD Model Results / Analysis . . . . .	74
<b>5. CONCLUSIONS . . . . .</b>	<b>80</b>
5.1 The Devon CCD Imaging System / Stellar Photometer . . . . .	80
5.2 The Ellipsoidal Variable HR 4646 . . . . .	82
<b>REFERENCES . . . . .</b>	<b>84</b>

<b>APPENDIX</b> . . . . .	86
<b>A Manual for the Operation of the Devon Observatory</b>	
<b>CCD Stellar Photometer</b>	
<b>1. CCD Observations</b> . . . . .	86
<b>1.1 Getting Started</b> . . . . .	86
<b>1.2 Camera Start-up</b> . . . . .	87
<b>1.3 Focus</b> . . . . .	89
<b>1.4 System Monitoring</b> . . . . .	89
<b>1.5 Obtaining and Storing Images</b> . . . . .	90
<b>1.6 Reduction Images</b> . . . . .	91
<b>1.7 Data Transfer</b> . . . . .	92
<b>2. Image Processing / Data Reduction</b> . . . . .	93
<b>2.1 Processing the Frames</b> . . . . .	94
<b>2.2 Stellar Photometry</b> . . . . .	96

## LIST OF TABLES

Table 1. Observed Stars . . . . .	40
Table 2. Observing Log . . . . .	40
Table 3. Differential Magnitudes Output from PHOT. . . . .	49
Table 4. Photometric Data for HR 4646 Phased in 0.01 Phase Bins . . . .	62
Table 5. Fourier Coefficients for Photometric Variation of HR 4646 . . . .	67
Table 6. Radial Velocities for HR 4646 . . . . .	69
Table 7. Spectroscopic Orbital Elements of HR 4646 . . . . .	69
Table 8. DC Output for HR 4646 . . . . .	75
Table 9. Devon Observatory CCD Imaging System Parameters . . . . .	81

## LIST OF FIGURES

Figure 1.	TK512 CCD quantum efficiency versus wavelength . . . . .	18
Figure 2.	Cooling effectiveness of the TEC . . . . .	24
Figure 3.	TK512 dark current as a function of temperature . . . . .	25
Figure 4.	A typical flat-field for the Devon CCD system . . . . .	27
Figure 5.	Spatial variation due to the shutter effect: 0.100 s exposure . .	29
Figure 6.	Spatial variation due to the shutter effect: 0.400 s exposure . .	30
Figure 7.	Spatial variation due to the shutter effect: 1.250 s exposure . .	31
Figure 8.	The linearity of the Devon CCD system with respect to signal.	34
Figure 9.	Flare-feature in a typical stellar profile . . . . .	36
Figure 10.	A typical program frame for the HR 4646 observations . . . . .	41
Figure 11.	A ruled-surface plot of an unprocessed program frame . . . . .	43
Figure 12.	An intensity plot of a bias frame. . . . .	44
Figure 13.	The program frame prior to flat-fielding . . . . .	46
Figure 14.	The program frame after flat-fielding . . . . .	47
Figure 15.	A ruled-surface plot of a processed program frame . . . . .	48
Figure 16.	The (HR 4646–SAO 7521) differential magnitudes . . . . .	61
Figure 17.	The HR 4646 fluxes phased in 100 phase bins . . . . .	63
Figure 18.	The Fourier-fit to the HR 4646 light curve . . . . .	68
Figure 19.	The radial-velocity curve for HR 4646 . . . . .	70
Figure 20.	The WD model of HR 4646: Stellar surface temperatures . .	77
Figure 21.	The WD model of HR 4646: Orbital inclination . . . . .	78
Figure 22.	The WD model fit to the radial-velocity curve for HR 4646 . .	79

broadside and dim as they turn end-on to the observer. Furthermore, variation should be seen even if no eclipses occur, provided the stars are not seen from directly above or below. This effect leads to an observed continuous brightness variation which varies as roughly the ratio of projected surface area to maximum disk area or  $\cos 2\theta$  where  $\theta$  is the phase.

Of course, in reality the situation is more complicated. The stars are generally not perfect ellipsoids but actually somewhat “egg-shaped”, with their narrower ends pointing towards each other (defined by a Roche geometry, see Shore 1992). This can lead to a difference in the intensities of emitted light towards minima due to the difference in the profiles of the two end-on configurations.

As well, there are other effects which are enhanced by this distortion. Limb darkening is a drop in intensity towards the edge of the projected stellar disks due to the line of sight emerging from cooler surface layers. This effect can be important for ellipsoidal variables. For uniform limb darkening one would expect the effective projected stellar disks to be altered as well as the axial ratios of the ellipses. Gravity darkening refers to the effects of the non-coincidence of equipotential and isothermal surfaces of the rotating stars. Noting that for a rotationally distorted star, flux varies approximately linearly with the local surface gravity, gravitational distortion requires the star to be brighter at the poles. The global conservation of flux then requires the rotational equator to be dimmed (see, for example Shore 1992).

Considering that the stars are so close, one might also expect “reflection” effects. That is, light of one component irradiates and heats the other component. The resulting increase in surface brightness radiates from the far component toward the observer. Also, it is possible in these systems for tidal forces to draw out gas streams into revolution about the system, providing small variations in intensities that would be difficult to model. The light

variations due to the combination of a few or all of these effects, however, would be very subtle as compared to the situation where the variability were due to eclipses.

### 1.2.2 The Ellipsoidal Variable Program

In July and August 1994, the author successfully observed the star SAO 20517 using a single channel photometer attached to the Devon Observatory 0.5 m telescope (Martin et. al. 1994). After SAO 20517 was identified as a possible ellipsoidal binary system, it was decided in January 1995 that a program of observations of suspected ellipsoidal variables might be possible with the newly installed CCD imaging system.

From a list of ellipsoidal candidates suggested by D. P. Hube, the author selected a subset of the best candidates for an observing program of suspected ellipsoidal variables. Of these, three program stars were chosen to be observed. These were HR 4646, B 1413, and B 1414.

HR 4646 was selected for the following reasons:

i. Radial velocity data for this star were known to exist and showed that it has the characteristics of short period and large radial velocity amplitude typical of ellipsoidal variables. Both characteristics are indicative of a small separation between components and, therefore, large tidal effects and physical distortion.

ii. HR 4646 had been included in a short observing campaign in the summer of 1994, and therefore a small amount of 3-colour photoelectric photometry, although unreduced, might be available. The fact that the star field was thus familiar to the author and known to be compatible with the CCD detector field was also a factor.

iii. HR 4646 is a circumpolar object, i.e., from the latitude of the Devon Observatory it never sets. This was of particular advantage, since the number

of available dark observing hours at this latitude ( $\sim 54^\circ$ ) in mid-winter is more than 14 hours. Thus, the object could be observed, after initial setup and barring very poor sky conditions, for perhaps 12 continuous hours a night. If one considers that HR 4646 has a period of roughly 32 hours, full phase coverage from sections of 3 consecutive cycles could easily be observed on 4 consecutive clear nights. Overlapping coverage from night to night could also serve to eliminate the possibility of spurious systematic variation.

The other two stars chosen were, at the outset, possibly better candidates. B 1413 ( $\alpha(2000)=22^h58^m46^s.56$ ,  $\delta(2000)=+62^\circ46'11''.27$ ,  $V=9.^m02$ ) and B 1414 ( $\alpha(2000)=23^h00^m53^s.46$ ,  $\delta(2000)=+62^\circ52'13''.84$ ,  $V=9.^m81$ ) have shorter periods and comparable radial velocity amplitudes. They are also circumpolar objects. Best of all, as viewed with the CCD, they are in the same rich star field. They are also, however, very faint. They are  $\sim 4$  to 5 magnitudes fainter than HR 4646. Problems associated with very long exposures suggested starting with the brighter HR 4646. At the time of writing, the observations with full phase coverage for the stars B 1413 and B 1414 are incomplete and will not be discussed further.

### 1.3 HR 4646

*The Eighth Catalogue of the Orbital Elements of Spectroscopic Binary Systems* (Batten, Fletcher, and MacCarthy 1989) lists the star HR 4646 ( $\alpha(2000)=12^h12^m11.^s8$ ,  $\delta(2000)=+77^\circ36'58''$ ,  $V=5.^m1$ , A5) as a single-lined spectroscopic binary with a period of  $1.^d2709334$ . This is based on spectroscopy due to Abt (1961). In the following chapters, analysis of these data combined with the photometry carried out January 20-24 and February 10-13, 1995 demonstrates two main results. First, the Devon CCD system can be operated as a stellar photometer, at least in the case of bright stars in uncrowded fields. Second, its first results in that capacity lead to evidence that HR 4646 is an ellipsoidal binary (Steinbring, Hube, and Martin 1995).



## 2. CCD PHOTOMETRY

### 2.1. The Application of CCDs to Stellar Photometry

#### 2.1.1 General Characteristics of CCDs

A CCD or Charge Coupled Device is a small light sensitive silicon chip. Incident photons absorbed by the active layer of the CCD (the “epitaxial” layer) generate electron-hole pairs. Charge accumulates in potential wells (pixels) over its surface and the number of electrons in each well is linear with exposed intensity. After the chip is exposed, the charge can be electronically transferred from well to well to an on-chip amplifier (in what is by analogy called a *bucket brigade*) and then sampled and digitized by the associated camera electronics. The capacitors of the CCD are arranged along rows and columns. After the exposure, charge packets which have accumulated in the wells under each capacitor gate are transferred to the readout electronics by shifting them from row to row along columns. The charges in the final row are then sent individually to the on-chip amplifier. The electrons in each pixel across the surface are binned by the Analogue to Digital (A/D) converter to produce a smaller number of Analogue to Digital Units (ADU). The resulting output is a map of intensities. The set of all pixel intensities, each with its Cartesian coordinates known, is called a field (sometimes referred to as a frame).

Differences between typical CCDs used for astronomical applications are in the configuration of electrodes, overall size of the detector and the number of pixels, as well as the thickness of the chip and its spectral response characteristics. Typical formats range from arrays of  $\sim 300 \times 500$  pixels, to very large detectors with  $2048 \times 2048$  pixels. The sizes of the pixels themselves are typically  $\sim 10\text{-}30\ \mu\text{m}$ . Two basic classes among these CCDs are so-called front illuminated and back illuminated devices. In front illuminated devices,

light passes through the electrodes to the silicon. In back illuminated devices, the silicon is thinned to  $\sim 10 \mu\text{m}$ . In this way, the side opposite the electrodes can be exposed, and the light will pass directly into the silicon. For wavelengths between 400 nm and 800 nm, the photon absorption length in silicon is  $\sim 10 \mu\text{m}$ . However, for wavelengths shorter than 400 nm, the photon absorption length is only  $\sim 10 \text{ nm}$ . Thus, the potential for achieving high ultraviolet sensitivity is much greater in back illuminated devices rather than thick, front illuminated devices (Walker 1987).

### 2.1.2 Stellar Photometry

Observation of variable stars involves a process referred to as differential photometry. The magnitude of the target star is measured and compared to that of nearby stars of similar magnitude and spectral type. The magnitude of a star in the instrumental system,  $m$ , can be described by the expression

$$m = m_0 - 2.5 \log(C - C_{sky}), \quad (1)$$

where  $m_0$  is the the zero point of the instrumental system,  $C$  is the total number of counts due to the star and background, and  $C_{sky}$  is the total number of counts in the sky background. If the comparison star is observed through the same air-mass as the target star, the differential magnitude in the instrumental system is found by

$$\Delta m = m_{prog} - m_{comp}, \quad (2)$$

where  $m_{prog}$  is the instrumental magnitude for the program star, and  $m_{comp}$  is the instrumental magnitude of the comparison star.

In “classical” single-channel photoelectric photometry, the brightness of background sky as well as program and comparison stars are measured using

a photomultiplier. The observations are made one at a time through the same set of filters. Observations must cycle between program star, comparison stars, and sky. The goal is to reduce the effects of changing background illumination by maintaining a short time interval between observations of program and comparison stars. Applications of single channel photometry at the Devon Observatory have yielded precisions of  $\sim 0.^m003$  under photometric conditions. Martin, Hube, and Lyder (1990) quote an average precision of  $\sim 0.^m006$  for observations of 42 Per (program and comparison stars of  $V \approx 6^m$ ). This situation can be improved by using a photomultiplier centered on each star. Another detector can be used to simultaneously observe the background. The problem is that the slightly different gains and instrumental drifts in these detectors, each with its own set of filters, can obviate the attempt to reduce errors. Utilizing the Devon Observatory 2-channel photometer Martin, Hube, and Brown (1991) quote a typical precision of  $0.^m005$  for their observations of 75 Peg ( $V \approx 5^m$ ).

An advantage over the two previous methods can be realized with the use of a CCD. The advantage of this detector is that it covers a large field of sky. In this way, and of specific importance to differential photometry, many stars can be simultaneously exposed to an array of linear detectors. The star and its comparisons are exposed concurrently. Thus, to a certain extent, differential effects such as thin haze obscuring the field of view can be eliminated. The stars are all observed through the same air-mass, eliminating the need for at least first order corrections for atmospheric extinction. As well, the values for background illumination can be determined directly, for each exposure, for the immediate region around each of the stars. It is in principle possible with proper data reduction to achieve precisions superior to  $0.^m001$ . Photometry with CCDs can typically achieve  $0.^m002$  precision (Gilliland et al. 1991, Kjeldsen and Frandsen 1992).

### 2.1.3 CCD Observations

#### 2.1.3.a Image Processing for CCD Observations

Discussion for the moment will concern three basic corrections necessary with CCD detectors and follows a discussion found in Kjeldsen and Frandsen (1992). An important consideration during this processing is the degradation of the  $S/N$  associated with each step. At each processing step correction frames are combined with each other and the program frame in order to account for the detector's base-level, variations in detector gain, etc.. At each instance where frames are combined, their intrinsic noise values compound. It is for this reason that all processing is kept to a minimum. Equations for the propagation of the  $S/N$  for an arbitrary pixel of signal  $S$  (in electrons) are given for each step in processing and are due to a treatment found in Newberry (1991).

i. A correction must be made for temporal and spatial variations in the detector's zero level. That is, the number of counts present in all pixels when they are receiving no signal. To accomplish this the chip can be digitized without any exposure. This is called a *bias* frame, and is an additive effect. Typically, many bias frames are made and a mean created. This averages the effects of small changes in spatial structure of the bias frames over time. Changes in mean bias levels between exposures can be corrected for by scanning a strip of bias frame along the edge of every frame. This zero level is then subtracted as a first step in processing. Thus, this correction has the form (Kjeldsen and Frandsen 1992)

$$\text{Frame}_b(x, y) = \text{Frame}_0(x, y) - \langle \text{Bias} \rangle(x, y), \quad (3)$$

where  $\text{Frame}_b$  is the bias corrected frame,  $\text{Frame}_0$  is the frame corrected for scanned mean bias level, and  $\langle \text{Bias} \rangle$  is the average of all bias frames. The zero level correction amounts to a subtraction of a constant from all frames

other than the bias frames and their resultant  $S/N$  is calculated via the expression (Newberry 1991)

$$S/N = \left[ 1 \pm \frac{\text{const}}{S_{\text{Frame}}} \right] (S/N)_{\text{Frame}}, \quad (4)$$

where

$$S = S_{\text{Frame}} \pm \text{const}. \quad (5)$$

Combining the  $n$  bias frames results in a  $S/N$  of the mean bias frame given by (Newberry 1991)

$$S/N = \sum_{i=1}^n \left[ \left( \frac{S_i}{(S/N)_i} \right)^2 \right]^{-1/2} S, \quad (6)$$

where

$$S = \sum_{i=1}^n S_i. \quad (7)$$

Subtracting the average bias frame from the raw program frame results in a  $S/N$  given by (Newberry 1991)

$$S/N = \left[ S_{\text{Frame}_0} - S_{\langle \text{Bias} \rangle} + B^2 \left( 1 + \frac{1}{n} \right) \right]^{-1/2} S, \quad (8)$$

where

$$S = S_{\text{Frame}_0} - S_{\langle \text{Bias} \rangle}, \quad (9)$$

and

$$B^2 = Q^2 + \frac{g^2 - 1}{12} + N_0^2. \quad (10)$$

The base-level noise  $B$  includes the noise due to zero-level correction  $N_0$ , as well as the intrinsic noise in each frame due to the readout noise  $Q$ . The latter are properties of the readout electronics and are discussed in § 2.2.3.a. The form of the term involving  $g$  arises from truncation of the signal when it is binned by the A/D converter (see Newberry 1991 and references therein).

ii. The chip cannot differentiate between electrons resulting from exposure to light and those resulting from ambient heat. Thermal photons are accounted for by taking an integration of the same length but not exposing the chip to any light, i.e., keeping the shutter closed. As long as the chip is at the same temperature in this *dark* frame as in the exposure frame, one can subtract the dark frame from all exposures to correct for the effect. The result is (Kjeldsen and Frandsen 1992)

$$\text{Frame}_{\text{bd}}(x, y) = \text{Frame}_{\text{b}}(x, y) - \langle \text{Dark}_0 \rangle(x, y), \quad (11)$$

where  $\text{Frame}_{\text{bd}}$  is the dark corrected frame and  $\langle \text{Dark}_0 \rangle$  is the average of zero level corrected dark frames. The analysis of the propagation of  $S/N$  for dark subtraction is similar to that for bias subtraction. Here, the form of the expression for  $S/N$  for zero corrected dark frames is the same as equation (4). Combining the dark frames follows equation (6). The average dark frame is subtracted and the resultant  $S/N$  of the dark corrected frames is calculated as in equation (8).

iii. Not all the pixels have the same response to light. This is corrected for by exposing the detector to spatially uniform illumination and measuring the differential response from pixel to pixel, and perhaps across the chip. Dividing the dark corrected fields by this *flat* field generates pixel values as if the detector had a uniform response.

This map of the detector gain is typically generated by one of three methods. The first method is to take an image of the inside of the illuminated observatory dome. It can, however, lead to some systematic errors. The colour-temperature of the dome illumination can be very different from that of actual stars or dark sky background. Since the detector is more sensitive to light of some wavelengths than others, this can give a biased result. Also, it is not always an easy matter to obtain uniform illumination for the

detector. A great deal of experimentation is often necessary. A second, and often superior method, is to take an image of the sky at either dawn or dusk. The illumination in this case is often much more uniform than that obtainable with the first method. However, the light at dawn and dusk contains atmospheric emission lines at different amplitudes than dark night sky, and thus has a different colour-temperature. The third method involves taking exposures of “blank”, night sky. This gives uniform illumination which is most like that of actual program exposures. The problem is that light levels are low and, therefore, the illumination of the CCD is often insufficient to map out the pixel to pixel variations. Also, the task can be made difficult by very faint stars in the fields. This requires the operator to take many frames in several different locations in order to average images and remove the stars.

With many detectors, and/or if higher precision is needed, more corrections to the program frames will need to be made. For example, optical effects at boundary layers in the chip can result in interference fringes appearing in the images. More correction frames will be required to remove this additive effect. Defective pixels can be masked by substituting an average value over neighbouring pixels. Smoothed dark sky flat-fields might be used for a second order correction for large scale gain variations. For the present analysis, the final reduction calculation includes corrections i., ii., and iii., and follows the expression (Kjeldsen and Frandsen 1992)

$$\text{Image}(x, y) \propto \frac{\text{Program}_{\text{bd}}(x, y)}{\langle \text{Flat}_{\text{bd}} \rangle(x, y)} [1 + \delta_{\text{nonlinear}}(\text{ADU}, x, y)], \quad (12)$$

where Image represents the processed image,  $\text{Program}_{\text{bd}}$  is the bias and dark corrected program frame, and  $\langle \text{Flat}_{\text{bd}} \rangle$  represents the average of bias and dark corrected flat-field frames. The term  $\delta_{\text{nonlinear}}(\text{ADU}, x, y)$  would, if they were present, contain information about nonlinearities in CCD response. The calculation of  $S/N$  for zero correction and averaging of the flat fields is

as in the case of bias subtraction. The division of the program frame by the averaged flat field results in a  $S/N$  of (Newberry 1991)

$$S/N = \left[ 1 + \left( \frac{(S/N)_{\text{Program}_{\text{bd}}}}{(S/N)_{\langle \text{Flat}_{\text{bd}} \rangle}} \right)^2 \right]^{-1/2} S, \quad (13)$$

where

$$S = (S/N)_{\text{Program}_{\text{bd}}}. \quad (14)$$

The processing noise contributes to the final  $S/N$  of observations. Consider an image of an object which covers  $n$  pixels of the detector. The total number of counts attributable to the object,  $Z_{\text{obj}}$ , is given by (Newberry 1991)

$$Z_{\text{obj}} = g \sum_{(x,y)} [z(x,y) - z_{\text{sky,est}}(x,y)], \quad (15)$$

where  $z(x,y)$  is the number of counts in a pixel due to both the object and sky background, and  $z_{\text{sky,est}}(x,y)$  is the estimated number of counts due to the background. The noise due to each of  $j$  different sources is uncorrelated and combine in quadrature, i.e., as  $\sum_j N_j^2$ . Thus, the total noise in a given pixel, after sky subtraction is given by (Newberry 1991)

$$N_{(x,y)}^2 = \sigma^2[gz(x,y)] + \sigma^2[gz_{\text{sky,est}}(x,y)], \quad (16)$$

where  $\sigma^2$  is the variance of the respective quantity. The total noise in  $Z_{\text{obj}}$  is then

$$\begin{aligned} N^2 &= \sum_{(x,y)} N_{(x,y)}^2 = \sum_{(x,y)} \sigma^2[gz_{\text{obj}}(x,y)] \\ &\quad + \sum_{(x,y)} \sigma^2[gz_{\text{sky}}(x,y)] \\ &\quad + \sum_{(x,y)} \sigma^2[gz_{\text{sky,est}}(x,y)], \end{aligned} \quad (17)$$



where the total noise before sky subtraction has been separated into its object and sky components. The sources of noise in each of the three terms of equation (17) are photon statistics, truncation noise, and processing noise. The stochastic noise contribution to  $\sum_{(x,y)}[gz(x,y)]$  is just  $gZ$ . The total noise is then given by

$$N^2 = gZ_{\text{obj}} + n(gz_{\text{sky,avg}} + B^2) + n \left[ \frac{1}{n_{\text{sky}}} (gz_{\text{sky,avg}} + B^2) \right], \quad (18)$$

where  $n_{\text{sky}}$  is the number of pixels over which the background is sampled, and

$$B^2 = Q^2 + \frac{g^2 - 1}{12} + P^2. \quad (19)$$

where  $P$  includes all the noise added due to processing the program frame (the resultant noise calculated using equation (13)). This can be written as

$$N^2 = gZ_{\text{obj}} + n(gz_{\text{sky,avg}} + B^2) \left(1 + \frac{1}{n_{\text{sky}}}\right), \quad (20)$$

and results in a  $S/N$  for the object of

$$S/N = \frac{gZ_{\text{obj}}}{\sqrt{gZ_{\text{obj}} + n(gz_{\text{sky,avg}} + B^2) \left(1 + \frac{1}{n_{\text{sky}}}\right)}}, \quad (21)$$

### 2.1.3.b CCD Aperture Photometry

A brief analysis of the internal noise for an idealized case of CCD aperture photometry is now presented. It follows a treatment due to Kjeldsen and Frandsen (1992) (see also Gilliland and Brown 1988; Frandsen, Dreyer, and Kjeldsen 1989) and will be used to generate a few useful results. Consider a circular photometric aperture centered on a star. Let  $R$  represent the radius of the aperture in pixels, where  $\rho^2 = (x - x_0)^2 + (y - y_0)^2$ , and  $(x_0, y_0)$  is the centre position of the aperture. The present analysis will concern noise

due to photon statistics and readout noise alone. In this case the variance in electrons for the magnitude of the star is given by, with  $z$  representing the counts in a pixel,

$$\begin{aligned}
N_R^2 = \sum_{\rho \leq R} N_{x,y}^2 &= \sum_{\rho \leq R} z(x,y)g \\
&+ \frac{g}{z_{\text{flat}}} \sum_{\rho \leq R} [z(x,y)]^2 \\
&+ R^2 \left[ Q^2 \left( 1 + \frac{1}{n_{\text{sky}}} \right) + \frac{z_{\text{sky}}(x,y)g}{n_{\text{sky}}} \right],
\end{aligned} \tag{22}$$

where  $z_{\text{flat}}$  and  $z_{\text{sky}}$  are the counts in one pixel of the flat-field and background sky respectively,  $n_{\text{sky}}$  is the number of pixels in the sky background,  $Q$  is the readout noise, and  $g$  is the CCD gain. If the shape of the stellar profile is approximated by a Gaussian distribution of form

$$z(x,y) \approx z_{\text{sky}}(x,y) + z_0 0.5^{(2\rho/\text{FWHM})^2}, \tag{23}$$

and the counts summed within the aperture, the result is

$$\sum_{\rho \leq R} [z(x,y) - z_{\text{sky}}(x,y)]^n \approx \int_0^R (z_0 0.5^{(2\rho/\text{FWHM})^2})^n 2\pi\rho d\rho. \tag{24}$$

Now, if  $\rho > \text{FWHM}$ ,

$$\sum_{\rho \leq R} [z(x,y) - z_{\text{sky}}(x,y)]^n \approx \frac{(\text{FWHM})^2 \pi z_0^n}{4n \ln 2}, \tag{25}$$

which can be written as

$$\sum_{\rho \leq R} [z(x,y) - z_{\text{sky}}(x,y)]^n \approx \frac{(4 \ln 2)^{n-1}}{[\pi(\text{FWHM})^2]^{n-1}} \frac{Z_{\text{star}}^n}{n}, \tag{26}$$

where

$$Z_{\text{star}} = \sum_{\rho \leq R} [z(x,y) - z_{\text{sky}}(x,y)]. \tag{27}$$

The size of the aperture is optimized when it is not so small that portions of the stellar image are excluded, while not being so large that too much sky is included. If the aperture is too small, significant star counts can be lost and imaging centering errors can be a factor. If the aperture is too large, sky noise is increased. The value of aperture radius  $R$  can be optimized by considering the case of sky-limited exposures. This discussion is due to Harris (1990). In this case

$$S/N \approx \frac{e_{\text{star}}}{\sqrt{\pi R^2 e_{\text{sky}}}}. \quad (34)$$

Now, the stellar intensity profile,  $z(\rho)$ , gives rise to a count rate of

$$e_{\text{star}} = \int_0^R z(\rho) 2\pi \rho d\rho. \quad (35)$$

this implies that

$$S/N \propto \frac{1}{R} \int_0^R z(\rho) \rho d\rho. \quad (36)$$

For a Gaussian profile, the intensity is given by

$$z(R) = z_0 \exp(-R^2/2\sigma^2) \quad (37)$$

and  $S/N$  is maximized for  $R_0 \approx 2\sigma \approx 0.85$  FWHM. Thus, the optimal aperture is approximately 1.7 FWHM.

## 2.2 The Devon Observatory CCD System

### 2.2.1 Introduction

The 0.5 m Cassegrain reflecting telescope at the Devon Astronomical Observatory has recently been fitted with a SpectraSource HPC-1 Peltier cooled CCD camera utilizing a Tektronix TK512 512×512 pixel CCD. This

is a back illuminated chip with an array size of  $13.8 \times 13.8 \text{ mm}^2$ , and a pixel size of  $27 \times 27 \text{ }\mu\text{m}^2$ .

The TK512 CCD has high quantum efficiency over the spectral range 400 nm to 800 nm. Quantum efficiency measures the probability of an incident photon being converted to a measured signal by the detector. Typical photographic films and photomultipliers have efficiencies of less than 1% and approximately 10% respectively. A plot of the quantum efficiency versus wavelength for the TK512 chip is presented in Figure 1. Note that the efficiency is well above 80% for most of the visible spectrum, which means that approximately 80% of these visible light photons incident on the CCD will be detected.

The camera is operated using a 33 MHz 486 personal computer located in the Observatory warm room. Digitization takes place onboard the PC via a peripheral card supplied by SpectraSource. Detector refrigeration is provided by the Thermo-Electric Cooling unit (TEC), located in a separate control box in the Observatory warm room. The Liquid Recirculation Unit (LRU) is also located in the warm room and helps to maintain detector temperature by continuously pumping coolant through the camera head. This removes heat generated by the camera electronics. The camera is temporarily mounted at the  $f/8$  Cassegrain focus with a single V filter and has an  $11.8 \times 11.8 \text{ arcmin}^2$  field. The pixel size of  $27 \text{ }\mu\text{m}$  corresponds to an angular scale of 1.38 arcsec.

The stock HPC-1 software supplied by SpectraSource provides control for all functions of the camera. This includes control of the shutter, the capturing of images as well as bias and dark exposures, and image display and storage. The PC can store 20 images in RAM and approximately 450 frames on hard disk. These are then transferred to 120 Mbyte data-cartridges at the end of the observing session using a tape drive. For a more complete discussion of the CCD camera operation, its associated software, and the

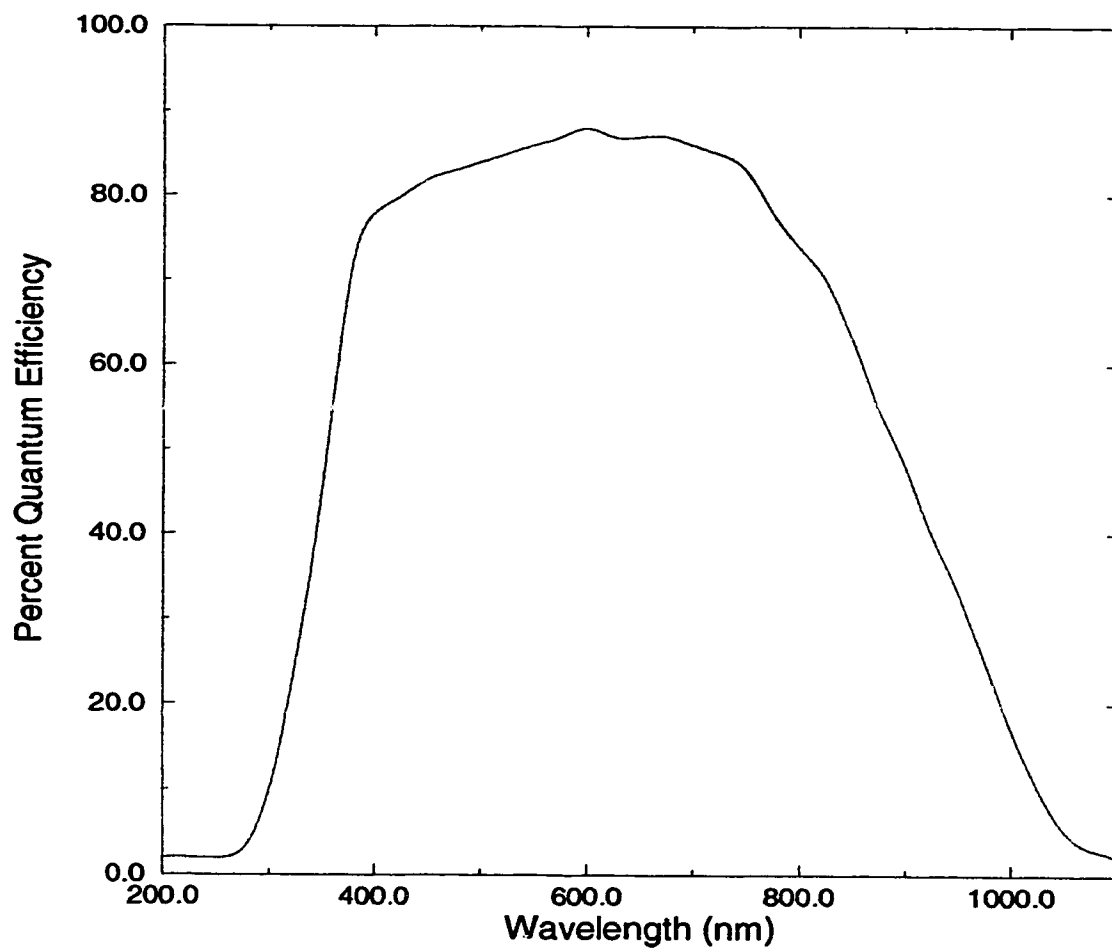


Fig. 1 - A plot of the TK512 CCD quantum efficiency versus wavelength The V filter used in observations is centered around 550 nm and has a band-pass of ~150 nm.

transfer and reduction of data see the Appendix.

Most of the major technical problems concerning observing with the new system were addressed in October and November of 1994. Many issues concerning camera operation presented themselves and were addressed. It came to light that there were problems with the telescope mechanics and optics, such as the telescope tracking rate and vignetting of the field. There were problems with the operation of the camera, including elevated dark counts and the effects of slow shutter speed on flat-fields, and of course, all the issues of set-up and operation had to be addressed before any successful observing could be done.

### 2.2.2 System Hardware

#### 2.2.2.a Focal Ratio

The issue first addressed was at what focal ratio the telescope should be operated with the new detector. The field observed by the camera at the original  $f/18$  focus was  $\sim 5 \times 5$  arcmin<sup>2</sup> and was usually too small for the concurrent observation of both program and comparison stars. The Devon telescope has the advantage of interchangeable front ends and the secondary mirror and housing for  $f/18$  was replaced with that for  $f/8$ . This provided the more usable field of  $11.8 \times 11.8$  arcmin<sup>2</sup> with an image scale of 1.38 arcsec pix<sup>-1</sup>.

#### 2.2.2.b Telescope Tracking

At this time, it was also noted that the telescope tracking needed adjustment. The stellar images taken were obviously “smeared out”, suggesting that the tracking was not synchronous with the apparent movement of the star. Until this was finally corrected, exposures were limited to 100 seconds. For longer exposures, images became too distorted for photometry to be carried out on the frames. That is, stellar images left trails larger than could

be accommodated by the available photometric reduction routines.

#### *2.2.2.c Vignetting*

The first problem associated with the new telescope front- end was the appearance of serious vignetting on one side of the field. This was for the most part addressed after several attempts at both collimation of the secondary and third mirrors and the modification of the filter holder in the camera mount. Finally, it was suspected that one of the telescope light baffles was interfering with the beam, and after this was removed and the mirrors aligned one last time, the vignetting problem was for the most part solved. Three corners of the field are still vignetted but this involves only  $\sim 1600$  pixels or about 0.6% of the detector surface area.

#### *2.2.2.d Equipment Setup*

Coincident with this, an observing procedure was developing (see the Appendix) and equipment setup took its final form. The camera control computer is located in a warm room adjacent to the dome. This way, the display is visible for focussing the camera by turning the monitor towards a window from this room to the dome. The TEC and the LRU were also located in the warm room.

#### *2.2.2.e The Cooling System*

It was observed that the detector temperature, which is displayed on the HPC-1 operation screen, was at intervals rising and falling by as much as 100 K. It was subsequently determined that this did not correspond to the actual temperature of the CCD detector. The temperature was monitored via a method outlined in SpectraSource documentation. A voltmeter was connected directly to the sensor via an output jack located on the TEC control box. At this output jack the measured voltage is linear with sensor temperature. It was observed that the rise in temperature displayed on the

HPC-1 screen corresponded to the TEC box overheating. The actual sensor temperature remained constant. In future, the CCD detector temperature will be monitored continuously via a voltmeter connected to the TEC box. The temperature of the TEC box itself can be maintained with better air circulation for its cooling vents.

It was also noted that during operation large air cavities could form in the coolant lines and could become lodged in the catacombs of the camera head. When this happened, the coolant in the LRU failed to circulate. After consultation with SpectraSource and technicians in the Physics Department Low Temperature Laboratory, a possible solution was arrived at. The problem was addressed by the fashioning of a reservoir bottle, approximately 1 litre in volume, which continuously flushes small bubbles from the lines. Once all the air was purged from the camera head this problem was completely solved.

### 2.2.3 CCD Characteristics

#### 2.2.3.a Gain and Readout Noise

The readout characteristics of the CCD were studied. That is, the values for CCD gain and readout noise were calculated. The CCD gain factor,  $g$ , is the number of recorded electrons in a well per digital unit (the bin size employed in the A/D converter). Typical values for gain are between  $1 \text{ e}^- \text{ ADU}^{-1}$  for very “shallow” wells, and  $10 \text{ e}^- \text{ ADU}^{-1}$  for “deep” wells. The readout noise,  $Q$ , is a property of imperfections in the CCD readout electronics and is usually quoted in electrons. Typical values for readout noise are between 2 and  $10 \text{ e}^-$  (Walker 1987).

The values of CCD gain and readout noise were calculated on several occasions using a method employed in the image reduction software IRAF. The IRAF package FINDGAIN compares the mean signal in two unprocessed



flats to the base-level calculated from two bias frames to estimate  $g$  and  $Q$ . The means and standard deviations are calculated for all four frames. The CCD gain is given by

$$g = \frac{[\langle \text{Flat}_1 \rangle + \langle \text{Flat}_2 \rangle] - [\langle \text{Bias}_1 \rangle + \langle \text{Bias}_2 \rangle]}{[\sigma(\text{Flat}_{1-2})]^2 - [\sigma(\text{Bias}_{1-2})]^2}, \quad (38)$$

where the brackets represent the mean counts over all pixels,  $\sigma$  is the standard deviation, and the readout noise in electrons is given by

$$Q = g \times \frac{\sigma(\text{Bias}_{1-2})}{\sqrt{2}}, \quad (39)$$

where

$$\text{Flat}_{1-2}(x, y) = \text{Flat}_1(x, y) - \text{Flat}_2(x, y), \quad (40)$$

and

$$\text{Bias}_{1-2}(x, y) = \text{Bias}_1(x, y) - \text{Bias}_2(x, y). \quad (41)$$

This calculation was carried out between several frames on different observing runs. The averaged results give a CCD gain of  $g = 4.9 \pm 0.2 \text{ e}^- \text{ ADU}^{-1}$  and readnoise of  $Q = 79 \pm 2 \text{ e}^-$ . Although a value of CCD gain of  $5 \text{ e}^- \text{ ADU}^{-1}$  is typical of similar CCDs, a readout noise level of  $80 \text{ e}^-$  is high. Typical values for readout noise for the present generation of CCDs (manufactured in the 1990s) are less than  $20 \text{ e}^-$ . For example, the Texas Instruments CCD TC213 (manufacturer quoted specifications for 1994 model year) has a readout noise of  $15 \text{ e}^-$ . The specification for the readout noise for the TK512 is  $< 10 \text{ e}^-$ . The reason for the high readout noise is not known and SpectraSource is being consulted in order to solve the problem.

The readout noise puts limits on the dynamic range of the CCD. This is estimated via the expression

$$\text{range} \simeq \frac{z_{\max}}{Q}, \quad (42)$$

where in this case,  $z_{max} = 65,535 \text{ ADU} \approx 3.21 \times 10^5 \text{ e}^-$ , and  $Q = 79 \text{ e}^-$ . The dynamic range for this CCD is, therefore, approximately 4100.

### 2.2.3.b Thermal Characteristics

During initial setup the necessary information about the CCD thermal characteristics was obtained. Large dark counts with rate  $\sim 50 \text{ ADU pix}^{-1} \text{ s}^{-1}$  at a detector temperature of  $-27^\circ \text{C}$  were present in all frames. This number is arrived at by taking an exposure of the same length as a program frame but with the shutter closed, averaging the counts in all pixels and dividing by the integration time in seconds. The dark count rate was studied in more depth. It was found to be approximately constant with exposure length. That is, the rate of dark counts does not appear to increase with longer exposures. A 1.000 s exposure has a dark count rate of approximately  $50 \text{ ADU pix}^{-1} \text{ s}^{-1}$ , as does a 30.0 s or 300.0 s exposure.

The relationship between dark counts and detector temperature was later studied in more depth and was found to be linear for temperatures within 10 K of the system operating temperature of  $\sim 246 \text{ K} \approx -27^\circ \text{C}$ . The operating temperature of the CCD maintained by the TEC was found to be stable to within 0.1 K. Plots of dark counts per second versus detector temperature are presented in Figures 2 and 3. Note that the full well depth for this 16-bit system is 65,535 ADU. In Figure 2 one can see that for the system uncooled (detector temperature  $\sim 290 \text{ K}$ ) the dark count rate reaches the level of nearly 1/3 full well depth or  $2 \times 10^4 \text{ ADU pix}^{-1} \text{ s}^{-1}$ . Near the operating temperature of 246 K, however, the rate is closer to  $50 \text{ ADU pix}^{-1} \text{ s}^{-1}$ . This can be seen in Figure 3, an enlargement of the region from 245 K to 255 K. The slope of the linear regression to the points in Figure 3 gives a rate of thermal counts of  $22 \pm 1 \text{ ADU pix}^{-1} \text{ s}^{-1} \text{ K}^{-1}$ .

Since the TEC cools the CCD based on (although not 1:1 with) the difference between ambient and detector temperature, one might expect the

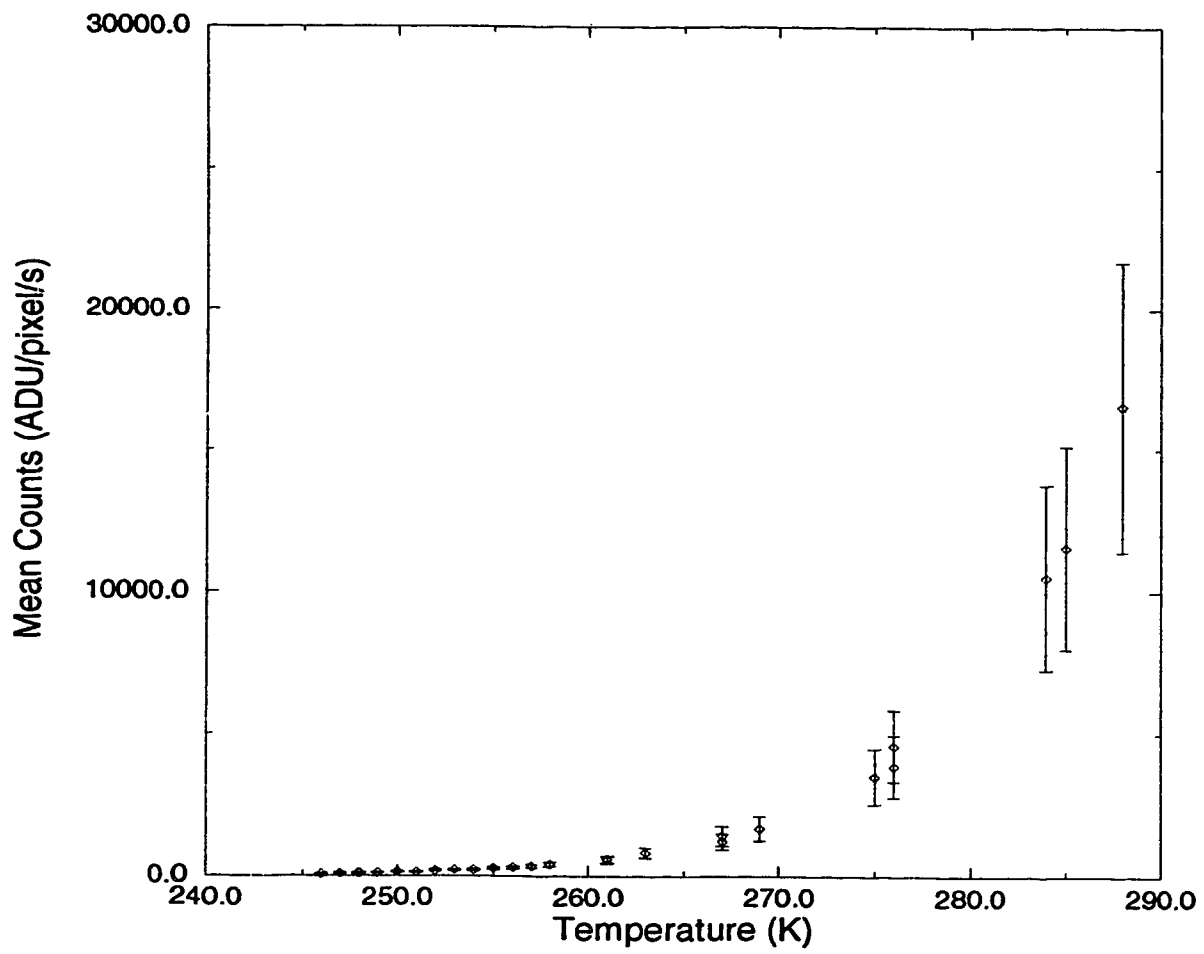


Fig 2. - Plot of the dark counts per second versus temperature, showing the cooling effectiveness of the TEC from room temperature down to 246 K  $\approx$  -27 °C. The elapsed time from room to operating temperatures is about 30 minutes.

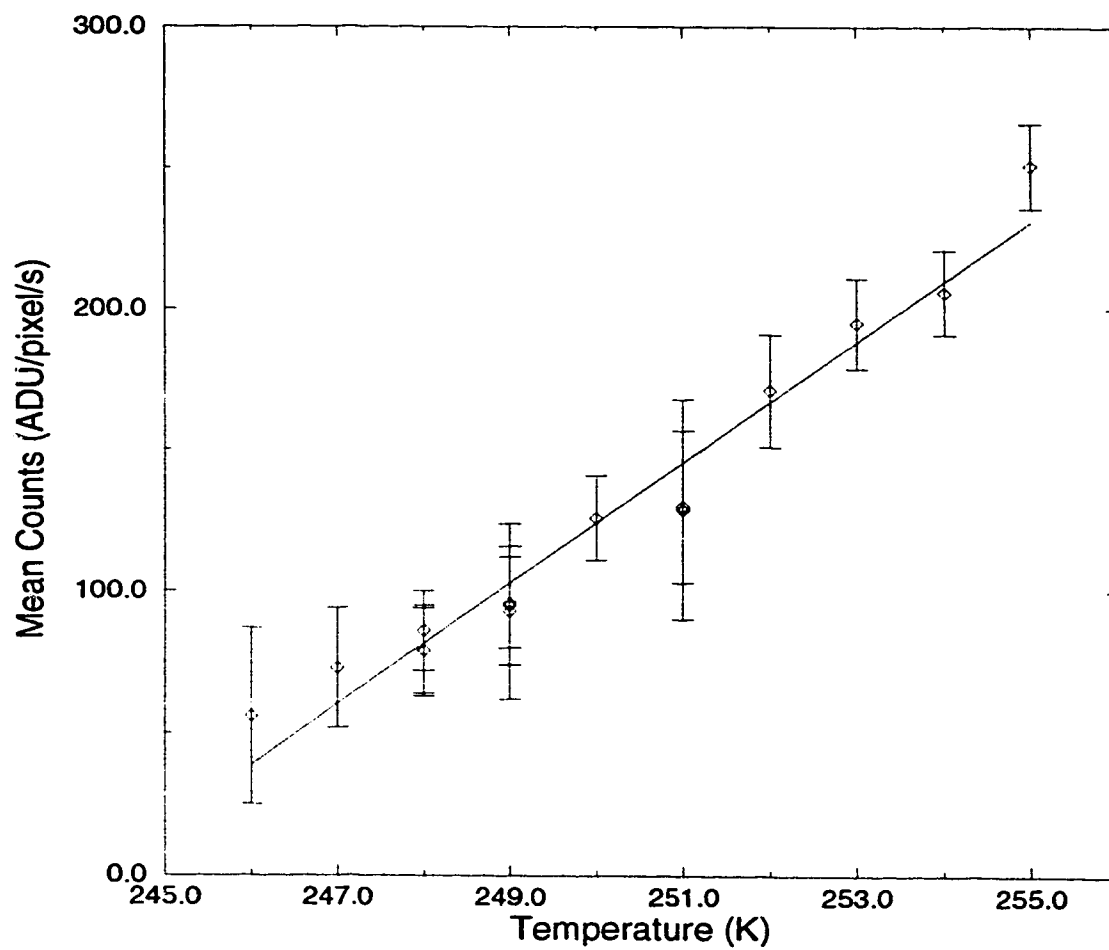


Fig 3. - Plot of the dark counts per second versus temperature near the operating regime of  $-20^{\circ}\text{C}$  to  $-30^{\circ}\text{C}$ . The slope of the linear regression to the points gives a rate of thermal counts of  $22 \pm 1 \text{ ADU pix}^{-1} \text{ s}^{-1} \text{ K}^{-1}$ .

detector to be somewhat colder when the ambient temperature is low, say, -10 °C to -20 °C. SpectraSource suggests that an enhanced cooling effect is possible at lower ambient temperatures. They suggest that this would correspond to a drop in detector temperature amounting to approximately 60% that of the ambient drop. Note that the data for the above plots were collected when both the camera and the TEC were at room temperature. Dark frames taken when the observations of HR 4646 were made (ambient temperature of -20 °C) suggest that the detector operating temperature was still only approximately -27 °C. Future workers will need to analyze the problem of detector refrigeration more in depth if lower dark counts are to be realized. SpectraSource is also being consulted with regard to this issue.

### *2.2.3.c Flat-Fields*

It was noted that properly taken dome flats could be sufficient for the flat-fielding of images, but only if exposures were not shorter than 0.350 s. It had been observed that very short exposures had a detectable “shutter effect”. That is, the slow mechanical shutter speed created noticeably higher illumination in the centre of the frame than at the edge (see Surma 1993). The flat fields have a region of greater intensity in the centre of the frame. This is evident in both dome and twilight illuminated flats and remains constant for longer exposures ( $\geq 2$  seconds). An intensity plot along the central row of a typical flat-field is shown in Figure 4. It is a 0.5 second image of twilight sky taken at dusk. No alteration in shape of the central “hot spot” was evident when the camera was rotated with respect to the optical axis in the mount and it is therefore believed to be a property of the telescope optics. It is possibly due to blockages in the optical train such as the secondary mirror and its support structure.

The effect of the slow shutter can be seen in Figures 5-7. Each image was created by dividing a short exposure dome flat-field by one of much

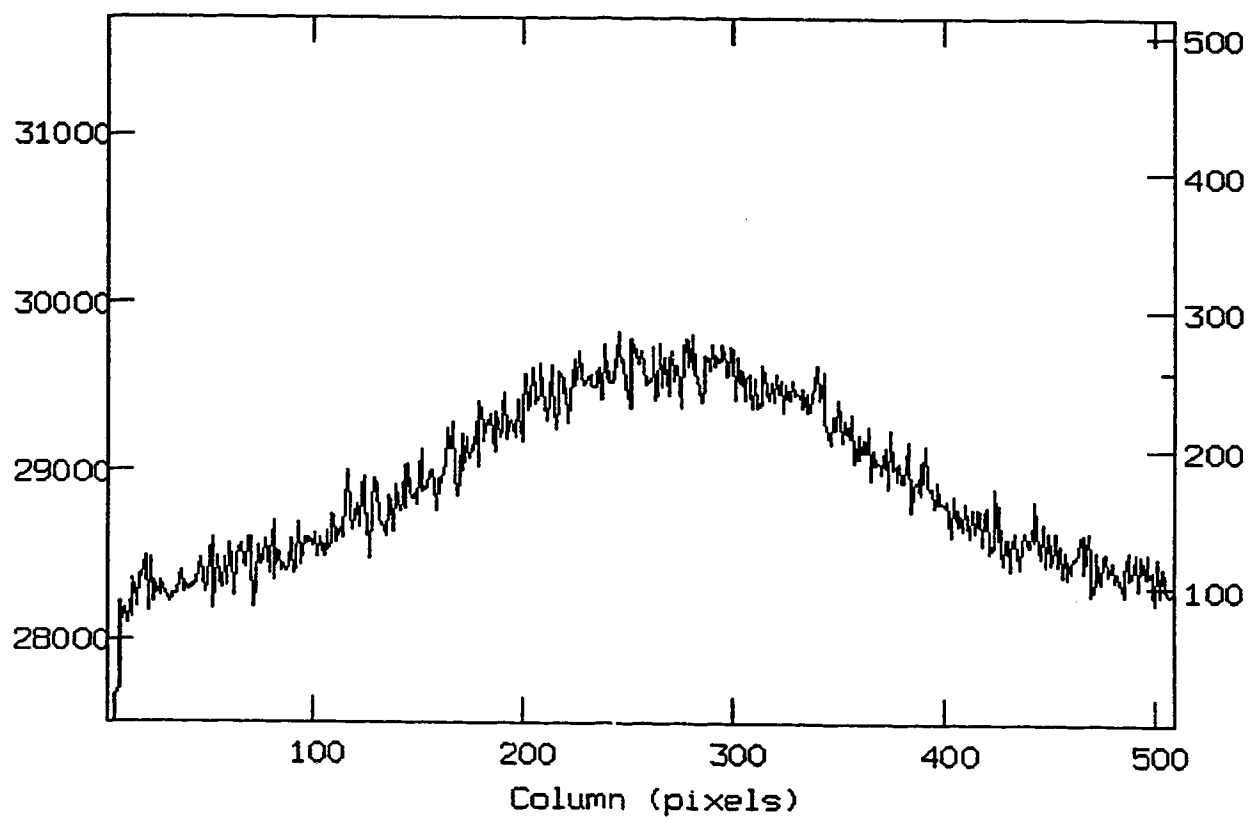


Fig. 4 - An intensity plot along the central row of a 0.5 second twilight sky flat field. The left hand scale is in counts (ADU) while the right hand scale indicates the row number with a tick-mark on the axis. The central hot spot is a property of the telescope optics and is 4-6% higher in intensity than the rest of the image.

longer integration. A 2.000 s dome-flat was used, by which point no effects due to the shutter speed can be detected. These results are from tests done with the camera unfiltered; however, testing involving integrations through a V-band filter were also made, with similar results. The result of dividing the fields is the variation across the field due only to the shutter effect. One can see that once integrations reach about 0.4 seconds the effect is greatly reduced. Figures 5, 6, and 7 are intensity plots along the central row (left to right across the image) of the results from integrations of duration 0.100 s, 0.400 s, and 1.250 s respectively. The ratio of intensities against the 2.000 s integration flat are along the left hand axis. One can see that the effect has fallen from approximately 4% variation across the chip in the 0.100 s integration to less than 1% in the 0.400 s integration. Note that the brightness of the dome illumination was decreased twice during the procedure, which accounts for the non-monotonic change in intercept in the plots.

It was planned that a more sophisticated method of obtaining dome flats would be set up. This would have involved at least a method of illumination with light of known Planck temperature. A slide projector or a set of halogen projection lamps colour-balanced by filters could be employed to produce approximately the Planck temperature of sunlight. This set-up has not yet been constructed and the only available illumination for dome flats is the incandescent dome lights. As well, the only means of changing camera filters at present is by unbolting the camera mount, removing the camera head and filter holder from the mount, and manually inserting the filter in the filter holder. Thus, the extensive testing of flat-fields by both the methods of twilight sky and dome illumination has only been done either unfiltered or through a V filter.

It is not known if the rate at which the shutter opens and closes is

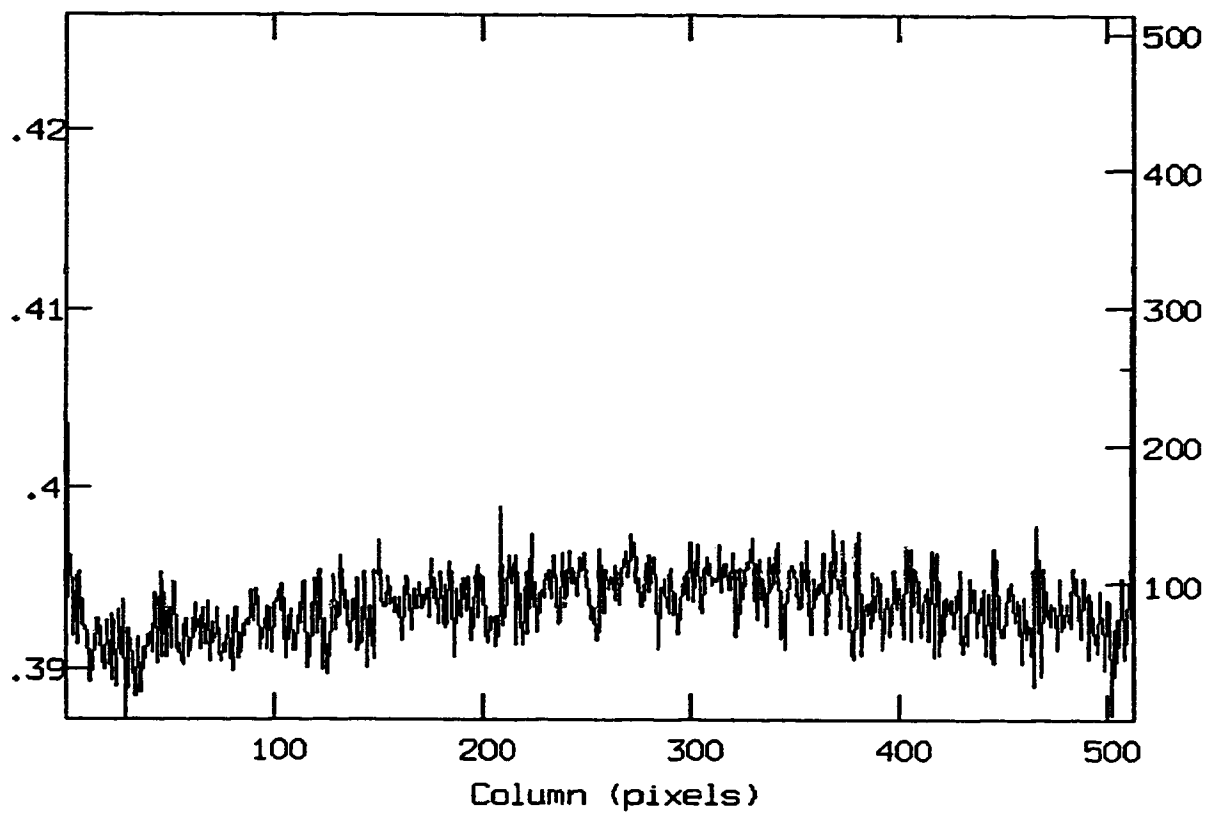


Fig. 6 - Intensity plot along the central row for the 0.400 s exposure. The variation is reduced to  $\sim 1\%$  across the field.



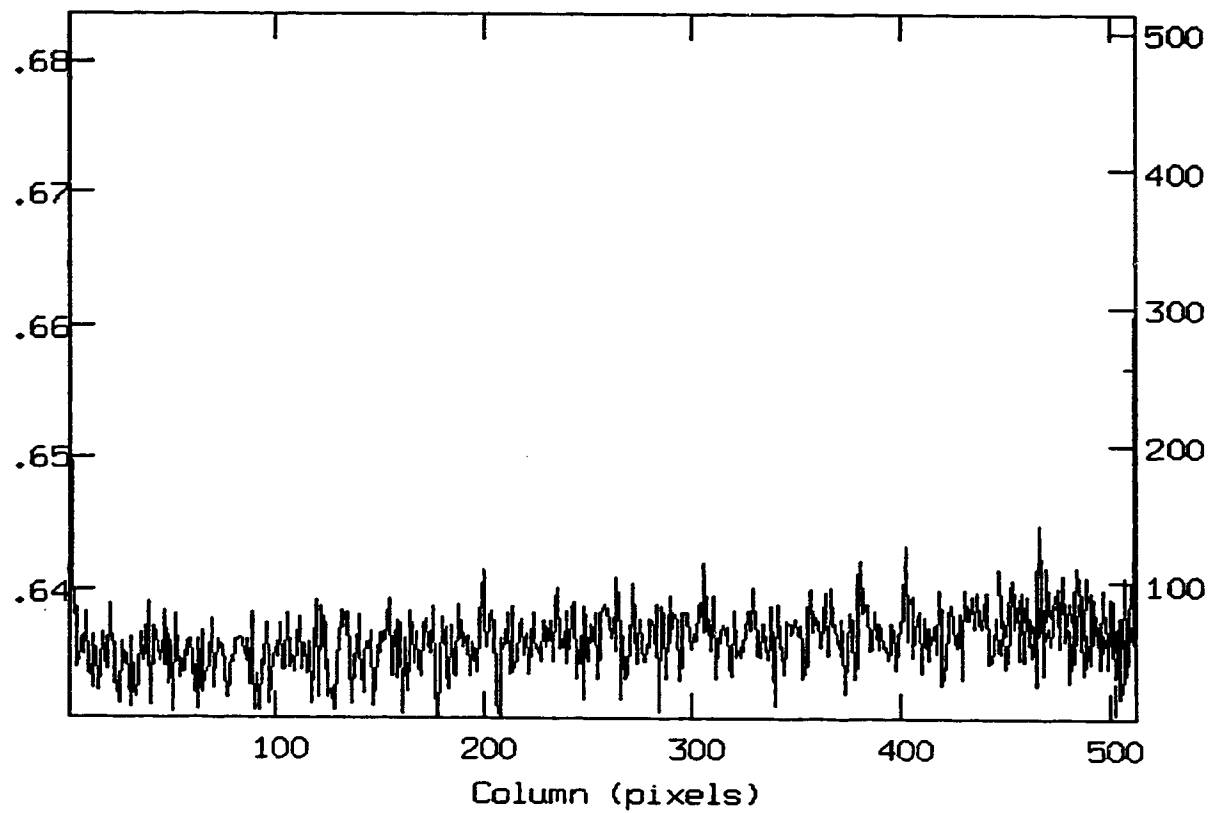


Fig. 7 . Intensity plot along the central row for the 1.250 s exposure. The variation is reduced to less than 0.5% across the field.

uniform for short exposures. That is, it is not known for a given integration time if this effect varies in intensity from exposure to exposure. Although the shutter has been hand-timed for integrations longer than 30 seconds and is found to be accurate to within 1 second, the testing of shutter speed for short exposures has not yet been done. Since it is not known if the dome lights provide constant illumination, a time series of short exposure flat-fields may not demonstrate variability in the shutter speed. Surma (1993) suggests a method of correcting for the effects of shutter speed by deconvolving a CCD camera's intrinsic flat-field from a 2-dimensional function describing the illumination due to the shutter. However, it was decided that at least for the first observations with the camera, this regime of very short exposures ( $< 0.35$  sec) could simply be avoided. A more sophisticated method of flat-fielding images must be developed later.

#### *2.2.3.d Other Effects*

Some other effects sometimes noticed in CCD imaging systems have not been a factor in this system. Fringing refers to Michelson interference fringes created from the interaction of incoming light with surface and boundary layers within the chip. This effect is sometimes seen for illumination with strong emission lines. No fringing patterns above the level of background noise were evident in any of the flat-field or program frames from the present work. Variation in bias levels over time is corrected for by the automatic overscanning of a 30-40 pixel wide strip of bias level along one edge of the frame immediately after each exposure. This level is then automatically subtracted in the processing stage. In order to account for bias structure, a sample of 10 to 20 bias frames were taken before and/or after each run, averaged, and used in processing. Variation in bias structure over the course of minutes or hours was not observed. Bias frames taken at different times were divided by and subtracted from each other in order to reveal any variation. The results were

uniform. The present work involved differential photometry of bright stars using exposures requiring a range of well depth from approximately  $1 \times 10^4$  ADU  $\text{pix}^{-1}$  to  $5 \times 10^4$  ADU  $\text{pix}^{-1}$ . This involves the middle 60% of the response curve of the chip. It has been shown that CCDs in general have deviations from linearity of only 0.1-0.5%. This is true even with exposures approaching pixel saturation (McCall, English, and Shelton 1989).

Following a method employed in McCall, English, and Shelton (1989), a rough check of the linearity was made using the flat-field exposures employed in § 2.2.3.c. A function of the form  $S - A = +Bt^\alpha$ , where  $S$  is signal and  $t$  is time was fitted to the points. The growth of the logarithm of  $S - A$ , was plotted against the logarithm of the integration time,  $t$ . A departure of  $\alpha$  from a value of 1.0 would be indicative of a nonlinearity in the system. This would not necessarily correspond to a nonlinearity in the response of the CCD, partly because of systematic errors due to the shutter speed as well as the possibility of temporal changes in intensity of the dome lights.

A plot of mean signal (the average of all pixels over the frame) versus time is shown in Figure 8. The brightness of the illumination was decreased twice over the course of the test in order to accommodate longer exposures. This is seen as changes in slope in the plotted data. The value of  $\alpha$  was determined for three regimes. Exposures from 0.010 s to 0.100 s had signals from  $5 \times 10^3$  ADU  $\text{pix}^{-1}$  to  $2 \times 10^4$  ADU  $\text{pix}^{-1}$  and yielded a value of  $\alpha = 1.036 \pm 0.009$  (s.d.). Exposures from 0.200 s to 0.900 s had a range of signals from  $9 \times 10^3$  ADU  $\text{pix}^{-1}$  to  $4 \times 10^4$  ADU  $\text{pix}^{-1}$  and yielded a value of  $\alpha = 0.994 \pm 0.004$  (s.d.). Exposures from 1.000 s to 2.000 s had signals from  $2 \times 10^4$  ADU  $\text{pix}^{-1}$  to  $5 \times 10^4$  ADU  $\text{pix}^{-1}$ , with a fit to the data yielding a value of  $\alpha = 0.989 \pm 0.027$  (s.d.). The first regime corresponds to the region of integration times that were avoided due to slow shutter speed. The second regime roughly corresponds to the range of exposure times and counts per

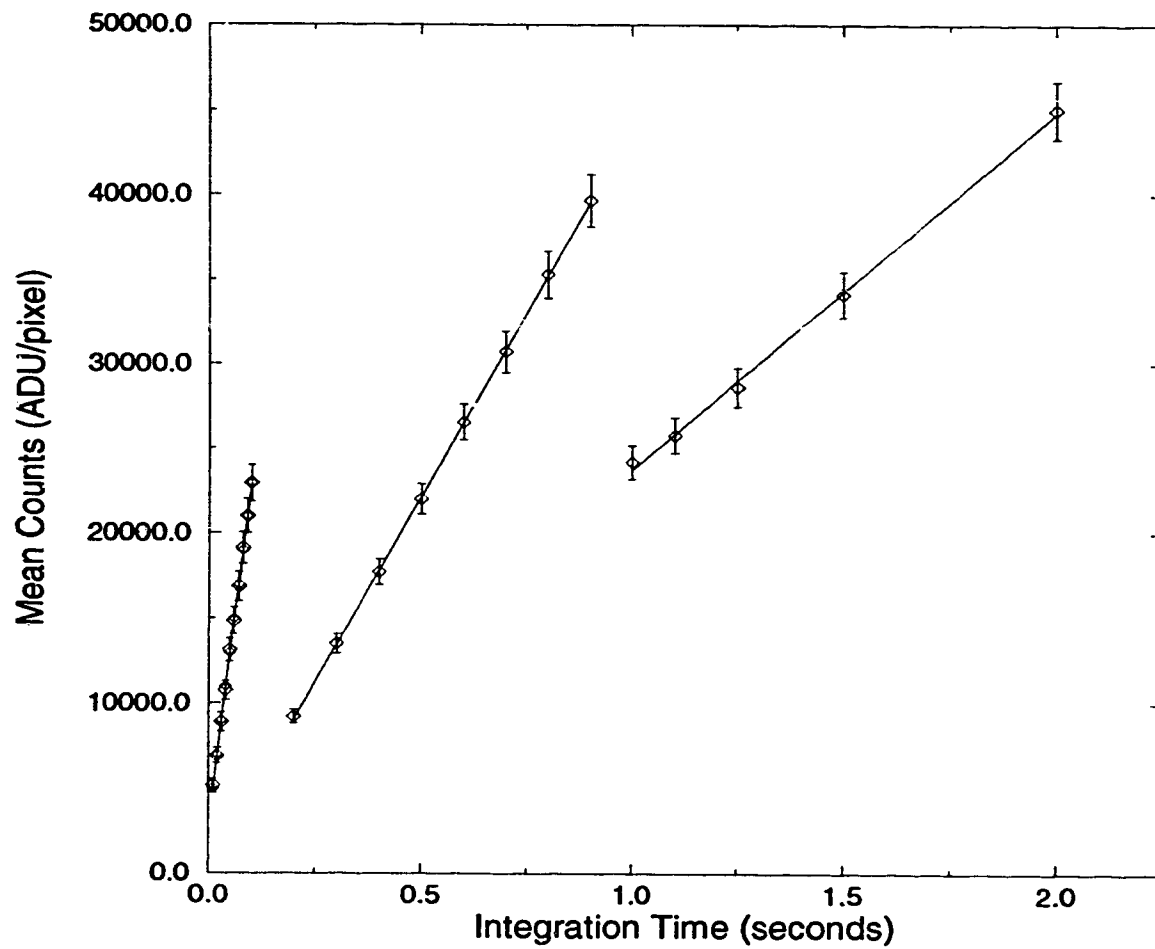


Fig. 8 - A plot of signal (averaged over the frame) versus time for the unfiltered flat fields employed in § 2.2.3.c.

pixel employed in the present work. It is true that the counts in many of the pixels under the brightest star would have been in the range of the third region at  $\sim 5 \times 10^4$  ADU  $\text{pix}^{-1}$ . However, the values for  $\alpha$  calculated from this data do not indicate nonlinearity greater than 1% in either of the latter two regimes.

## 2.2.4 Images

### 2.2.4.a Image Quality and Sampling

With the mirrors collimated and the problem of vignetting corrected, the only issue of the telescope's optics that was not addressed is image quality. Typical stellar FWHM is approximately 6 arcsec, but this is only after very careful focussing of the telescope. Typically, there is a flare consistently on one side of the stellar image. See Figure 9.

In order to properly sample a stellar image, the Nyquist theorem requires that the FWHM be greater than 2 pixels. Otherwise, information about spatial image structure will be lost due to aliasing (Walker 1987). Now, for a 6 arcsec FWHM, it is required that 1 pixel be  $\leq 3$  arcsec. Note that the image scale with the present set-up is 1.38 arcsec  $\text{pix}^{-1}$ . Thus, in the present configuration, the Nyquist condition is met.

### 2.2.4.b Maintenance of Telescope Focus

The amount of flex with temperature variation in the telescope optics is considerable. The observer can notice when monitoring the stellar images on the HPC-1 display that a drop in ambient temperature of only a few degrees in the dome will correspond to the stellar images becoming badly out of focus. This can make the maintenance of focus difficult and stellar image quality can sometimes suffer. Note the flare emerging from the right of the star profile in Figure 9. For the present work, the apertures for photometry

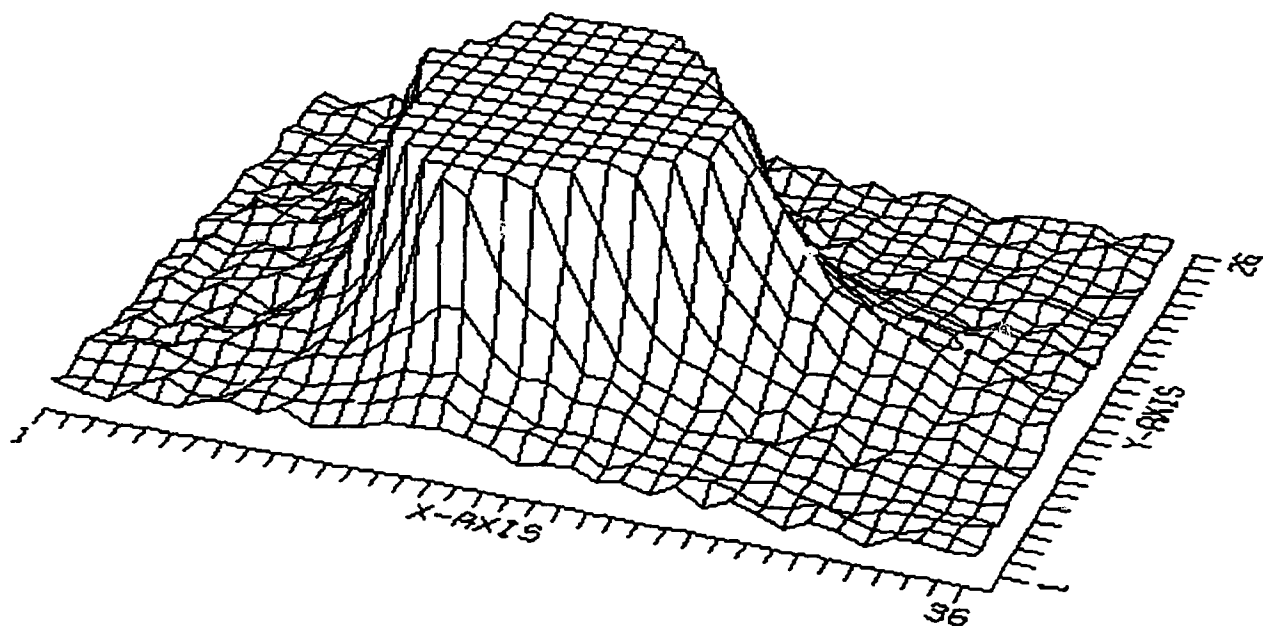


Fig. 9 - A ruled-surface plot of section of image showing the apparently bright (5<sup>th</sup> magnitude) star HR 4646. The integration length is 0.500 s. The peak has been truncated at a height of 2000 ADU and the flare is evident to the right of the plateau.

chosen were very large  $\sim 16$ -20 arcsec, and never excluded this flare feature when it appeared.

#### *2.2.4.c General Observing Procedures*

In the present work, before each night's run, 10-20 flat fields were taken using a  $0.5 \times 0.5 \text{ m}^2$  white plastic square permanently affixed to the inside of the dome and using the dome lights for illumination. To avoid the shutter effect, integrations were always longer than 0.35 seconds and were the same duration as in the program frames. Care was taken to make the illumination of the square uniform (see the Appendix). As well, 10 - 20 bias frames were taken before and/or after each run. Dark fields were taken with integration times the same as those of program exposures. Usually only 5 frames were taken per night. If average dark frame intensities were less than 25 ADU  $\text{pix}^{-1}$ , dark reductions would not be necessary and more frames were not taken (see § 3.2.1). Some care was taken to keep stars in the same locations on the detector throughout an observing session despite small telescope tracking errors. The method employed was to mark the HPC-1 display screen with a piece of black electrician's tape. Thus, the locations of the centroids of stellar images in the fields can only be considered to be within  $\sim 50$  pixels of their original locations at the beginning of the observing session.

#### *2.2.4.d General Reduction Procedures*

Reduction procedures were developed to handle the large number of observations per night. The general procedures are outlined in detail in the Appendix. Processing was carried out at the University of Alberta on a Sun Sparc-station using the image reduction software IRAF. As well, some simple post-processing subroutines were written in FORTRAN 77. These read the differential magnitudes from IRAF output files and matched them with the Julian Date, which was calculated from the time encoded in the

HPC-1 image header file.

The procedures are basically as follows. The entire set of program frames for one night is imported into IRAF. Then they are processed as one batch. After this, aperture photometry is carried out as one batch. Finally, the differential magnitudes for the entire night are read from the IRAF magnitude files to a single output file for subsequent analysis. In this way, the entire night's work, usually hundreds of exposures, can be reduced in one afternoon. The only real impediment to quick reductions is computer speed.



### 3. OBSERVATIONS / REDUCTIONS

#### 3.1 Observations of HR 4646

The data consist of 1599 observations over 7 nights. The January 20-24 1995 observations were 0.350 s integrations at approximately 2 minute intervals ( $\sim 0.001$  in phase). In the February 10-13 1995 observations, the telescope was stopped down to  $\sim 0.35$  m and the integrations increased to 0.550 s. This was intended to ensure a wide range of possible integration times in that variable sky conditions sometimes required shorter exposures. Exposures less than 0.350 s were not advisable due to the effects of slow shutter speed. A typical program frame is presented in Figure 10. The program, check, and comparison stars are labelled by the numbers 1, 2, and 3. The coordinates for the stars given in Table 1. The large field  $\sim 10 \times 3$  arcmin<sup>2</sup>, encompassing object, comparison and check stars, necessitated one minor adjustment. The comparison star sometimes drifted slightly closer to the edge of the detector due to imperfect telescope tracking. To alleviate this, the camera mounting was rotated 30 ° after the January observations so that the star field better fit the frame. Note that the observing procedure was to take flat-fields for each night's run, so any change in the optics associated with rotating the camera or stopping down the telescope would be accounted for.

#### 3.2 Data Reductions

##### 3.2.1 Image Processing

The set of bias frames was combined with the IRAF package ZERO-COMBINE in CCDRED. The flats were bias subtracted using this averaged frame and then combined using FLATCOMBINE. This provided two averaged processing frames for each night. Program fields were freed of bias and then flat-fielded using the package CCDPROC. Note that the additional

TABLE 1  
Observed Stars

star	$\alpha(2000)$	$\delta(2000)$	V / sp. type
1. HR 4646	$12^h 12^m 11^s.8$	$+77^\circ 36' 58''$	$5.^m1$ , A5
2. SAO 7519	$12^h 11^m 37^s.0$	$+77^\circ 31' 38''$	$8.^m9$
3. SAO 7521	$12^h 11^m 48^s.3$	$+77^\circ 26' 27''$	$6.^m6$ , A0

TABLE 2  
Observing Log

date	observations	JD – 2449000.0	duration	notes
Jan 20/21, 1995	198	738.622-738.964	8 hours	thick haze
Jan 21/22, 1995	268	739.647-740.070	10 hours	
Jan 22/23, 1995	216	740.593-740.940	8 hours	aurora
Jan 23/24, 1995	219	741.560-741.945	9 hours	
Feb 10/11, 1995	322	759.606-760.038	10 hours	
Feb 11/12, 1995	89	760.590-760.713	3 hours	cloud
Feb 12/13, 1995	247	761.651-761.970	8 hours	

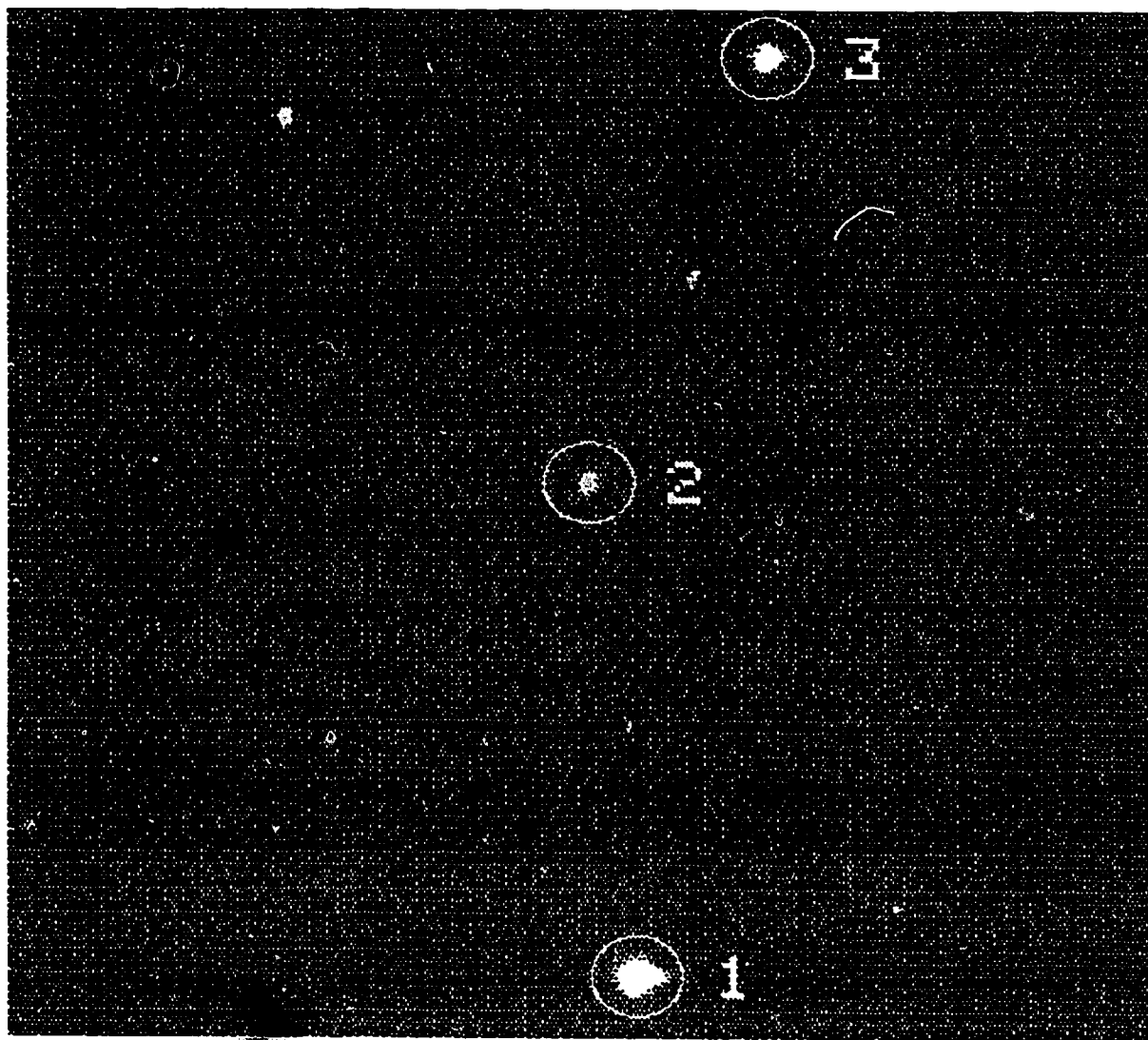


Fig. 10 - A typical program frame for HR 4646 observations. North is down and west is to the right. The program star HR 4646 is labelled as number 1. The comparison stars SAO 7519 and SAO 7521 are labelled as number 2 and number 3, respectively.

noise from simply adding two frames with readout noise of  $16 \text{ ADU pix}^{-1}$  is  $\sim \sqrt{2}(\text{readnoise}) \approx 23 \text{ ADU pix}^{-1}$ . Since the dark counts ( $\sim 20 \text{ ADU pix}^{-1}$ ) were on the order of the readout noise, dark corrections were not made to the frames.

The basic processing steps are seen in Figures 12 through 16. Figure 11 is a ruled-surface map of the raw (unprocessed) program frame. After automatic correction for zero level (subtraction of the mean bias level in each frame), the mean-bias frame is subtracted. The intensity plot along the central row of the bias frame is shown in Figure 12. Ratios of two consecutive bias-frames and two consecutive flat-field frames were created. Estimates of the signal in bias and flat-field frames were obtained by averaging counts in  $50 \times 50 \text{ pix}^2$  regions of the ratio images and using an expression found in McCall, English, and Shelton (1988). For signal  $r$  and noise  $\sigma_r$  of the ratio image, the noise (in  $\text{e}^- \text{ pix}^{-1}$ ) of the frame is given by  $\sigma_{\text{Frame}} = (\sigma_r/r) \frac{S}{\sqrt{2}}$ , where  $S$  is the signal per pixel of the frame. The signal and noise of the ratio image was taken to be the mean and standard deviation. This yielded a value of  $S/N = 94$  for the bias frame and  $S/N = 392$  for the flat-field. The mean signal in regions under star profiles in the unprocessed frame is  $\sim 5.5 \times 10^4 \text{ e}^- \text{ pix}^{-1}$  with a noise of  $\sim 2 \times 10^2 \text{ e}^- \text{ pix}^{-1}$  (photon shot noise). After zero-level correction (base-level of  $7.4 \times 10^3 \text{ e}^- \text{ pix}^{-1}$ ) applying equation (4) yields a  $S/N$  of 203 for the program frame. The individual bias frames are combined. A sample of 5 bias frames from the first observing session have a combined signal of  $7.5 \times 10^2 \text{ e}^- \text{ pix}^{-1}$ . The noise for an individual bias frame is  $\approx 2 \text{ e}^- \text{ pix}^{-1}$ , which yields a  $S/N$  of 210 for the mean-bias frame using equation (6). From equation (8), the mean-bias subtracted program frame is found to have  $S/N = 137$ . The major contributors to this degradation of  $S/N$  are noise due to zero-level correction ( $236 \text{ e}^-$ ) and the readout noise ( $79 \text{ e}^-$ ) appearing in equation (10).

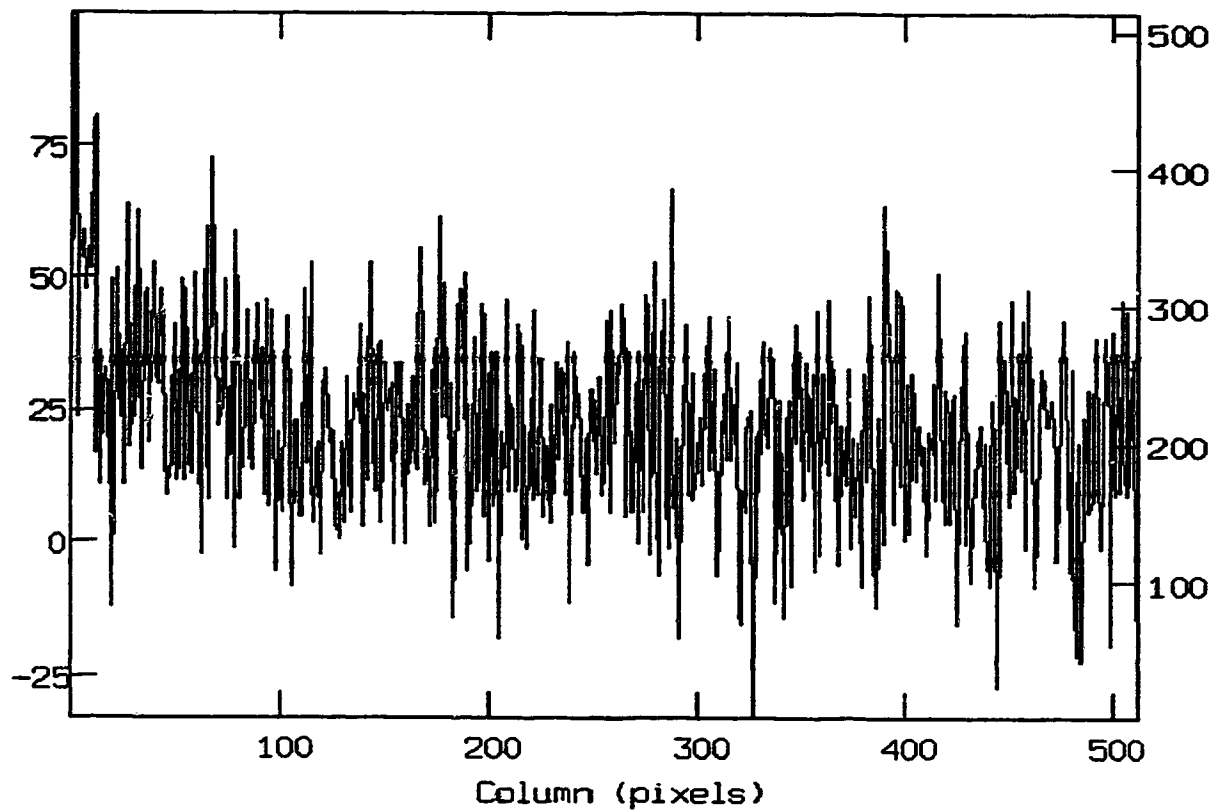


Fig. 12 - The central row of the bias frame. This frame is subtracted as the second step in processing. The left hand scale is counts in ADU while the right hand scale gives an indicator to show the row number.

Finally, the mean-bias subtracted frame is divided by the mean flat-field, shown in Figures 13 and 14, and the result is shown in Figure 15. The mean flat-field has a signal of  $1.4 \times 10^5 \text{ e}^- \text{ pix}^{-1}$  with a noise of  $5.8 \times 10^2 \text{ e}^- \text{ pix}^{-1}$ . Thus, after zero-level correction and bias-subtraction, the flat-field has a value of  $S/N = 243$ . Applying equation (13) yields a  $S/N = 119$  for the flat-fielded program frame. The maximum count levels in the program images have been truncated at  $2000 \text{ ADU pix}^{-1}$  in order for both to be plotted on the same scale.

### 3.2.2 Differential Aperture Photometry

Aperture photometry was carried out on the processed program frames with the IRAF package DAOPHOT. The star SAO 7521 ( $V=6.^m6$ ) was used as a comparison with SAO 7519 ( $V=8.^m9$ ) serving as a check star. In order to automate the differential photometry, the coordinates in the first frame of the three relevant stars were found using DAOFIND. The apertures for differential photometry were typically set to 16 pixels ( $\approx 22 \text{ arcsec}$ ) with a 4 pixel ( $\approx 6 \text{ arcsec}$ ) sky annulus. Afterwards, using IMALIGN, each of the entire set of frames for the night was shifted so the stars were at the same coordinates as in the first frame. This effectively formed a template from the coordinate file of the first frame that PHOT could use to automatically perform aperture photometry on all subsequent frames. The post-processing programs read the differential magnitudes from the DAOPHOT output files and matched them with the Julian Date, which was calculated from the time encoded in the HPC-1 image header file. The output of the first post-processing program is presented in Table 3. Observations of program, check, and comparison stars through the V filter are labelled by  $v_1$ ,  $v_2$ , and  $v_3$ , respectively. Note that these magnitudes have not been transformed from the local to the standard UBV system. Also, note that the individual apparent magnitudes are calculated from an arbitrary base-level of  $26^{\text{th}}$  magnitude set

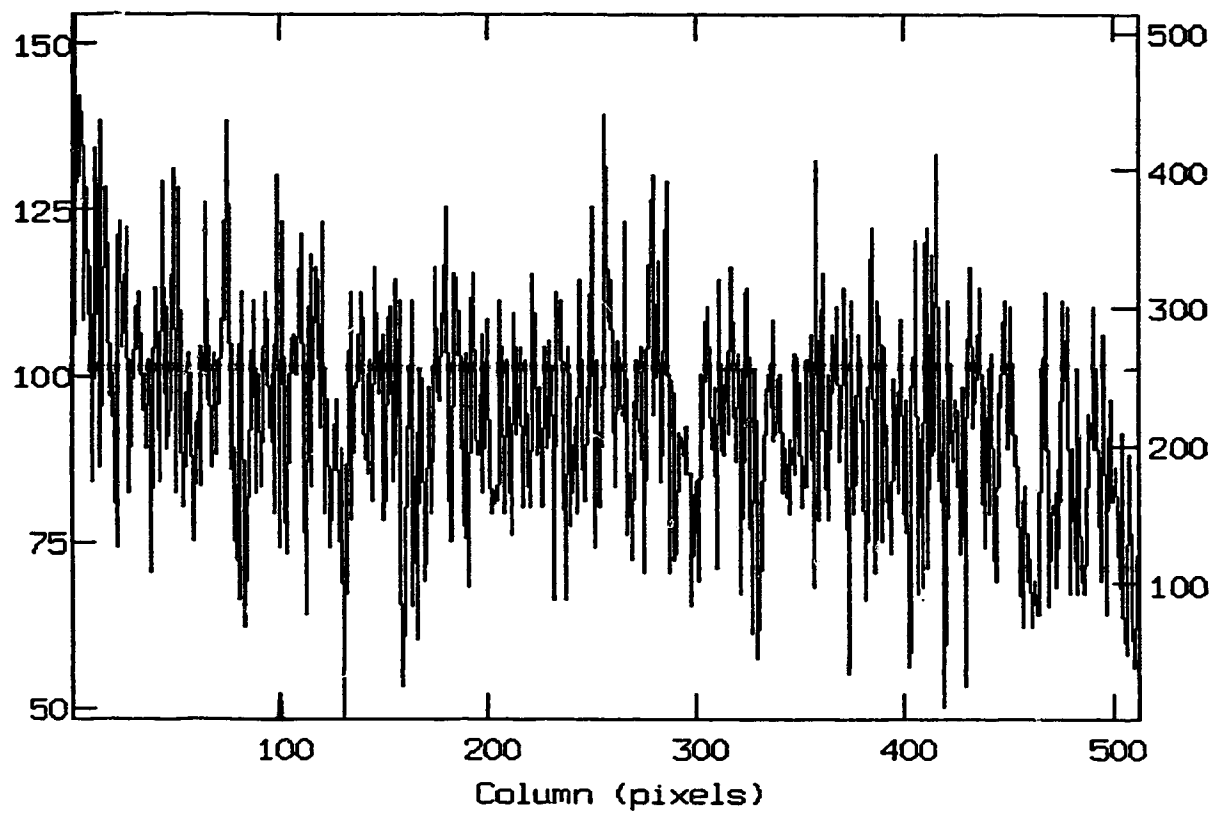


Fig. 13 - Intensity plot along the central row of the program field prior to flat-fielding.

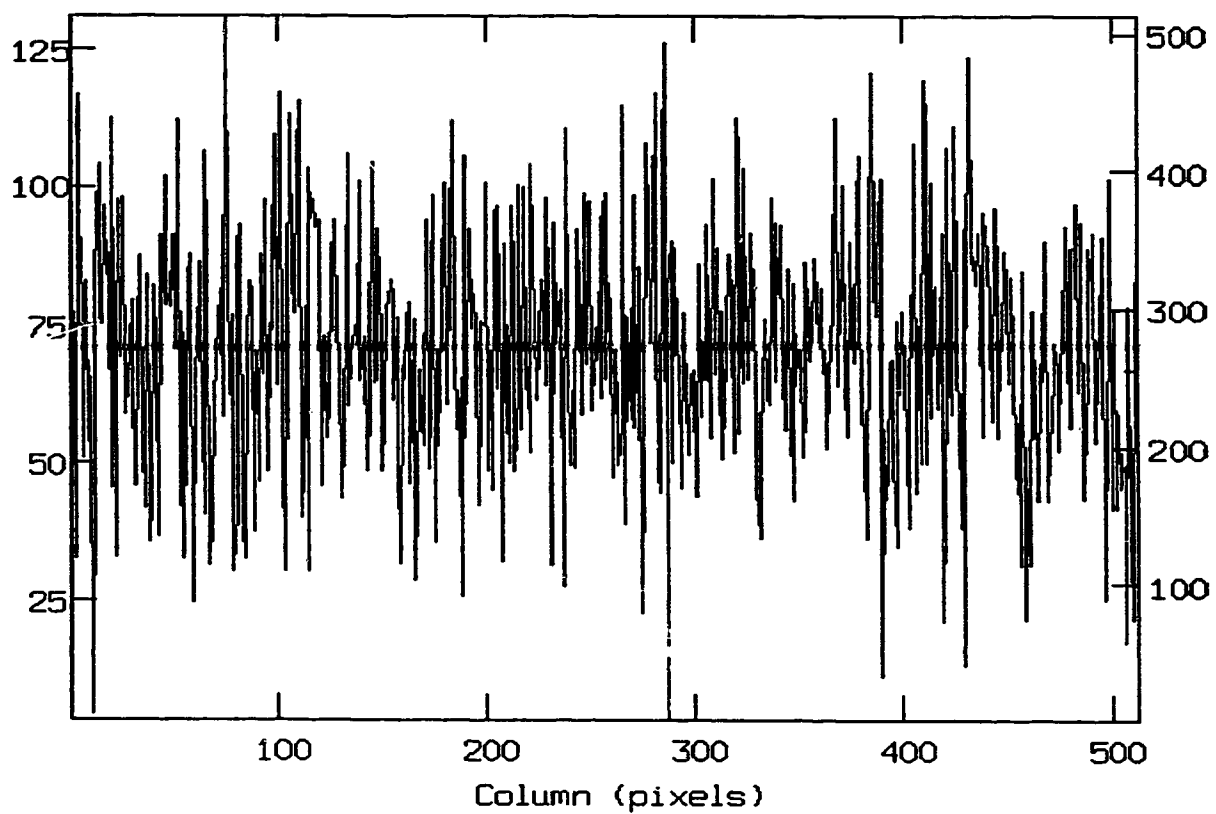


Fig. 14 - Intensity plot along the central row of the program field after flat-fielding.



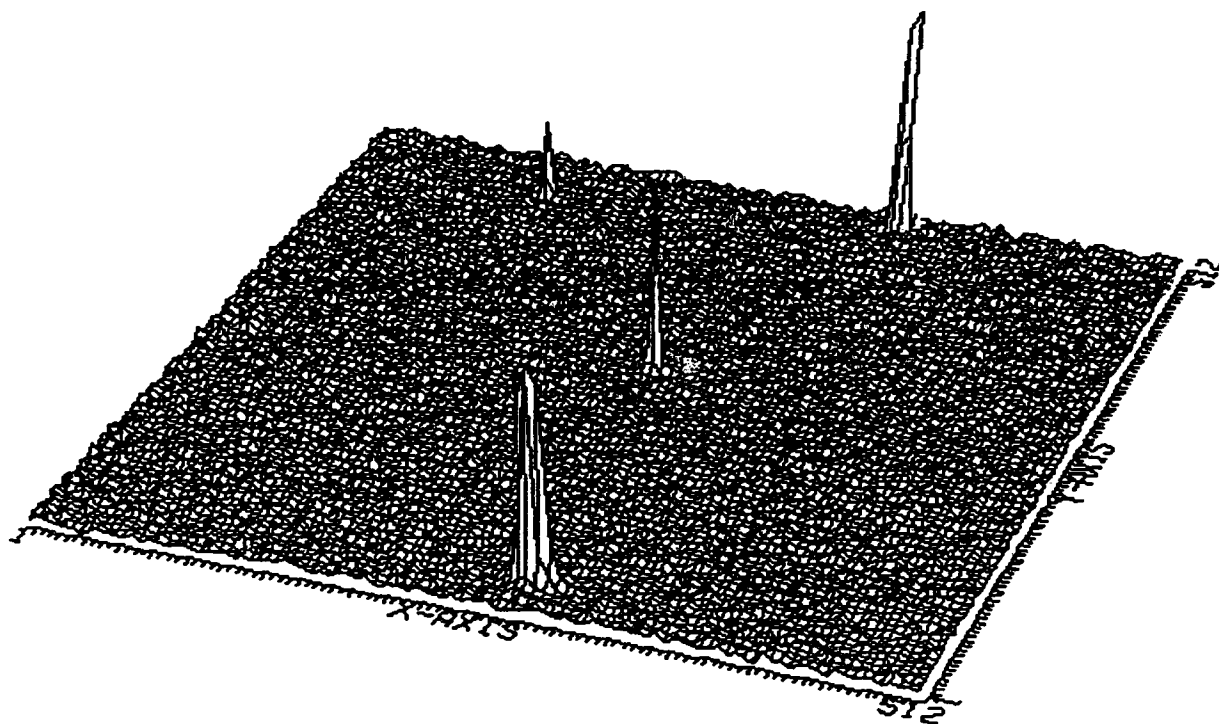


Fig. 15 - The processed frame, after zero level correction, bias frame subtraction and flat-fielding. The background is at a level of  $\sim 75 \pm 25$  ADU  $\text{pix}^{-1}$ .

TABLE 3  
Differential Magnitudes Output from PHOT  
epoch = JD + 2449000.0

JD	V <sub>1</sub>	V <sub>2</sub>	V <sub>3</sub>	V <sub>1-2</sub>	V <sub>1-3</sub>	V <sub>2-3</sub>	JD	V <sub>1</sub>	V <sub>2</sub>	V <sub>3</sub>	V <sub>1-2</sub>	V <sub>1-3</sub>	V <sub>2-3</sub>
738.622	9.688	13.120	11.503	-1.815	-3.432	1.617	738.799	10.213	13.626	12.014	-1.801	-3.413	1.612
738.623	9.752	13.122	11.513	-1.761	-3.370	1.609	738.800	10.159	13.727	11.997	-1.838	-3.568	1.730
738.624	9.662	13.118	11.474	-1.812	-3.456	1.644	738.802	10.191	13.608	11.946	-1.755	-3.417	1.662
738.624	9.672	13.126	11.434	-1.762	-3.454	1.692	738.803	10.215	13.698	12.001	-1.786	-3.483	1.697
738.625	9.716	13.103	11.460	-1.744	-3.387	1.643	738.804	10.165	13.656	12.003	-1.838	-3.491	1.653
738.626	9.714	13.091	11.489	-1.775	-3.377	1.602	738.806	10.190	13.601	12.010	-1.820	-3.411	1.591
738.627	9.709	13.113	11.499	-1.792	-3.406	1.614	738.808	10.210	13.726	12.043	-1.791	-3.566	1.775
738.628	9.707	13.078	11.474	-1.767	-3.371	1.604	738.810	10.221	13.726	12.043	-1.822	-3.505	1.683
738.629	9.707	13.126	11.472	-1.765	-3.419	1.654	738.811	10.246	13.681	12.067	-1.871	-3.435	1.614
738.631	9.705	13.118	11.477	-1.772	-3.413	1.641	738.813	10.237	13.730	12.089	-1.852	-3.493	1.641
738.632	9.699	13.119	11.496	-1.797	-3.420	1.623	738.814	10.298	13.744	12.170	-1.872	-3.446	1.574
738.635	9.687	13.121	11.495	-1.808	-3.434	1.626	738.815	10.371	13.738	12.208	-1.837	-3.367	1.530
738.636	9.692	13.070	11.465	-1.773	-3.378	1.605	738.817	10.421	13.858	12.210	-1.789	-3.437	1.648
738.638	9.688	13.117	11.526	-1.838	-3.429	1.591	738.818	10.340	13.854	12.177	-1.837	-3.514	1.677
738.639	9.691	13.113	11.480	-1.789	-3.422	1.633	738.820	10.335	13.883	12.158	-1.823	-3.488	1.725
738.640	9.687	13.109	11.466	-1.779	-3.422	1.643	738.822	10.334	13.782	12.143	-1.809	-3.448	1.639
738.642	9.689	13.113	11.463	-1.774	-3.424	1.650	738.824	10.250	13.788	12.057	-1.807	-3.538	1.731
738.643	9.717	13.144	11.457	-1.740	-3.427	1.687	738.825	10.262	13.664	12.042	-1.780	-3.402	1.622
738.647	9.723	13.127	11.468	-1.745	-3.414	1.669	738.827	10.290	13.749	12.134	-1.844	-3.459	1.615
738.649	9.689	13.134	11.494	-1.805	-3.465	1.660	738.828	10.336	13.793	12.146	-1.810	-3.457	1.647
738.650	9.705	13.120	11.476	-1.771	-3.415	1.644	738.829	10.280	13.811	12.134	-1.854	-3.531	1.677
738.652	9.692	13.129	11.493	-1.801	-3.437	1.636	738.831	10.280	13.713	12.097	-1.817	-3.433	1.616
738.653	9.730	13.146	11.485	-1.755	-3.416	1.661	738.832	10.256	13.699	12.069	-1.813	-3.443	1.630
738.654	9.705	13.142	11.474	-1.769	-3.437	1.668	738.833	10.280	13.886	12.120	-1.840	-3.606	1.766
738.656	9.683	13.112	11.488	-1.805	-3.429	1.624	738.836	10.279	13.793	12.106	-1.827	-3.514	1.687
738.657	9.715	13.132	11.465	-1.750	-3.417	1.657	738.838	10.328	13.877	12.110	-1.791	-3.458	1.758
738.658	9.690	13.109	11.469	-1.779	-3.419	1.640	738.839	10.346	13.802	12.193	-1.847	-3.456	1.698
738.661	9.742	13.090	11.489	-1.747	-3.348	1.601	738.840	10.326	13.967	12.130	-1.804	-3.641	1.837
738.664	9.826	13.125	11.462	-1.636	-3.299	1.663	738.842	10.282	13.795	12.065	-1.783	-3.513	1.730
738.665	9.688	13.158	11.452	-1.764	-3.470	1.706	738.843	10.285	13.800	12.100	-1.815	-3.515	1.700
738.668	9.680	13.053	11.471	-1.791	-3.373	1.582	738.845	10.263	13.645	12.041	-1.778	-3.382	1.604
738.670	9.790	13.135	11.485	-1.695	-3.345	1.650	738.846	10.189	13.825	12.075	-1.886	-3.638	1.750
738.671	9.702	13.104	11.462	-1.760	-3.402	1.642	738.847	10.210	13.768	12.027	-1.817	-3.558	1.741
738.672	9.694	13.087	11.465	-1.771	-3.393	1.622	738.850	10.196	13.728	12.011	-1.815	-3.532	1.717
738.674	9.667	13.066	11.487	-1.820	-3.399	1.579	738.852	10.215	13.599	12.013	-1.798	-3.384	1.586
738.677	9.735	13.101	11.441	-1.686	-3.346	1.660	738.853	10.206	13.749	12.003	-1.797	-3.543	1.746
738.680	10.198	13.656	11.998	-1.860	-3.452	1.632	738.854	10.192	13.747	12.086	-1.754	-3.252	1.761
738.681	10.204	13.683	12.002	-1.798	-3.476	1.681	738.856	10.192	13.697	12.022	-1.793	-3.505	1.670
738.682	10.234	13.627	11.986	-1.752	-3.393	1.641	738.857	10.215	13.711	12.068	-1.793	-3.456	1.703
738.683	10.182	13.608	12.004	-1.822	-3.426	1.604	738.858	10.182	13.643	11.968	-1.786	-3.461	1.675
738.685	10.203	13.621	12.015	-1.812	-3.418	1.606	738.860	10.192	13.732	12.005	-1.813	-3.540	1.727
738.686	10.209	13.616	12.017	-1.788	-3.407	1.619	738.861	10.203	13.672	12.010	-1.807	-3.469	1.662
738.688	10.192	13.603	12.018	-1.826	-3.411	1.585	738.864	10.180	13.601	11.996	-1.816	-3.421	1.605
738.689	10.191	13.643	11.976	-1.785	-3.452	1.667	738.865	10.217	13.785	12.014	-1.797	-3.568	1.771
738.692	10.222	13.637	11.982	-1.760	-3.415	1.655	738.867	10.184	13.634	11.998	-1.814	-3.450	1.636
738.693	10.231	13.693	11.982	-1.751	-3.462	1.711	738.868	10.177	13.672	12.005	-1.828	-3.495	1.667
738.695	10.209	13.696	12.014	-1.805	-3.487	1.682	738.870	10.193	13.610	11.985	-1.792	-3.417	1.625
738.696	10.210	13.631	12.033	-1.843	-3.421	1.578	738.871	10.212	13.373	12.010	-1.798	-3.361	1.563
738.697	10.214	13.684	12.067	-1.822	-3.445	1.623	738.872	10.203	13.663	12.024	-1.821	-3.460	1.639
738.699	10.292	13.730	12.088	-1.796	-3.438	1.642	738.874	10.230	13.648	12.003	-1.773	-3.418	1.645
738.700	10.287	13.699	12.041	-1.754	-3.412	1.658	738.875	10.214	13.695	12.030	-1.816	-3.481	1.665
738.702	10.356	13.824	12.126	-1.770	-3.468	1.698	738.878	10.207	13.730	11.993	-1.786	-3.523	1.737
738.703	10.308	13.812	12.109	-1.801	-3.504	1.738	738.879	10.179	13.729	12.048	-1.869	-3.550	1.681
738.706	10.360	13.751	12.139	-1.778	-3.401	1.623	738.881	10.188	13.645	12.047	-1.859	-3.457	1.598
738.707	10.265	13.802	12.175	-1.802	-3.475	1.674	738.882	10.193	13.616	12.009	-1.816	-3.523	1.707
738.708	10.347	13.711	12.117	-1.770	-3.363	1.593	738.882	10.193	13.716	12.009	-1.816	-3.523	1.707
738.710	10.283	13.802	12.095	-1.812	-3.519	1.707	738.883	10.178	13.599	11.994	-1.846	-3.421	1.575
738.711	10.243	13.676	12.013	-1.770	-3.433	1.663	738.885	10.185	13.537	11.994	-1.809	-3.352	1.543
738.713	10.202	13.712	11.986	-1.784	-3.510	1.726	738.888	10.201	13.669	12.002	-1.801	-3.468	1.667
738.715	10.345	13.765	12.176	-1.831	-3.420	1.589	738.905	10.169	13.666	11.961	-1.792	-3.497	1.705
738.717	10.240	13.644	12.027	-1.787	-3.404	1.617	738.906	10.178	13.698	11.973	-1.795	-3.520	1.725
738.718	10.202	13.663	12.017	-1.815	-3.461	1.646	738.907	10.162	13.751	11.980	-1.824	-3.589	1.765
738.721	10.218	13.615	11.983	-1.765	-3.397	1.632	738.908	10.160	13.618	11.980	-1.820	-3.458	1.638
738.724	10.204	13.662	12.009	-1.805	-3.458	1.653	738.910	10.152	13.636	11.981	-1.829	-3.484	1.655
738.725	10.181	13.585	11.992	-1.811	-3.404	1.593	738.911	10.160	13.616	11.991	-1.831	-3.456	1.625
738.726	10.195	13.640	12.026	-1.831	-3.445	1.614	738.913	10.167	13.628	11.949	-1.782	-3.461	1.679
738.728	10.214	13.627	11.990	-1.756	-3.393	1.637	738.914	10.170	13.565	12.018	-1.848	-3.395	1.547
738.729	10.214	13.565	12.022	-1.808	-3.371	1.543	738.916	10.180	13.645	11.970	-1.790	-3.463	1.675
738.731	10.208	13.650	11.970	-1.762	-3.412	1.680	738.918	10.172	13.705	11.989	-1.817	-3.533	1.716
738.732	10.229	13.611	11.984	-1.755	-3.382	1.627	738.920	10.190	13.777	12.010	-1.820	-3.587	1.767
738.734	10.200	13.624	11.988	-1.788	-3.424	1.636	738.921	10.217	13.777	12.028	-1.811	-3.560	1.749
738.735	10.189	13.626	11.979	-1.790	-3.437	1.647	738.922	10.218	13.733	12.029	-1.811	-3.515	1.704
738.736	10.197	13.649	12.003	-1.806	-3.452	1.646	738.924	10.226	13.696	12.029	-1.803	-3.470	1.667
738.754	10.170	13.661	11.970	-1.800	-3.494	1.694	738.925	10.241	13.798	12.023	-1.782	-3.557	1.775
738.757	10.182	13.604	11.987	-1.805	-3.422	1.671	738.928	10.223	13.800	12.018	-1.795	-3.577	1.782
738.758	10.159	13.637	12.012	-1.853	-3.478	1.625	738.929	10.221	13.712	12.044	-1.823	-3.491	1.668
738.760	10.204	13.615	11.999	-1.795	-3.411	1.616	738.932	10.223	13.745	12.017	-1.794	-3.522	1.628
738.761	10.218	13.636	12.003	-1.785	-3.418	1.633	738.933	10.215	13.745	11.997	-1.782	-3.530	1.748
738.763	10.198	13.644	11.968	-1.770	-3.446	1.67							

TABLE 3 (continued)  
epoch = JD + 2449000.0

JD	V <sub>1</sub>	V <sub>2</sub>	V <sub>3</sub>	V <sub>1-2</sub>	V <sub>1-3</sub>	V <sub>2-3</sub>	JD	V <sub>1</sub>	V <sub>2</sub>	V <sub>3</sub>	V <sub>1-2</sub>	V <sub>1-3</sub>	V <sub>2-3</sub>
739.649	10.047	13.418	11.820	-1.773	-3.371	1.598	739.810	10.037	13.524	11.801	-1.764	-3.487	1.723
739.650	10.063	13.491	11.832	-1.769	-3.428	1.659	739.811	10.040	13.509	11.808	-1.768	-3.469	1.701
739.652	10.055	13.456	11.847	-1.792	-3.401	1.609	739.813	10.038	13.534	11.827	-1.789	-3.496	1.707
739.653	10.042	13.455	11.829	-1.787	-3.413	1.626	739.814	10.036	13.599	11.808	-1.772	-3.563	1.791
739.654	10.049	13.496	11.834	-1.785	-3.447	1.662	739.815	10.031	13.510	11.826	-1.795	-3.479	1.684
739.656	10.079	13.432	11.841	-1.762	-3.353	1.591	739.817	10.037	13.540	11.797	-1.760	-3.503	1.740
739.657	10.032	13.440	11.851	-1.819	-3.408	1.589	739.819	10.030	13.408	11.802	-1.772	-3.378	1.606
739.659	10.034	13.438	11.840	-1.806	-3.404	1.598	739.820	10.047	13.486	11.798	-1.751	-3.439	1.688
739.660	10.047	13.466	11.819	-1.772	-3.419	1.647	739.821	10.039	13.529	11.789	-1.750	-3.490	1.740
739.661	10.038	13.459	11.828	-1.770	-3.401	1.631	739.822	10.043	13.557	11.793	-1.750	-3.514	1.764
739.663	10.051	13.443	11.815	-1.764	-3.392	1.628	739.824	10.037	13.516	11.822	-1.785	-3.479	1.694
739.664	10.057	13.557	11.837	-1.780	-3.500	1.720	739.825	10.043	13.510	11.777	-1.734	-3.467	1.733
739.665	10.056	13.518	11.877	-1.821	-3.462	1.641	739.826	10.039	13.419	11.789	-1.750	-3.380	1.630
739.667	10.058	13.468	11.839	-1.781	-3.410	1.729	739.829	10.035	13.529	11.793	-1.758	-3.494	1.736
739.668	10.065	13.516	11.814	-1.749	-3.451	1.702	739.831	10.042	13.530	11.781	-1.739	-3.488	1.749
739.670	10.074	13.511	11.830	-1.756	-3.437	1.681	739.832	10.052	13.431	11.795	-1.743	-3.379	1.636
739.671	10.069	13.486	11.821	-1.752	-3.417	1.665	739.833	10.033	13.555	11.785	-1.752	-3.522	1.770
739.672	10.054	13.533	11.849	-1.795	-3.479	1.684	739.835	10.021	13.474	11.790	-1.769	-3.453	1.684
739.674	10.064	13.400	11.833	-1.763	-3.336	1.567	739.836	10.038	13.501	11.793	-1.755	-3.463	1.708
739.675	10.030	13.403	11.833	-1.803	-3.373	1.570	739.838	10.036	13.518	11.789	-1.753	-3.479	1.726
739.677	10.027	13.429	11.839	-1.812	-3.402	1.590	739.839	10.035	13.585	11.788	-1.753	-3.550	1.797
739.678	10.053	13.536	11.877	-1.824	-3.483	1.659	739.840	10.040	13.582	11.813	-1.773	-3.542	1.769
739.679	10.053	13.413	11.827	-1.774	-3.360	1.586	739.842	10.034	13.559	11.787	-1.753	-3.525	1.772
739.681	10.029	13.492	11.823	-1.794	-3.464	1.670	739.843	10.049	13.512	11.781	-1.732	-3.463	1.731
739.682	10.059	13.516	11.814	-1.756	-3.438	1.682	739.845	10.036	13.568	11.777	-1.741	-3.530	1.789
739.683	10.059	13.457	11.819	-1.760	-3.457	1.697	739.846	10.037	13.496	11.778	-1.745	-3.459	1.718
739.685	10.056	13.490	11.845	-1.789	-3.434	1.645	739.847	10.041	13.525	11.804	-1.763	-3.484	1.721
739.686	10.047	13.479	11.818	-1.771	-3.432	1.661	739.849	10.038	13.565	11.820	-1.782	-3.527	1.745
739.688	10.050	13.461	11.811	-1.761	-3.411	1.650	739.850	10.019	13.611	11.790	-1.771	-3.592	1.821
739.689	10.044	13.466	11.847	-1.803	-3.422	1.619	739.852	10.022	13.439	11.802	-1.780	-3.417	1.637
739.690	10.051	13.453	11.859	-1.808	-3.402	1.594	739.853	10.030	13.558	11.768	-1.738	-3.528	1.790
739.692	10.060	13.453	11.821	-1.761	-3.393	1.632	739.856	10.035	13.523	11.786	-1.751	-3.488	1.737
739.693	10.056	13.507	11.810	-1.754	-3.451	1.697	739.857	10.042	13.519	11.794	-1.752	-3.477	1.725
739.695	10.054	13.455	11.855	-1.801	-3.401	1.600	739.858	10.059	13.522	11.768	-1.709	-3.463	1.754
739.696	10.081	13.493	11.843	-1.762	-3.412	1.650	739.860	10.022	13.496	11.795	-1.773	-3.474	1.701
739.697	10.058	13.428	11.855	-1.797	-3.370	1.573	739.861	10.017	13.486	11.790	-1.773	-3.469	1.696
739.699	10.069	13.438	11.844	-1.752	-3.364	1.589	739.863	10.040	13.490	11.802	-1.762	-3.450	1.688
739.702	10.081	13.483	11.833	-1.752	-3.408	1.656	739.864	10.043	13.545	11.784	-1.741	-3.502	1.761
739.703	10.091	13.445	11.841	-1.750	-3.354	1.604	739.867	10.025	13.470	11.808	-1.783	-3.445	1.662
739.704	10.051	13.430	11.837	-1.786	-3.379	1.593	739.867	10.021	13.555	11.803	-1.782	-3.534	1.752
739.706	10.060	13.479	11.837	-1.777	-3.419	1.642	739.868	10.047	13.460	11.763	-1.716	-3.413	1.697
739.707	10.060	13.535	11.860	-1.793	-3.468	1.675	739.869	10.044	13.508	11.786	-1.742	-3.464	1.722
739.709	10.030	13.522	11.818	-1.768	-3.492	1.704	739.871	10.029	13.572	11.802	-1.773	-3.543	1.770
739.710	10.040	13.488	11.832	-1.792	-3.448	1.656	739.873	10.032	13.531	11.785	-1.753	-3.499	1.746
739.711	10.044	13.452	11.843	-1.799	-3.408	1.609	739.874	10.035	13.540	11.772	-1.737	-3.505	1.768
739.713	10.054	13.502	11.822	-1.768	-3.448	1.680	739.876	10.039	13.586	11.788	-1.749	-3.547	1.798
739.714	10.058	13.438	11.846	-1.788	-3.380	1.592	739.877	10.058	13.566	11.796	-1.738	-3.508	1.770
739.715	10.057	13.550	11.828	-1.771	-3.493	1.722	739.878	10.075	13.577	11.824	-1.749	-3.502	1.753
739.717	10.044	13.500	11.848	-1.804	-3.456	1.652	739.879	10.031	13.490	11.781	-1.750	-3.459	1.709
739.719	10.062	13.452	11.837	-1.775	-3.390	1.615	739.881	10.035	13.587	11.819	-1.784	-3.552	1.768
739.720	10.041	13.453	11.842	-1.801	-3.412	1.611	739.882	10.040	13.549	11.787	-1.747	-3.509	1.762
739.721	10.046	13.558	11.820	-1.774	-3.512	1.738	739.883	10.031	13.519	11.807	-1.776	-3.488	1.712
739.723	10.061	13.485	11.839	-1.778	-3.424	1.646	739.886	9.989	13.512	11.761	-1.772	-3.523	1.751
739.724	9.946	13.556	11.731	-1.785	-3.410	1.625	739.888	10.043	13.496	11.805	-1.762	-3.453	1.691
739.725	10.071	13.507	11.861	-1.790	-3.436	1.646	739.889	10.031	13.580	11.804	-1.773	-3.549	1.776
739.727	10.047	13.510	11.874	-1.777	-3.463	1.686	739.890	10.046	13.566	11.812	-1.766	-3.520	1.754
739.730	10.023	13.505	11.809	-1.786	-3.482	1.696	739.893	10.028	13.543	11.808	-1.753	-3.518	1.740
739.731	10.019	13.533	11.795	-1.776	-3.514	1.738	739.895	10.036	13.503	11.791	-1.755	-3.467	1.712
739.733	10.007	13.443	11.806	-1.799	-3.436	1.637	739.895	10.020	13.566	11.803	-1.764	-3.546	1.763
739.734	10.026	13.568	11.805	-1.779	-3.542	1.763	739.896	10.031	13.551	11.783	-1.752	-3.520	1.768
739.735	10.042	13.525	11.820	-1.778	-3.483	1.705	739.898	10.046	13.547	11.818	-1.772	-3.501	1.729
739.736	10.036	13.508	11.819	-1.763	-3.472	1.689	739.899	10.035	13.580	11.798	-1.765	-3.545	1.782
739.738	10.040	13.450	11.801	-1.761	-3.410	1.649	739.900	10.023	13.559	11.787	-1.764	-3.536	1.772
739.739	10.053	13.504	11.815	-1.762	-3.451	1.689	739.902	10.028	13.533	11.775	-1.747	-3.505	1.758
739.741	10.036	13.504	11.807	-1.771	-3.468	1.697	739.903	10.023	13.581	11.784	-1.761	-3.558	1.797
739.743	10.040	13.455	11.809	-1.769	-3.415	1.646	739.904	10.043	13.536	11.788	-1.745	-3.493	1.748
739.745	10.060	13.533	11.781	-1.721	-3.473	1.752	739.906	10.045	13.595	11.805	-1.761	-3.550	1.789
739.746	10.045	13.493	11.808	-1.765	-3.458	1.694	739.907	10.044	13.566	11.803	-1.760	-3.523	1.763
739.747	10.042	13.501	11.808	-1.766	-3.459	1.694	739.909	10.027	13.569	11.794	-1.767	-3.542	1.775
739.749	10.036	13.502	11.819	-1.783	-3.466	1.683	739.932	10.045	13.610	11.787	-1.742	-3.565	1.823
739.750	10.036	13.488	11.793	-1.757	-3.452	1.635	739.934	10.055	13.585	11.808	-1.753	-3.530	1.777
739.752	10.051	13.593	11.806	-1.755	-3.542	1.787	739.935	10.050	13.660	11.818	-1.768	-3.610	1.842
739.753	10.060	13.436	11.834	-1.774	-3.376	1.602	739.936	10.029	13.632	11.830	-1.801	-3.603	1.802
739.754	10.046	13.556	11.828	-1.782	-3.510	1.728	739.938	10.039	13.510	11.837	-1.798	-3.471	1.673
739.772	10.052	13.537	11.822	-1.770	-3.485	1.715	739.939	10.034	13.554	11.832	-1.798	-3.520	1.722
739.774	10.042	13.543	11.806	-1.764	-3.501	1.737	739.941	10.040	13.503	11.815	-1.775	-3.463	1.688
739.775	10.045	13.507	11.799	-1.754	-3.462	1.708	739.942	10.046	13.642	11.822	-1.776	-3.596	1.820
739.776	10.043	13.478	11.810	-1.767	-3.435	1.668	739.943	10.099	13.515	11.869	-1.770	-3.416	1.646
739.778	10.058	13.431	11.786										

TABLE 3 (continued)  
epoch = JD + 2449000.0

JD	v <sub>1</sub>	v <sub>2</sub>	v <sub>3</sub>	v <sub>1-3</sub>	v <sub>1-2</sub>	v <sub>2-3</sub>	JD	v <sub>1</sub>	v <sub>2</sub>	v <sub>3</sub>	v <sub>1-3</sub>	v <sub>1-2</sub>	v <sub>2-3</sub>
739.977	10.028	13.549	11.795	-1.767	-3.521	1.754	740.639	10.049	13.467	11.819	-1.770	-3.418	1.648
739.978	10.014	13.538	11.780	-1.766	-3.534	1.768	740.640	10.071	13.514	11.820	-1.749	-3.443	1.594
739.980	10.015	13.502	11.780	-1.765	-3.487	1.722	740.642	10.055	13.436	11.804	-1.749	-3.381	1.632
739.981	10.018	13.456	11.773	-1.765	-3.438	1.683	740.643	10.082	13.485	11.843	-1.761	-3.403	1.642
739.982	10.038	13.493	11.800	-1.762	-3.455	1.693	740.645	10.071	13.510	11.802	-1.731	-3.439	1.708
739.984	10.009	13.557	11.802	-1.793	-3.548	1.755	740.648	10.061	13.476	11.808	-1.747	-3.415	1.668
739.985	10.029	13.485	11.782	-1.753	-3.456	1.703	740.650	10.033	13.441	11.841	-1.808	-3.408	1.600
739.989	10.016	13.611	11.774	-1.758	-3.595	1.837	740.652	10.067	13.487	11.837	-1.770	-3.420	1.650
739.991	10.038	13.589	11.797	-1.759	-3.550	1.791	740.653	10.024	13.485	11.834	-1.810	-3.461	1.651
739.992	10.022	13.547	11.768	-1.746	-3.523	1.779	740.654	10.031	13.433	11.814	-1.783	-3.402	1.619
739.994	10.027	13.493	11.795	-1.768	-3.466	1.698	740.656	10.041	13.450	11.837	-1.796	-3.409	1.613
739.995	10.028	13.592	11.793	-1.765	-3.564	1.799	740.659	10.061	13.496	11.842	-1.781	-3.435	1.654
739.996	10.020	13.536	11.780	-1.760	-3.516	1.756	740.660	10.074	13.439	11.825	-1.751	-3.365	1.614
739.997	10.051	13.578	11.781	-1.730	-3.527	1.797	740.661	10.061	13.489	11.813	-1.752	-3.428	1.676
739.999	10.029	13.583	11.829	-1.800	-3.554	1.754	740.663	10.082	13.556	11.866	-1.784	-3.474	1.690
740.000	10.009	13.491	11.767	-1.758	-3.489	1.724	740.664	10.089	13.528	11.813	-1.724	-3.439	1.715
740.002	10.016	13.563	11.775	-1.759	-3.547	1.788	740.665	10.025	13.497	11.854	-1.829	-3.472	1.643
740.003	10.016	13.496	11.811	-1.795	-3.480	1.685	740.667	10.063	13.477	11.833	-1.770	-3.414	1.644
740.004	10.053	13.542	11.762	-1.709	-3.489	1.780	740.668	10.052	13.475	11.803	-1.751	-3.423	1.672
740.006	10.008	13.558	11.814	-1.806	-3.550	1.744	740.670	10.040	13.503	11.817	-1.777	-3.463	1.686
740.007	10.013	13.537	11.802	-1.789	-3.524	1.735	740.671	10.058	13.489	11.800	-1.742	-3.431	1.689
740.008	10.037	13.577	11.785	-1.748	-3.540	1.792	740.672	10.039	13.464	11.801	-1.769	-3.432	1.663
740.010	10.047	13.476	11.792	-1.745	-3.429	1.684	740.675	10.042	13.456	11.798	-1.756	-3.414	1.658
740.011	10.029	13.538	11.772	-1.743	-3.509	1.766	740.677	10.044	13.481	11.795	-1.751	-3.437	1.686
740.013	10.014	13.594	11.771	-1.757	-3.580	1.873	740.678	10.057	13.462	11.810	-1.753	-3.405	1.652
740.014	10.007	13.552	11.808	-1.801	-3.552	1.751	740.679	10.067	13.480	11.814	-1.747	-3.413	1.666
740.017	10.022	13.576	11.807	-1.805	-3.544	1.765	740.681	10.025	13.470	11.812	-1.787	-3.445	1.658
740.018	10.005	13.550	11.758	-1.753	-3.514	1.792	740.682	10.041	13.499	11.827	-1.747	-3.419	1.672
740.020	10.051	13.609	11.759	-1.728	-3.558	1.830	740.683	10.059	13.510	11.819	-1.760	-3.419	1.681
740.021	10.026	13.601	11.783	-1.757	-3.575	1.818	740.685	10.067	13.506	11.825	-1.758	-3.439	1.681
740.022	10.022	13.592	11.790	-1.768	-3.570	1.802	740.686	10.059	13.470	11.820	-1.761	-3.411	1.650
740.024	10.032	13.509	11.792	-1.759	-3.476	1.717	740.688	10.051	13.454	11.796	-1.745	-3.403	1.658
740.025	10.039	13.552	11.803	-1.764	-3.513	1.749	740.689	10.066	13.467	11.813	-1.748	-3.402	1.654
740.027	10.014	13.548	11.775	-1.761	-3.534	1.773	740.690	10.063	13.512	11.827	-1.758	-3.443	1.685
740.028	10.036	13.545	11.795	-1.759	-3.509	1.750	740.692	10.057	13.483	11.852	-1.758	-3.426	1.631
740.029	10.054	13.551	11.828	-1.774	-3.497	1.723	740.693	10.054	13.473	11.829	-1.775	-3.419	1.644
740.031	10.104	13.632	11.861	-1.757	-3.528	1.771	740.695	10.085	13.499	11.811	-1.726	-3.414	1.688
740.032	10.170	13.747	11.954	-1.784	-3.607	1.823	740.696	10.078	13.474	11.826	-1.748	-3.396	1.648
740.034	10.083	13.578	11.863	-1.780	-3.495	1.715	740.698	10.063	13.487	11.851	-1.788	-3.424	1.636
740.035	10.018	13.579	11.789	-1.771	-3.561	1.790	740.699	10.046	13.474	11.835	-1.785	-3.428	1.639
740.036	10.023	13.508	11.789	-1.766	-3.485	1.719	740.700	10.072	13.471	11.822	-1.750	-3.399	1.649
740.038	10.025	13.501	11.816	-1.791	-3.476	1.685	740.722	10.067	13.442	11.857	-1.790	-3.375	1.585
740.039	10.027	13.549	11.795	-1.768	-3.522	1.754	740.722	10.055	13.521	11.846	-1.791	-3.466	1.675
740.041	10.026	13.530	11.799	-1.773	-3.504	1.731	740.724	10.069	13.514	11.845	-1.776	-3.445	1.669
740.042	10.028	13.499	11.793	-1.768	-3.474	1.706	740.725	10.077	13.494	11.862	-1.785	-3.417	1.632
740.045	10.036	13.506	11.794	-1.768	-3.470	1.712	740.727	10.082	13.454	11.880	-1.798	-3.463	1.665
740.046	10.017	13.528	11.813	-1.796	-3.511	1.715	740.728	10.087	13.486	11.887	-1.806	-3.405	1.599
740.047	10.025	13.495	11.805	-1.780	-3.470	1.690	740.729	10.094	13.504	11.859	-1.765	-3.410	1.604
740.049	10.005	13.530	11.819	-1.814	-3.525	1.711	740.731	10.142	13.596	11.923	-1.781	-3.454	1.673
740.050	10.025	13.471	11.774	-1.749	-3.446	1.697	740.732	10.152	13.596	11.953	-1.801	-3.444	1.643
740.052	10.017	13.465	11.762	-1.745	-3.448	1.703	740.733	10.202	13.599	11.964	-1.762	-3.397	1.635
740.053	10.035	13.440	11.798	-1.763	-3.405	1.642	740.735	10.257	13.639	12.022	-1.763	-3.382	1.617
740.055	10.044	13.495	11.786	-1.742	-3.451	1.709	740.736	10.230	13.689	12.014	-1.764	-3.439	1.675
740.056	10.041	13.548	11.764	-1.723	-3.507	1.784	740.738	10.241	13.622	12.018	-1.777	-3.381	1.604
740.057	10.018	13.508	11.790	-1.772	-3.490	1.718	740.739	10.244	13.654	12.035	-1.791	-3.410	1.619
740.059	10.021	13.565	11.787	-1.766	-3.544	1.778	740.740	10.269	13.653	12.028	-1.759	-3.384	1.625
740.060	10.014	13.445	11.778	-1.764	-3.435	1.671	740.742	10.278	13.717	12.063	-1.785	-3.439	1.654
740.061	10.019	13.453	11.793	-1.801	-3.499	1.693	740.743	10.268	13.633	12.061	-1.793	-3.365	1.572
740.060	10.014	13.449	11.778	-1.764	-3.435	1.671	740.745	10.281	13.706	12.039	-1.815	-3.483	1.665
740.061	10.019	13.513	11.820	-1.801	-3.494	1.693	740.746	10.269	13.690	12.025	-1.756	-3.421	1.665
740.063	9.997	13.437	11.788	-1.791	-3.440	1.649	740.749	10.152	13.543	11.953	-1.801	-3.391	1.590
740.064	10.018	13.522	11.796	-1.778	-3.504	1.726	740.750	10.154	13.576	11.903	-1.749	-3.422	1.673
740.066	10.017	13.517	11.781	-1.744	-3.488	1.743	740.752	10.113	13.541	11.874	-1.761	-3.428	1.667
740.067	10.022	13.517	11.798	-1.756	-3.495	1.739	740.753	10.088	13.501	11.865	-1.777	-3.413	1.636
740.068	10.037	13.544	11.800	-1.763	-3.507	1.744	740.754	10.087	13.483	11.848	-1.787	-3.396	1.633
740.070	10.026	13.530	11.801	-1.775	-3.504	1.729	740.756	10.067	13.468	11.831	-1.764	-3.401	1.617
740.073	10.089	13.476	11.877	-1.788	-3.387	1.599	740.757	10.028	13.490	11.802	-1.774	-3.462	1.688
740.075	10.128	13.507	11.861	-1.733	-3.379	1.646	740.759	10.050	13.476	11.814	-1.764	-3.426	1.662
740.076	10.110	13.538	11.874	-1.764	-3.428	1.664	740.760	10.043	13.558	11.826	-1.783	-3.515	1.732
740.077	10.095	13.515	11.869	-1.774	-3.420	1.646	740.761	10.045	13.476	11.836	-1.791	-3.431	1.640
740.079	10.081	13.490	11.855	-1.774	-3.409	1.635	740.763	10.055	13.441	11.823	-1.768	-3.386	1.618
740.080	10.082	13.538	11.831	-1.749	-3.456	1.707	740.764	10.061	13.477	11.843	-1.782	-3.416	1.634
740.082	10.092	13.509	11.865	-1.773	-3.417	1.644	740.766	10.065	13.499	11.871	-1.806	-3.434	1.628
740.083	10.082	13.439	11.853	-1.771	-3.357	1.586	740.767	10.049	13.502	11.804	-1.755	-3.453	1.698
740.084	10.098	13.466	11.830	-1.732	-3.368	1.636	740.769	10.047	13.446	11.848	-1.801	-3.399	1.598
740.086	10.073	13.521	11.875	-1.802	-3.448	1.676	740.770	10.060	13.444	11.817	-1.757	-3.384	1.627
740.087	10.097	13.499	11.829	-1.737	-3.402	1.670	740.771	10.050	13.467	11.797	-1.747	-3.417	1.670
740.089	10.084	13.481	11.847	-1.763	-3.397	1.634	740.772	10.039	13.535	11.819	-1.780	-3.496	1.716
740.090	10.060	13.498	11.845										

TABLE 3 (continued)  
epoch = JD + 2449000.0

JD	V <sub>1</sub>	V <sub>2</sub>	V <sub>3</sub>	V <sub>1-3</sub>	V <sub>1-2</sub>	V <sub>2-3</sub>	JD	V <sub>1</sub>	V <sub>2</sub>	V <sub>3</sub>	V <sub>1-3</sub>	V <sub>1-2</sub>	V <sub>2-3</sub>
740.809	10.016	13.437	11.808	-1.792	-3.421	1.629	741.621	10.010	13.471	11.812	-1.802	-3.461	1.659
740.810	10.054	13.502	11.845	-1.791	-3.448	1.657	741.622	10.068	13.452	11.786	-1.718	-3.377	1.653
740.811	10.059	13.513	11.882	-1.823	-3.454	1.631	741.625	10.072	13.471	11.809	-1.764	-3.407	1.643
740.811	10.059	13.513	11.882	-1.823	-3.454	1.631	741.627	10.072	13.471	11.764	-1.692	-3.399	1.707
740.811	10.059	13.513	11.882	-1.823	-3.454	1.631	741.628	10.126	13.508	11.779	-1.653	-3.379	1.726
740.813	10.082	13.501	11.887	-1.805	-3.419	1.614	741.630	10.043	13.435	11.870	-1.877	-3.392	1.565
740.814	10.052	13.491	11.863	-1.811	-3.439	1.628	741.631	10.016	13.500	11.781	-1.766	-3.485	1.719
740.816	10.050	13.472	11.823	-1.773	-3.422	1.649	741.631	10.016	13.500	11.781	-1.766	-3.485	1.719
740.817	10.069	13.480	11.826	-1.757	-3.411	1.654	741.632	10.036	13.510	11.821	-1.785	-3.474	1.689
740.818	10.023	13.473	11.815	-1.792	-3.450	1.658	741.634	10.085	13.453	11.769	-1.684	-3.368	1.684
740.820	10.042	13.430	11.821	-1.779	-3.388	1.609	741.635	10.047	13.491	11.818	-1.771	-3.444	1.673
740.821	10.052	13.482	11.834	-1.782	-3.430	1.648	741.636	10.158	13.483	11.787	-1.629	-3.325	1.696
740.822	10.067	13.455	11.865	-1.798	-3.388	1.590	741.638	9.982	13.453	11.781	-1.799	-3.471	1.672
740.824	10.082	13.535	11.843	-1.761	-3.453	1.622	741.639	10.032	13.481	11.812	-1.780	-3.449	1.669
740.825	10.066	13.465	11.852	-1.786	-3.399	1.613	741.641	10.059	13.450	11.772	-1.713	-3.376	1.678
740.827	10.081	13.461	11.849	-1.768	-3.380	1.612	741.642	10.070	13.446	11.755	-1.685	-3.376	1.678
740.829	10.067	13.487	11.853	-1.786	-3.420	1.634	741.643	10.048	13.391	11.812	-1.794	-3.343	1.549
740.831	10.053	13.503	11.834	-1.781	-3.450	1.669	741.645	10.033	13.496	11.797	-1.764	-3.463	1.699
740.832	10.048	13.546	11.822	-1.781	-3.498	1.717	741.646	10.050	13.391	11.781	-1.731	-3.341	1.610
740.834	10.052	13.475	11.819	-1.767	-3.423	1.656	741.646	10.050	13.391	11.781	-1.731	-3.341	1.610
740.835	10.045	13.469	11.823	-1.778	-3.424	1.646	741.649	10.032	13.414	11.766	-1.734	-3.382	1.648
740.836	10.058	13.472	11.815	-1.757	-3.414	1.657	741.651	10.049	13.389	11.805	-1.756	-3.340	1.584
740.838	10.065	13.486	11.825	-1.760	-3.421	1.661	741.652	10.086	13.440	11.779	-1.693	-3.354	1.661
740.839	10.050	13.462	11.840	-1.790	-3.412	1.622	741.653	10.051	13.437	11.834	-1.783	-3.386	1.603
740.840	10.061	13.462	11.840	-1.779	-3.401	1.622	741.654	10.059	13.494	11.768	-1.709	-3.435	1.726
740.842	10.035	13.506	11.828	-1.793	-3.471	1.678	741.656	10.057	13.465	11.773	-1.722	-3.414	1.692
740.843	10.050	13.512	11.819	-1.769	-3.462	1.693	741.656	10.072	13.463	11.834	-1.732	-3.397	1.595
740.845	10.042	13.464	11.828	-1.786	-3.422	1.636	741.659	10.063	13.363	11.798	-1.732	-3.300	1.565
740.846	10.044	13.459	11.844	-1.800	-3.415	1.615	741.660	10.047	13.450	11.772	-1.725	-3.403	1.678
740.847	10.066	13.496	11.809	-1.743	-3.430	1.687	741.661	10.065	13.547	11.808	-1.743	-3.482	1.739
740.849	10.066	13.507	11.828	-1.762	-3.441	1.679	741.663	10.096	13.390	11.796	-1.700	-3.294	1.594
740.851	10.027	13.424	11.813	-1.786	-3.397	1.611	741.664	10.079	13.484	11.771	-1.721	-3.411	1.690
740.852	10.048	13.448	11.831	-1.783	-3.400	1.617	741.665	10.045	13.426	11.834	-1.750	-3.381	1.591
740.853	10.028	13.467	11.809	-1.781	-3.439	1.658	741.667	10.065	13.419	11.775	-1.710	-3.354	1.644
740.854	10.041	13.446	11.807	-1.766	-3.405	1.639	741.668	10.060	13.436	11.772	-1.712	-3.376	1.664
740.875	10.024	13.448	11.808	-1.784	-3.424	1.640	741.670	10.052	13.427	11.812	-1.760	-3.375	1.615
740.876	10.034	13.451	11.822	-1.786	-3.417	1.631	741.671	10.059	13.471	11.784	-1.726	-3.413	1.687
740.877	10.039	13.429	11.809	-1.770	-3.390	1.620	741.672	10.032	13.469	11.833	-1.801	-3.437	1.636
740.878	10.029	13.454	11.818	-1.789	-3.425	1.636	741.674	10.029	13.470	11.790	-1.761	-3.441	1.680
740.879	10.053	13.434	11.826	-1.773	-3.381	1.608	741.675	10.101	13.375	11.763	-1.662	-3.274	1.612
740.881	10.039	13.446	11.783	-1.744	-3.407	1.663	741.675	10.101	13.375	11.763	-1.662	-3.274	1.612
740.882	10.031	13.418	11.797	-1.766	-3.387	1.621	741.678	10.046	13.330	11.769	-1.723	-3.284	1.561
740.883	10.033	13.448	11.782	-1.749	-3.415	1.666	741.679	10.034	13.447	11.804	-1.770	-3.413	1.643
740.885	10.057	13.434	11.807	-1.730	-3.377	1.656	741.681	10.036	13.394	11.761	-1.745	-3.358	1.633
740.886	9.922	13.433	11.721	-1.799	-3.421	1.622	741.682	10.071	13.438	11.815	-1.744	-3.367	1.623
740.888	10.053	13.464	11.815	-1.762	-3.411	1.649	741.684	10.060	13.434	11.784	-1.744	-3.368	1.640
740.889	10.033	13.459	11.799	-1.766	-3.426	1.660	741.685	10.041	13.452	11.802	-1.761	-3.451	1.690
740.890	10.026	13.441	11.796	-1.770	-3.415	1.645	741.686	10.062	13.413	11.803	-1.741	-3.351	1.610
740.892	10.041	13.508	11.806	-1.765	-3.467	1.702	741.688	10.029	13.354	11.821	-1.792	-3.325	1.533
740.893	10.037	13.443	11.808	-1.771	-3.406	1.635	741.689	10.019	13.360	11.787	-1.768	-3.341	1.573
740.895	10.041	13.409	11.820	-1.779	-3.368	1.589	741.691	10.075	13.482	11.806	-1.731	-3.407	1.676
740.896	10.021	13.435	11.809	-1.788	-3.414	1.626	741.692	10.047	13.410	11.786	-1.739	-3.363	1.624
740.897	10.025	13.434	11.816	-1.791	-3.409	1.618	741.693	10.059	13.428	11.771	-1.712	-3.369	1.654
740.899	10.031	13.434	11.816	-1.785	-3.403	1.618	741.695	10.092	13.470	11.782	-1.690	-3.378	1.688
740.900	10.048	13.461	11.795	-1.780	-3.446	1.696	741.696	10.017	13.483	11.805	-1.788	-3.466	1.678
740.903	10.056	13.437	11.839	-1.783	-3.381	1.598	741.699	10.052	13.436	11.801	-1.749	-3.384	1.635
740.904	10.063	13.457	11.818	-1.755	-3.391	1.639	741.699	10.049	13.476	11.774	-1.743	-3.445	1.674
740.906	10.028	13.465	11.802	-1.774	-3.437	1.663	741.700	10.002	13.447	11.774	-1.741	-3.445	1.674
740.907	10.048	13.428	11.808	-1.760	-3.380	1.620	741.702	10.073	13.516	11.792	-1.719	-3.443	1.724
740.909	10.030	13.469	11.802	-1.772	-3.439	1.667	741.703	10.042	13.500	11.766	-1.724	-3.458	1.734
740.910	10.027	13.477	11.802	-1.775	-3.450	1.675	741.723	10.027	13.420	11.818	-1.791	-3.393	1.602
740.911	10.027	13.443	11.789	-1.762	-3.416	1.654	741.724	10.070	13.456	11.768	-1.730	-3.402	1.672
740.913	10.061	13.434	11.808	-1.747	-3.373	1.626	741.725	10.070	13.456	11.768	-1.730	-3.402	1.672
740.915	10.043	13.440	11.818	-1.775	-3.397	1.622	741.727	10.044	13.485	11.820	-1.776	-3.411	1.665
740.915	10.015	13.481	11.841	-1.826	-3.466	1.640	741.728	10.039	13.365	11.782	-1.743	-3.326	1.583
740.917	10.048	13.512	11.805	-1.761	-3.464	1.703	741.730	10.013	13.443	11.764	-1.751	-3.430	1.679
740.918	10.015	13.434	11.797	-1.782	-3.419	1.637	741.731	10.021	13.414	11.789	-1.768	-3.393	1.625
740.920	10.037	13.484	11.805	-1.768	-3.447	1.679	741.732	10.050	13.427	11.757	-1.707	-3.377	1.670
740.921	10.019	13.516	11.777	-1.758	-3.497	1.739	741.734	10.024	13.427	11.759	-1.735	-3.303	1.568
740.922	10.030	13.445	11.774	-1.744	-3.415	1.671	741.735	10.040	13.353	11.756	-1.716	-3.313	1.597
740.924	10.020	13.465	11.807	-1.787	-3.445	1.658	741.736	10.038	13.385	11.788	-1.750	-3.347	1.597
740.925	10.043	13.431	11.793	-1.750	-3.388	1.638	741.738	10.049	13.423	11.772	-1.723	-3.374	1.651
740.927	10.043	13.439	11.791	-1.748	-3.396	1.648	741.739	10.020	13.363	11.771	-1.751	-3.343	1.592
740.929	10.016	13.464	11.805	-1.793	-3.449	1.655	741.740	10.024	13.432	11.790	-1.768	-3.410	1.642
740.931	10.036	13.473	11.805	-1.769	-3.437	1.668	741.742	10.057	13.365	11.772	-1.715	-3.310	1.595
740.932	10.036	13.467	11.801	-1.765	-3.431	1.666	741.743	10.014	13.465	11.762	-1.748	-3.451	1.703
740.934	10.034	13.435	11.802	-1.768	-3.401	1.633	741.745	10.027	13.395	11.821	-1.794	-3.368	1.574
740.935	10.013	13.435	11.788	-1.775	-3.422	1.647	741.746	10.060	13.430	11.801	-1.741	-3.352	1.629
740.936	10.035	13.471	11.796</										

TABLE 3 (continued)  
epoch = JD + 2449600.0

JD	v <sub>1</sub>	v <sub>2</sub>	v <sub>3</sub>	v <sub>1-3</sub>	v <sub>1-2</sub>	v <sub>2-3</sub>	JD	v <sub>1</sub>	v <sub>2</sub>	v <sub>3</sub>	v <sub>1-3</sub>	v <sub>1-2</sub>	v <sub>2-3</sub>
741.781	10.051	13.471	11.806	-1.755	-3.420	1.665	741.945	9.999	13.438	11.762	-1.763	-3.439	1.676
741.782	10.062	13.435	11.806	-1.744	-3.373	1.629	741.946	9.999	13.438	11.762	-1.763	-3.439	1.676
741.784	10.036	13.442	11.806	-1.732	-3.406	1.674	741.947	9.999	13.438	11.762	-1.763	-3.439	1.676
741.785	10.006	13.448	11.794	-1.778	-3.442	1.664	741.948	9.999	13.438	11.762	-1.763	-3.439	1.676
741.786	10.046	13.416	11.794	-1.752	-3.430	1.664	741.949	9.999	13.438	11.762	-1.763	-3.439	1.676
741.788	10.051	13.412	11.747	-1.696	-3.361	1.665	741.950	9.999	13.438	11.762	-1.763	-3.439	1.676
741.789	10.030	13.424	11.774	-1.744	-3.394	1.650	741.951	9.999	13.438	11.762	-1.763	-3.439	1.676
741.790	10.023	13.436	11.760	-1.737	-3.413	1.676	741.952	9.999	13.438	11.762	-1.763	-3.439	1.676
741.792	10.019	13.475	11.789	-1.770	-3.456	1.686	741.953	9.999	13.438	11.762	-1.763	-3.439	1.676
741.793	10.009	13.503	11.780	-1.771	-3.496	1.725	741.954	9.999	13.438	11.762	-1.763	-3.439	1.676
741.795	10.044	13.452	11.765	-1.721	-3.408	1.687	741.955	9.999	13.438	11.762	-1.763	-3.439	1.676
741.796	10.047	13.405	11.765	-1.718	-3.358	1.640	741.956	9.999	13.438	11.762	-1.763	-3.439	1.676
741.797	10.019	13.379	11.801	-1.782	-3.360	1.578	741.957	9.999	13.438	11.762	-1.763	-3.439	1.676
741.799	10.010	13.420	11.789	-1.779	-3.410	1.631	741.958	9.999	13.438	11.762	-1.763	-3.439	1.676
741.800	10.003	13.361	11.769	-1.766	-3.358	1.592	741.959	9.999	13.438	11.762	-1.763	-3.439	1.676
741.802	10.014	13.437	11.779	-1.655	-3.418	1.638	741.960	9.999	13.438	11.762	-1.763	-3.439	1.676
741.802	10.024	13.442	11.768	-1.744	-3.418	1.638	741.961	9.999	13.438	11.762	-1.763	-3.439	1.676
741.804	9.999	13.406	11.766	-1.767	-3.407	1.640	741.962	9.999	13.438	11.762	-1.763	-3.439	1.676
741.806	10.028	13.387	11.781	-1.753	-3.359	1.606	741.963	9.999	13.438	11.762	-1.763	-3.439	1.676
741.807	10.026	13.350	11.760	-1.734	-3.324	1.590	741.964	9.999	13.438	11.762	-1.763	-3.439	1.676
741.809	10.024	13.413	11.764	-1.740	-3.389	1.649	741.965	9.999	13.438	11.762	-1.763	-3.439	1.676
741.810	10.045	13.411	11.770	-1.725	-3.366	1.641	741.966	9.999	13.438	11.762	-1.763	-3.439	1.676
741.811	10.037	13.412	11.757	-1.720	-3.375	1.655	741.967	9.999	13.438	11.762	-1.763	-3.439	1.676
741.813	10.029	13.455	11.771	-1.742	-3.426	1.684	741.968	9.999	13.438	11.762	-1.763	-3.439	1.676
741.814	10.029	13.420	11.780	-1.751	-3.391	1.640	741.969	9.999	13.438	11.762	-1.763	-3.439	1.676
741.815	10.030	13.387	11.781	-1.751	-3.357	1.606	741.970	9.999	13.438	11.762	-1.763	-3.439	1.676
741.816	10.038	13.442	11.738	-1.772	-3.284	1.604	741.971	9.999	13.438	11.762	-1.763	-3.439	1.676
741.818	10.017	13.350	11.781	-1.772	-3.340	1.568	741.972	9.999	13.438	11.762	-1.763	-3.439	1.676
741.820	10.039	13.408	11.765	-1.726	-3.369	1.643	741.973	9.999	13.438	11.762	-1.763	-3.439	1.676
741.821	10.028	13.438	11.802	-1.774	-3.410	1.636	741.974	9.999	13.438	11.762	-1.763	-3.439	1.676
741.822	10.029	13.460	11.781	-1.752	-3.431	1.679	741.975	9.999	13.438	11.762	-1.763	-3.439	1.676
741.823	10.040	13.380	11.796	-1.756	-3.440	1.584	741.976	9.999	13.438	11.762	-1.763	-3.439	1.676
741.824	10.037	13.452	11.798	-1.761	-3.395	1.634	741.977	9.999	13.438	11.762	-1.763	-3.439	1.676
741.827	10.035	13.465	11.769	-1.734	-3.430	1.696	741.978	9.999	13.438	11.762	-1.763	-3.439	1.676
741.828	10.026	13.433	11.764	-1.738	-3.407	1.669	741.979	9.999	13.438	11.762	-1.763	-3.439	1.676
741.829	10.015	13.434	11.782	-1.767	-3.419	1.652	741.980	9.999	13.438	11.762	-1.763	-3.439	1.676
741.832	10.034	13.436	11.753	-1.719	-3.402	1.683	741.981	9.999	13.438	11.762	-1.763	-3.439	1.676
741.834	10.048	13.431	11.797	-1.749	-3.383	1.634	741.982	9.999	13.438	11.762	-1.763	-3.439	1.676
741.835	10.040	13.438	11.786	-1.746	-3.398	1.652	741.983	9.999	13.438	11.762	-1.763	-3.439	1.676
741.836	10.047	13.435	11.762	-1.715	-3.388	1.673	741.984	9.999	13.438	11.762	-1.763	-3.439	1.676
741.838	9.988	13.427	11.771	-1.783	-3.439	1.656	741.985	9.999	13.438	11.762	-1.763	-3.439	1.676
741.839	10.022	13.384	11.785	-1.763	-3.362	1.599	741.986	9.999	13.438	11.762	-1.763	-3.439	1.676
741.841	10.009	13.460	11.802	-1.793	-3.451	1.658	741.987	9.999	13.438	11.762	-1.763	-3.439	1.676
741.842	10.034	13.355	11.782	-1.748	-3.321	1.573	741.988	9.999	13.438	11.762	-1.763	-3.439	1.676
741.844	10.017	13.493	11.773	-1.756	-3.476	1.720	741.989	9.999	13.438	11.762	-1.763	-3.439	1.676
741.845	10.023	13.355	11.783	-1.760	-3.394	1.572	741.990	9.999	13.438	11.762	-1.763	-3.439	1.676
741.846	10.024	13.401	11.769	-1.745	-3.332	1.632	741.991	9.999	13.438	11.762	-1.763	-3.439	1.676
741.848	10.041	13.496	11.750	-1.709	-3.455	1.746	741.992	9.999	13.438	11.762	-1.763	-3.439	1.676
741.849	10.025	13.536	11.796	-1.771	-3.511	1.740	741.993	9.999	13.438	11.762	-1.763	-3.439	1.676
741.850	10.021	13.433	11.779	-1.758	-3.412	1.654	741.994	9.999	13.438	11.762	-1.763	-3.439	1.676
741.852	10.011	13.418	11.762	-1.751	-3.407	1.656	741.995	9.999	13.438	11.762	-1.763	-3.439	1.676
741.853	10.024	13.490	11.781	-1.757	-3.466	1.709	741.996	9.999	13.438	11.762	-1.763	-3.439	1.676
741.854	10.010	13.499	11.765	-1.755	-3.489	1.734	741.997	9.999	13.438	11.762	-1.763	-3.439	1.676
741.856	10.001	13.494	11.772	-1.771	-3.493	1.722	741.998	9.999	13.438	11.762	-1.763	-3.439	1.676
741.857	10.000	13.416	11.784	-1.784	-3.416	1.632	741.999	9.999	13.438	11.762	-1.763	-3.439	1.676
741.877	10.016	13.482	11.750	-1.734	-3.466	1.732	742.000	9.999	13.438	11.762	-1.763	-3.439	1.676
741.878	10.023	13.448	11.767	-1.744	-3.425	1.681	742.001	9.999	13.438	11.762	-1.763	-3.439	1.676
741.880	10.014	13.452	11.710	-1.716	-3.438	1.728	742.002	9.999	13.438	11.762	-1.763	-3.439	1.676
741.881	10.014	13.427	11.743	-1.749	-3.419	1.670	742.003	9.999	13.438	11.762	-1.763	-3.439	1.676
741.882	10.005	13.386	11.752	-1.747	-3.381	1.634	742.004	9.999	13.438	11.762	-1.763	-3.439	1.676
741.884	10.012	13.338	11.731	-1.719	-3.326	1.607	742.005	9.999	13.438	11.762	-1.763	-3.439	1.676
741.885	10.019	13.444	11.737	-1.718	-3.425	1.707	742.006	9.999	13.438	11.762	-1.763	-3.439	1.676
741.886	10.014	13.451	11.762	-1.743	-3.437	1.689	742.007	9.999	13.438	11.762	-1.763	-3.439	1.676
741.888	10.014	13.403	11.784	-1.777	-3.406	1.619	742.008	9.999	13.438	11.762	-1.763	-3.439	1.676
741.889	10.008	13.443	11.748	-1.740	-3.435	1.695	742.009	9.999	13.438	11.762	-1.763	-3.439	1.676
741.891	9.996	13.435	11.764	-1.768	-3.439	1.671	742.010	9.999	13.438	11.762	-1.763	-3.439	1.676
741.892	9.985	13.436	11.734	-1.749	-3.451	1.702	742.011	9.999	13.438	11.762	-1.763	-3.439	1.676
741.893	10.003	13.571	11.752	-1.749	-3.568	1.819	742.012	9.999	13.438	11.762	-1.763	-3.439	1.676
741.895	10.004	13.395	11.745	-1.741	-3.391	1.650	742.013	9.999	13.438	11.762	-1.763	-3.439	1.676
741.896	9.990	13.391	11.760	-1.770	-3.401	1.631	742.014	9.999	13.438	11.762	-1.763	-3.439	1.676
741.897	10.023	13.442	11.768	-1.745	-3.419	1.674	742.015	9.999	13.438	11.762	-1.763	-3.439	1.676
741.901	10.000	13.468	11.767	-1.767	-3.468	1.701	742.016	9.999	13.438	11.762	-1.763	-3.439	1.676
741.902	10.017	13.344	11.788	-1.771	-3.327	1.556	742.017	9.999	13.438	11.762	-1.763	-3.439	1.676
741.903	10.026	13.424	11.780	-1.754	-3.398	1.644	742.018	9.999	13.438	11.762	-1.763	-3.439	1.676
741.907	10.013	13.402	11.764	-1.751	-3.389	1.638	742.019	9.999	13.438	11.762	-1.763	-3.439	1.676
741.909	10.001	13.492	11.761	-1.760	-3.491	1.731	742.020	9.999	13.438	11.762	-1.763	-3.439	1.676
741.910	9.996	13.478	11.771	-1.775	-3.482	1.707	742.021	9.999	13.438	11.762	-1.763	-3.439	1.676
741.911	10.014	13.464	11.746	-1.732	-3.450	1.718	742.022	9.999	13.438	11.762	-1.763	-3.439	1.676
741.913	10.011	13.386	11.760	-1.749	-3.375	1.626	742.023	9.999	13.438	11.762	-1.76		

TABLE 3 (continued)  
epoch = JD + 2449000.0

JD	v <sub>1</sub>	v <sub>2</sub>	v <sub>3</sub>	v <sub>1-3</sub>	v <sub>1-2</sub>	v <sub>2-3</sub>	JD	v <sub>1</sub>	v <sub>2</sub>	v <sub>3</sub>	v <sub>1-3</sub>	v <sub>1-2</sub>	v <sub>2-3</sub>
759.737	9.845	13.262	11.656	-1.811	-3.417	1.606	759.872	9.817	13.336	11.611	-1.794	-3.519	1.725
759.741	9.841	13.263	11.628	-1.787	-3.422	1.635	759.874	9.817	13.313	11.630	-1.813	-3.496	1.683
759.742	9.851	13.344	11.653	-1.802	-3.493	1.691	759.875	9.811	13.306	11.671	-1.860	-3.495	1.635
759.742	9.833	13.300	11.636	-1.803	-3.467	1.664	759.877	9.838	13.289	11.661	-1.823	-3.451	1.628
759.743	9.858	13.257	11.691	-1.833	-3.399	1.566	759.878	9.830	13.304	11.655	-1.865	-3.474	1.609
759.743	9.870	13.189	11.663	-1.854	-3.423	1.571	759.879	9.836	13.373	11.659	-1.823	-3.537	1.714
759.746	9.826	13.251	11.680	-1.854	-3.369	1.526	759.881	9.836	13.286	11.663	-1.827	-3.450	1.623
759.747	9.830	13.215	11.662	-1.832	-3.385	1.553	759.883	9.814	13.372	11.662	-1.818	-3.558	1.710
759.749	9.805	13.368	11.618	-1.813	-3.363	1.750	759.884	9.834	13.324	11.613	-1.779	-3.490	1.711
759.750	9.822	13.290	11.621	-1.799	-3.468	1.669	759.885	9.819	13.417	11.619	-1.800	-3.398	1.798
759.751	9.828	13.312	11.651	-1.823	-3.484	1.661	759.886	9.834	13.313	11.649	-1.815	-3.479	1.664
759.752	9.839	13.270	11.684	-1.845	-3.431	1.586	759.888	9.840	13.313	11.672	-1.832	-3.473	1.641
759.753	9.824	13.333	11.654	-1.830	-3.509	1.579	759.889	9.828	13.329	11.664	-1.836	-3.471	1.635
759.755	9.825	13.280	11.690	-1.865	-3.455	1.590	759.891	9.846	13.350	11.626	-1.790	-3.454	1.664
759.756	9.822	13.223	11.680	-1.858	-3.401	1.543	759.892	9.826	13.300	11.647	-1.821	-3.474	1.653
759.758	9.825	13.199	11.652	-1.827	-3.374	1.547	759.893	9.783	13.388	11.591	-1.808	-3.605	1.797
759.761	9.813	13.249	11.698	-1.885	-3.436	1.551	759.895	9.822	13.392	11.682	-1.860	-3.570	1.710
759.761	9.831	13.318	11.651	-1.820	-3.487	1.667	759.897	9.833	13.336	11.673	-1.840	-3.503	1.663
759.763	9.844	13.268	11.665	-1.826	-3.428	1.602	759.898	9.816	13.281	11.671	-1.855	-3.465	1.610
759.764	9.810	13.309	11.676	-1.832	-3.465	1.633	759.899	9.827	13.332	11.664	-1.837	-3.505	1.668
759.766	9.831	13.355	11.611	-1.810	-3.524	1.714	759.900	9.832	13.309	11.627	-1.795	-3.477	1.682
759.767	9.826	13.313	11.667	-1.841	-3.487	1.646	759.902	9.816	13.289	11.677	-1.861	-3.443	1.582
759.768	9.833	13.334	11.664	-1.831	-3.501	1.670	759.903	9.853	13.322	11.682	-1.829	-3.469	1.640
759.770	9.829	13.333	11.671	-1.842	-3.444	1.598	759.904	9.836	13.321	11.645	-1.809	-3.485	1.670
759.771	9.816	13.231	11.684	-1.868	-3.419	1.547	759.906	9.836	13.281	11.682	-1.806	-3.506	1.700
759.772	9.814	13.224	11.654	-1.840	-3.410	1.570	759.906	9.828	13.343	11.639	-1.867	-3.459	1.592
759.774	9.832	13.264	11.622	-1.790	-3.432	1.642	759.907	9.841	13.350	11.634	-1.793	-3.479	1.686
759.775	9.835	13.301	11.680	-1.845	-3.466	1.621	759.909	9.827	13.386	11.698	-1.771	-3.455	1.688
759.776	9.847	13.246	11.695	-1.848	-3.399	1.550	759.910	9.879	13.441	11.710	-1.831	-3.562	1.731
759.777	9.832	13.288	11.698	-1.856	-3.456	1.600	759.911	9.844	13.358	11.667	-1.823	-3.514	1.691
759.778	9.829	13.249	11.687	-1.858	-3.420	1.562	759.913	9.932	13.453	11.785	-1.853	-3.521	1.668
759.779	9.830	13.231	11.666	-1.836	-3.401	1.565	759.914	9.855	13.370	11.691	-1.836	-3.515	1.679
759.779	9.820	13.279	11.670	-1.850	-3.459	1.609	759.916	9.838	13.359	11.683	-1.845	-3.521	1.676
759.781	9.814	13.361	11.628	-1.814	-3.517	1.733	759.917	9.843	13.370	11.672	-1.829	-3.527	1.698
759.782	9.843	13.261	11.641	-1.818	-3.438	1.620	759.918	9.835	13.315	11.682	-1.847	-3.480	1.633
759.784	9.834	13.330	11.646	-1.812	-3.496	1.684	759.920	9.843	13.353	11.664	-1.821	-3.510	1.689
759.785	9.834	13.315	11.669	-1.835	-3.481	1.646	759.921	9.827	13.257	11.701	-1.874	-3.430	1.556
759.786	9.829	13.247	11.683	-1.854	-3.418	1.564	759.922	9.815	13.363	11.653	-1.815	-3.495	1.680
759.788	9.827	13.336	11.668	-1.841	-3.509	1.668	759.924	9.834	13.290	11.658	-1.824	-3.456	1.632
759.789	9.827	13.337	11.564	-1.837	-3.510	1.673	759.925	9.830	13.360	11.677	-1.847	-3.530	1.683
759.790	9.811	13.436	11.609	-1.798	-3.685	1.887	759.927	9.837	13.350	11.667	-1.830	-3.513	1.683
759.792	9.820	13.370	11.665	-1.835	-3.469	1.624	759.928	9.828	13.430	11.599	-1.771	-3.607	1.831
759.793	9.827	13.311	11.662	-1.835	-3.484	1.649	759.929	9.836	13.345	11.662	-1.824	-3.507	1.683
759.795	9.824	13.231	11.673	-1.849	-3.407	1.558	759.931	9.840	13.344	11.686	-1.816	-3.514	1.698
759.796	9.814	13.318	11.648	-1.834	-3.504	1.670	759.932	9.818	13.302	11.646	-1.828	-3.484	1.656
759.797	9.829	13.323	11.636	-1.807	-3.494	1.687	759.934	9.840	13.355	11.647	-1.807	-3.545	1.738
759.799	9.827	13.289	11.517	-1.790	-3.862	2.072	759.935	9.828	13.230	11.673	-1.845	-3.402	1.557
759.800	9.824	13.286	11.665	-1.835	-3.460	1.621	759.936	9.824	13.359	11.664	-1.840	-3.545	1.705
759.802	9.819	13.285	11.686	-1.817	-3.467	1.530	759.938	9.834	13.356	11.641	-1.807	-3.522	1.715
759.803	9.832	13.327	11.659	-1.827	-3.495	1.668	759.939	9.831	13.337	11.645	-1.814	-3.506	1.692
759.805	9.829	13.287	11.657	-1.828	-3.458	1.630	759.942	9.836	13.388	11.669	-1.833	-3.552	1.719
759.806	9.834	13.374	11.631	-1.797	-3.540	1.743	759.942	9.838	13.329	11.682	-1.844	-3.491	1.647
759.807	9.835	13.304	11.662	-1.827	-3.469	1.642	759.943	9.833	13.318	11.671	-1.838	-3.485	1.647
759.809	9.822	13.309	11.668	-1.823	-3.483	1.641	759.945	9.836	13.331	11.659	-1.823	-3.495	1.672
759.810	9.816	13.379	11.639	-1.808	-3.563	1.740	759.946	9.833	13.370	11.674	-1.828	-3.469	1.656
759.811	9.845	13.340	11.653	-1.828	-3.495	1.687	759.948	9.818	13.387	11.674	-1.857	-3.569	1.712
759.813	9.826	13.311	11.667	-1.841	-3.485	1.644	759.949	9.829	13.282	11.696	-1.867	-3.453	1.586
759.814	9.837	13.315	11.674	-1.837	-3.478	1.641	759.950	9.839	13.272	11.684	-1.845	-3.433	1.588
759.816	9.820	13.435	11.615	-1.795	-3.615	1.820	759.952	9.841	13.371	11.642	-1.801	-3.530	1.729
759.817	9.835	13.238	11.684	-1.849	-3.403	1.554	759.953	9.837	13.346	11.649	-1.812	-3.509	1.697
759.818	9.775	13.228	11.614	-1.839	-3.453	1.614	759.954	9.828	13.300	11.627	-1.799	-3.472	1.673
759.820	9.832	13.349	11.674	-1.842	-3.517	1.675	759.956	9.839	13.354	11.665	-1.826	-3.515	1.689
759.821	9.829	13.629	11.594	-1.765	-3.800	2.035	759.957	9.835	13.388	11.658	-1.823	-3.553	1.730
759.821	9.832	13.309	11.674	-1.842	-3.477	1.635	759.959	9.837	13.384	11.674	-1.837	-3.547	1.710
759.822	9.826	13.313	11.686	-1.860	-3.487	1.627	759.960	9.829	13.352	11.629	-1.800	-3.523	1.723
759.824	9.826	13.278	11.678	-1.851	-3.473	1.620	759.961	9.838	13.358	11.658	-1.817	-3.560	1.781
759.825	9.824	13.357	11.678	-1.819	-3.453	1.714	759.964	9.825	13.357	11.639	-1.814	-3.478	1.664
759.827	9.823	13.353	11.661	-1.838	-3.530	1.692	759.964	9.841	13.375	11.670	-1.832	-3.496	1.698
759.828	9.830	13.294	11.684	-1.854	-3.464	1.610	759.966	9.838	13.325	11.670	-1.827	-3.487	1.655
759.829	9.837	13.381	11.680	-1.843	-3.544	1.701	759.967	9.832	13.342	11.644	-1.812	-3.510	1.698
759.831	9.826	13.325	11.685	-1.859	-3.499	1.640	759.969	9.845	13.335	11.669	-1.824	-3.490	1.666
759.832	9.848	13.292	11.671	-1.823	-3.444	1.621	759.970	9.839	13.283	11.686	-1.847	-3.444	1.597
759.834	9.833	13.346	11.666	-1.813	-3.493	1.680	759.971	9.835	13.364	11.643	-1.804	-3.525	1.721
759.835	9.866	13.340	11.680	-1.814	-3.477	1.660	759.972	9.859	13.476	11.615	-1.756	-3.489	1.733
759.836	9.823	13.351	11.655	-1.832	-3.528	1.696	759.974	9.834	13.377	11.651	-1.823	-3.492	1.669
759.838	9.817	13.295	11.692	-1.875	-3.478	1.603	759.975	9.846	13.382	11.663	-1.817	-3.536	1.719
759.839	9.841	13.363	11.680	-1.839	-3.522	1.683	759.977	9.845	13.353	11.678	-1.833	-3.508	1.675
759.841	9.837	13.291	11.674	-1.837	-3.454	1.617	759.978	9.840	13.313	11.639	-1.799	-3.473	1.674
759.842	9.836	13.328	11.670	-1.834	-3.492	1.658	759.979	9.845	13.371	11.617	-1.772	-3.526	1.754
759.843	9.824	13.318	11.640										

TABLE 3 (continued)  
epoch = JD + 2449000.0

JD	V <sub>1</sub>	V <sub>2</sub>	V <sub>3</sub>	V <sub>1-3</sub>	V <sub>1-2</sub>	V <sub>2-3</sub>	JD	V <sub>1</sub>	V <sub>2</sub>	V <sub>3</sub>	V <sub>1-3</sub>	V <sub>1-2</sub>	V <sub>2-3</sub>
760.009	9.846	13.264	11.688	-1.842	-3.418	1.576	760.696	9.978	13.463	11.777	-1.799	-3.475	1.676
760.010	9.843	13.263	11.674	-1.831	-3.493	1.662	760.699	10.185	13.387	12.108	-1.923	-3.472	1.849
760.012	9.857	13.243	11.738	-1.881	-3.386	1.505	760.700	9.961	13.456	11.782	-1.821	-3.495	1.674
760.013	9.850	13.376	11.679	-1.829	-3.526	1.697	760.702	10.133	13.693	11.971	-1.778	-3.500	1.722
760.014	9.855	13.456	11.656	-1.801	-3.601	1.800	760.703	10.079	13.578	11.916	-1.837	-3.499	1.662
760.015	9.867	13.383	11.657	-1.790	-3.516	1.726	760.704	10.025	13.503	11.839	-1.814	-3.478	1.664
760.017	9.854	13.471	11.657	-1.803	-3.617	1.814	760.706	9.946	13.424	11.753	-1.801	-3.478	1.671
760.018	9.846	13.304	11.686	-1.803	-3.458	1.718	760.707	9.946	13.536	11.677	-1.731	-3.590	1.859
760.020	9.840	13.386	11.674	-1.834	-3.546	1.712	760.709	9.895	13.361	11.675	-1.780	-3.466	1.685
760.021	9.844	13.452	11.643	-1.799	-3.608	1.809	760.710	9.889	13.453	11.678	-1.789	-3.561	1.775
760.022	9.852	13.605	11.625	-1.773	-3.753	1.929	760.712	9.900	13.370	11.732	-1.832	-3.470	1.638
760.024	9.847	13.291	11.699	-1.852	-3.444	1.597	760.713	9.908	13.466	11.703	-1.795	-3.558	1.763
760.025	9.850	13.331	11.707	-1.857	-3.481	1.624	761.651	10.002	13.659	11.847	-1.845	-3.657	1.812
760.027	9.847	13.259	11.699	-1.852	-3.412	1.660	761.651	9.884	13.478	11.761	-1.847	-3.464	1.587
760.028	9.850	13.401	11.645	-1.795	-3.551	1.766	761.652	9.879	13.471	11.801	-1.829	-3.450	1.621
760.030	9.854	13.305	11.692	-1.838	-3.451	1.613	761.653	10.018	13.646	11.835	-1.817	-3.668	1.851
760.031	9.853	13.784	11.645	-1.792	-3.931	2.139	761.661	9.626	13.186	11.489	-1.863	-3.560	1.697
760.032	9.859	13.342	11.696	-1.857	-3.503	1.646	761.661	9.633	13.179	11.481	-1.852	-3.546	1.694
760.033	9.852	13.309	11.719	-1.861	-3.457	1.596	761.662	9.648	13.222	11.461	-1.819	-3.574	1.755
760.034	9.835	13.423	11.651	-1.816	-3.588	1.772	761.662	9.648	13.222	11.467	-1.819	-3.574	1.755
760.035	9.853	13.424	11.659	-1.806	-3.571	1.765	761.663	9.814	13.285	11.657	-1.843	-3.471	1.628
760.036	9.853	13.503	11.630	-1.777	-3.650	1.873	761.664	9.808	13.224	11.655	-1.847	-3.416	1.569
760.038	9.860	13.467	11.647	-1.787	-3.607	1.820	761.664	9.804	13.449	11.616	-1.812	-3.645	1.833
760.590	9.881	13.522	11.701	-1.820	-3.641	1.821	761.666	9.794	13.373	11.621	-1.827	-3.579	1.752
760.591	9.727	13.545	11.531	-1.804	-3.848	2.046	761.666	9.801	13.323	11.618	-1.817	-3.522	1.705
760.592	9.410	12.975	11.749	-1.839	-3.665	1.726	761.668	9.793	13.471	11.614	-1.821	-3.579	1.758
760.593	9.769	13.339	11.607	-1.838	-3.570	1.732	761.670	9.789	13.343	11.624	-1.838	-3.551	1.716
760.596	10.035	14.031	11.892	-1.857	-3.996	2.139	761.671	9.775	13.179	11.651	-1.876	-3.404	1.528
760.597	9.814	13.735	11.650	-1.836	-3.921	2.085	761.672	9.801	13.397	11.607	-1.806	-3.596	1.790
760.599	9.784	13.306	11.613	-1.829	-3.522	1.693	761.674	9.810	13.206	11.650	-1.840	-3.396	1.556
760.600	9.756	13.445	11.575	-1.819	-3.689	1.870	761.675	9.798	13.281	11.625	-1.827	-3.483	1.656
760.602	9.811	13.450	11.589	-1.778	-3.639	1.861	761.676	9.776	13.198	11.676	-1.900	-3.422	1.524
760.603	9.750	13.331	11.550	-1.800	-3.584	1.784	761.678	9.811	13.282	11.689	-1.878	-3.471	1.628
760.605	9.700	13.285	11.507	-1.807	-3.585	1.778	761.679	9.800	13.269	11.627	-1.827	-3.469	1.642
760.606	9.835	13.254	11.699	-1.864	-3.419	1.553	761.681	9.782	13.300	11.595	-1.813	-3.518	1.705
760.607	9.812	13.653	11.630	-1.818	-3.841	2.023	761.682	9.782	13.229	11.652	-1.870	-3.447	1.577
760.614	9.790	13.257	11.600	-1.816	-3.490	1.680	761.684	9.782	13.268	11.598	-1.816	-3.486	1.670
760.614	9.811	13.257	11.660	-1.845	-3.486	1.637	761.684	9.809	13.203	11.683	-1.874	-3.394	1.520
760.614	9.799	13.232	11.643	-1.844	-3.433	1.589	761.685	9.882	13.279	11.735	-1.852	-3.397	1.544
760.615	9.796	13.354	11.605	-1.809	-3.558	1.749	761.686	9.881	13.356	11.688	-1.807	-3.475	1.668
760.616	9.792	13.371	11.601	-1.809	-3.579	1.770	761.688	9.888	13.321	11.719	-1.831	-3.433	1.602
760.617	9.796	13.423	11.600	-1.816	-3.639	1.823	761.689	9.873	13.260	11.732	-1.859	-3.387	1.528
760.618	9.796	13.313	11.593	-1.797	-3.517	1.720	761.691	9.893	13.375	11.719	-1.826	-3.482	1.656
760.620	9.807	13.403	11.611	-1.804	-3.596	1.792	761.692	9.898	13.268	11.749	-1.851	-3.370	1.519
760.622	9.801	13.312	11.649	-1.848	-3.511	1.663	761.692	9.890	13.270	11.730	-1.840	-3.380	1.540
760.623	9.803	13.539	11.581	-1.778	-3.736	1.958	761.693	9.868	13.289	11.711	-1.843	-3.421	1.678
760.624	9.799	13.392	11.625	-1.826	-3.593	1.767	761.693	9.887	13.323	11.687	-1.800	-3.436	1.636
760.625	9.795	13.423	11.620	-1.845	-3.448	1.603	761.694	9.866	13.300	11.744	-1.878	-3.434	1.556
760.627	9.749	13.743	11.714	-1.765	-3.786	2.021	761.695	9.868	13.237	11.757	-1.889	-3.369	1.480
760.629	10.043	13.488	11.897	-1.854	-3.445	1.591	761.696	9.870	13.373	11.706	-1.836	-3.503	1.667
760.630	10.210	13.745	12.082	-1.872	-3.535	1.663	761.696	9.827	13.401	11.639	-1.812	-3.574	1.762
760.631	10.042	13.553	11.901	-1.859	-3.551	1.692	761.693	9.885	13.290	11.723	-1.838	-3.405	1.567
760.632	9.856	13.424	11.716	-1.860	-3.568	1.708	761.699	9.903	13.206	11.762	-1.859	-3.303	1.444
760.633	9.781	13.323	11.592	-1.801	-3.542	1.741	761.700	9.888	13.459	11.690	-1.802	-3.571	1.769
760.634	9.747	13.333	11.566	-1.798	-3.599	1.771	761.701	9.870	13.438	11.715	-1.845	-3.568	1.723
760.635	9.729	13.299	11.529	-1.800	-3.570	1.770	761.703	9.866	13.190	11.743	-1.877	-3.324	1.447
760.637	9.829	13.359	11.674	-1.845	-3.530	1.685	761.704	9.894	13.304	11.748	-1.864	-3.410	1.546
760.638	10.211	14.075	11.901	-1.697	-3.871	2.174	761.706	9.870	13.264	11.725	-1.865	-3.394	1.536
760.639	9.786	13.424	11.578	-1.792	-3.638	1.846	761.707	9.884	13.251	11.759	-1.879	-3.371	1.492
760.641	9.764	13.406	11.562	-1.798	-3.642	1.844	761.709	9.884	13.230	11.761	-1.909	-3.378	1.469
760.642	9.710	13.181	11.541	-1.831	-3.471	1.640	761.710	9.884	13.281	11.740	-1.863	-3.404	1.541
760.643	9.710	13.287	11.499	-1.759	-3.577	1.788	761.712	9.870	13.303	11.742	-1.873	-3.445	1.610
760.645	9.714	13.257	11.507	-1.793	-3.543	1.750	761.712	9.870	13.283	11.743	-1.873	-3.433	1.540
760.646	9.715	13.508	11.503	-1.788	-3.793	2.005	761.713	9.875	13.271	11.699	-1.823	-3.395	1.542
760.647	9.735	13.288	11.501	-1.766	-3.553	1.787	761.714	9.875	13.351	11.693	-1.815	-3.473	1.656
760.649	9.701	13.150	11.554	-1.850	-3.446	1.596	761.716	9.884	13.320	11.705	-1.821	-3.436	1.615
760.650	9.701	13.270	11.509	-1.866	-3.567	1.761	761.717	9.875	13.266	11.709	-1.834	-3.391	1.557
760.652	9.708	13.147	11.552	-1.844	-3.439	1.595	761.718	9.873	13.311	11.757	-1.884	-3.444	1.560
760.657	9.951	13.526	11.784	-1.833	-3.575	1.742	761.719	9.857	13.323	11.699	-1.842	-3.466	1.624
760.658	10.011	13.418	11.803	-1.792	-3.407	1.615	761.720	9.871	13.317	11.687	-1.816	-3.446	1.630
760.659	9.927	13.482	11.699	-1.772	-3.555	1.783	761.721	9.856	13.394	11.689	-1.833	-3.538	1.705
760.660	9.856	13.259	11.700	-1.844	-3.403	1.559	761.723	9.885	13.332	11.740	-1.855	-3.447	1.592
760.660	9.810	13.407	11.609	-1.799	-3.597	1.798	761.724	9.859	13.279	11.716	-1.857	-3.420	1.563
760.662	9.754	13.375	11.558	-1.804	-3.621	1.817	761.725	9.874	13.260	11.735	-1.861	-3.386	1.525
760.663	9.747	13.324	11.541	-1.794	-3.577	1.783	761.727	9.853	13.272	11.729	-1.851	-3.419	1.568
760.664	9.778	13.428	11.613	-1.835	-3.650	1.815	761.728	9.871	13.275	11.729	-1.858	-3.404	1.546
760.665	9.765	13.405	11.596	-1.831	-3.640	1.809	761.729	9.867	13.252	11.735	-1.868	-3.425	1.587
760.666	9.759	13.326	11.546	-1.787	-3.567	1.780	761.731	9.846	13.302	11.731	-1.885	-3.456	1.571
760.667	9.737	13.298	11.541	-1.804	-3.561	1.757	761.734	9.852	13.285	11.720	-1.868	-3.433	1.565
760.668	9.826	13.448											



TABLE 3 (continued)  
epoch = JD + 2449000.0

JD	V <sub>1</sub>	V <sub>2</sub>	V <sub>3</sub>	V <sub>1-3</sub>	V <sub>1-2</sub>	V <sub>2-3</sub>	JD	V <sub>1</sub>	V <sub>2</sub>	V <sub>3</sub>	V <sub>1-3</sub>	V <sub>1-2</sub>	V <sub>2-3</sub>
761.763	9.858	13.252	11.703	-1.845	-3.394	1.549	761.893	9.835	13.312	11.658	-1.823	-3.477	1.654
761.764	9.853	13.402	11.665	-1.812	-3.549	1.737	761.895	9.824	13.352	11.672	-1.848	-3.528	1.680
761.766	9.825	13.298	11.677	-1.832	-3.473	1.621	761.896	9.833	13.347	11.703	-1.870	-3.514	1.644
761.766	9.848	13.231	11.706	-1.858	-3.383	1.525	761.898	9.831	13.299	11.658	-1.827	-3.468	1.641
761.767	9.831	13.422	11.654	-1.823	-3.531	1.768	761.899	9.856	13.346	11.660	-1.804	-3.490	1.686
761.769	9.846	13.255	11.727	-1.831	-3.479	1.498	761.900	9.824	13.365	11.645	-1.821	-3.541	1.720
761.770	9.849	13.464	11.667	-1.818	-3.615	1.797	761.902	9.851	13.270	11.667	-1.816	-3.419	1.603
761.771	9.848	13.212	11.706	-1.858	-3.364	1.506	761.903	9.839	13.430	11.641	-1.802	-3.491	1.689
761.772	9.843	13.227	11.722	-1.874	-3.379	1.505	761.905	9.849	13.331	11.659	-1.810	-3.482	1.672
761.774	9.845	13.292	11.732	-1.887	-3.447	1.560	761.906	9.849	13.378	11.614	-1.765	-3.526	1.761
761.777	9.884	13.258	11.718	-1.884	-3.424	1.540	761.907	9.809	13.266	11.673	-1.864	-3.457	1.593
761.778	9.837	13.263	11.730	-1.893	-3.426	1.533	761.909	9.845	13.353	11.654	-1.809	-3.508	1.695
761.779	9.870	13.371	11.678	-1.808	-3.501	1.693	761.910	9.838	13.301	11.646	-1.808	-3.463	1.655
761.780	9.852	13.312	11.694	-1.842	-3.460	1.618	761.912	9.833	13.288	11.666	-1.833	-3.455	1.622
761.780	9.846	13.221	11.712	-1.846	-3.375	1.509	761.913	9.816	13.296	11.684	-1.868	-3.479	1.611
761.781	9.851	13.308	11.656	-1.835	-3.457	1.652	761.913	9.829	13.296	11.659	-1.830	-3.467	1.637
761.781	9.844	13.320	11.717	-1.823	-3.479	1.603	761.914	9.838	13.245	11.733	-1.895	-3.407	1.512
761.782	9.849	13.328	11.651	-1.802	-3.479	1.677	761.915	9.838	13.385	11.644	-1.803	-3.544	1.741
761.784	9.843	13.467	11.634	-1.791	-3.624	1.833	761.917	9.821	13.275	11.639	-1.862	-3.458	1.586
761.785	9.846	13.257	11.714	-1.868	-3.451	1.583	761.918	9.845	13.281	11.700	-1.852	-3.436	1.581
761.786	9.862	13.275	11.668	-1.806	-3.513	1.707	761.919	9.863	13.412	11.650	-1.787	-3.549	1.762
761.788	9.847	13.232	11.726	-1.879	-3.385	1.506	761.920	9.857	13.315	11.665	-1.808	-3.458	1.650
761.789	9.845	13.259	11.704	-1.849	-3.504	1.635	761.921	9.852	13.284	11.647	-1.795	-3.432	1.637
761.790	9.848	13.342	11.708	-1.860	-3.494	1.634	761.922	9.839	13.434	11.623	-1.784	-3.595	1.811
761.792	9.837	13.257	11.725	-1.888	-3.420	1.532	761.924	9.843	13.206	11.649	-1.806	-3.468	1.662
761.794	9.843	13.348	11.641	-1.798	-3.505	1.707	761.925	9.830	13.373	11.674	-1.844	-3.443	1.695
761.795	9.845	13.377	11.667	-1.822	-3.532	1.710	761.927	9.848	13.294	11.628	-1.780	-3.446	1.666
761.796	9.850	13.337	11.669	-1.819	-3.487	1.668	761.928	9.850	13.431	11.620	-1.770	-3.581	1.811
761.797	9.845	13.380	11.647	-1.802	-3.535	1.733	761.929	9.849	13.331	11.635	-1.786	-3.482	1.696
761.799	9.827	13.571	11.638	-1.831	-3.744	1.913	761.931	9.852	13.382	11.606	-1.754	-3.530	1.776
761.801	9.840	13.311	11.723	-1.883	-3.471	1.588	761.932	9.858	13.306	11.675	-1.817	-3.448	1.631
761.801	9.845	13.268	11.706	-1.861	-3.423	1.562	761.934	9.849	13.290	11.653	-1.804	-3.441	1.637
761.803	9.854	13.451	11.627	-1.773	-3.597	1.824	761.935	9.844	13.196	11.688	-1.844	-3.352	1.508
761.804	9.865	13.243	11.722	-1.853	-3.374	1.521	761.936	9.854	13.311	11.647	-1.793	-3.457	1.664
761.804	9.844	13.266	11.715	-1.871	-3.412	1.541	761.938	9.843	13.290	11.685	-1.842	-3.447	1.605
761.806	9.826	13.512	11.616	-1.821	-3.686	1.856	761.939	9.852	13.356	11.642	-1.790	-3.534	1.744
761.807	9.848	13.492	11.655	-1.807	-3.644	1.837	761.941	9.873	13.376	11.666	-1.793	-3.503	1.710
761.809	9.870	13.346	11.659	-1.789	-3.476	1.687	761.942	9.840	13.330	11.612	-1.772	-3.490	1.718
761.810	9.850	13.434	11.628	-1.778	-3.584	1.806	761.943	9.778	13.305	11.540	-1.762	-3.527	1.765
761.811	9.865	13.594	11.648	-1.783	-3.729	1.946	761.945	9.858	13.265	11.700	-1.842	-3.407	1.565
761.813	9.853	13.299	11.698	-1.845	-3.446	1.601	761.946	9.867	13.318	11.682	-1.815	-3.451	1.636
761.814	9.849	13.289	11.682	-1.833	-3.440	1.607	761.947	9.859	13.288	11.656	-1.797	-3.429	1.632
761.816	9.841	13.274	11.695	-1.854	-3.433	1.579	761.949	9.866	13.308	11.656	-1.790	-3.439	1.649
761.817	9.862	13.331	11.684	-1.822	-3.469	1.647	761.951	9.865	13.240	11.698	-1.833	-3.375	1.542
761.818	9.829	13.327	11.672	-1.843	-3.498	1.655	761.952	9.851	13.393	11.617	-1.766	-3.542	1.776
761.820	9.833	13.254	11.710	-1.877	-3.421	1.544	761.953	9.863	13.360	11.672	-1.809	-3.497	1.688
761.822	9.840	13.330	11.714	-1.874	-3.490	1.616	761.955	9.860	13.267	11.696	-1.836	-3.407	1.571
761.822	9.845	13.338	11.665	-1.867	-3.453	1.673	761.956	9.859	13.336	11.658	-1.799	-3.477	1.678
761.824	9.831	13.264	11.718	-1.887	-3.433	1.546	761.957	9.852	13.376	11.647	-1.795	-3.524	1.729
761.826	9.834	13.280	11.693	-1.864	-3.446	1.582	761.960	9.859	13.267	11.700	-1.841	-3.408	1.567
761.828	9.851	13.284	11.703	-1.852	-3.433	1.581	761.960	9.848	13.491	11.622	-1.774	-3.643	1.869
761.831	9.831	13.247	11.703	-1.872	-3.416	1.544	761.962	9.853	13.260	11.700	-1.847	-3.407	1.560
761.833	9.838	13.276	11.702	-1.864	-3.438	1.574	761.963	9.858	13.238	11.704	-1.846	-3.380	1.534
761.834	9.852	13.341	11.686	-1.834	-3.489	1.655	761.964	9.868	13.292	11.710	-1.842	-3.424	1.582
761.835	9.818	13.425	11.621	-1.803	-3.607	1.804	761.964	9.849	13.286	11.721	-1.872	-3.407	1.535
761.837	9.839	13.299	11.707	-1.868	-3.460	1.592	761.967	9.857	13.382	11.677	-1.820	-3.525	1.705
761.838	9.834	13.482	11.636	-1.802	-3.648	1.846	761.968	9.853	13.292	11.670	-1.817	-3.439	1.622
761.839	9.844	13.336	11.676	-1.832	-3.492	1.660	761.970	9.852	13.451	11.624	-1.772	-3.599	1.827
761.841	9.835	13.415	11.660	-1.825	-3.580	1.755	761.970	9.838	13.245	11.684	-1.846	-3.407	1.561
761.842	9.834	13.321	11.715	-1.861	-3.487	1.606							
761.843	9.838	13.307	11.697	-1.859	-3.469	1.610							
761.844	9.843	13.365	11.655	-1.812	-3.522	1.710							
761.845	9.828	13.282	11.697	-1.869	-3.454	1.585							
761.846	9.843	13.319	11.693	-1.850	-3.476	1.626							
761.846	9.837	13.360	11.682	-1.825	-3.543	1.718							
761.849	9.852	13.307	11.690	-1.838	-3.455	1.617							
761.850	9.836	13.329	11.640	-1.804	-3.493	1.689							
761.852	9.733	13.220	11.532	-1.799	-3.487	1.688							
761.854	9.852	13.360	11.708	-1.856	-3.508	1.652							
761.854	9.848	13.278	11.665	-1.817	-3.430	1.613							
761.856	9.834	13.355	11.682	-1.848	-3.521	1.673							
761.857	9.850	13.423	11.649	-1.799	-3.573	1.774							
761.859	9.843	13.319	11.690	-1.847	-3.476	1.629							
761.860	9.841	13.393	11.658	-1.817	-3.552	1.735							
761.861	9.846	13.394	11.633	-1.787	-3.548	1.761							
761.863	9.838	13.348	11.650	-1.812	-3.510	1.698							
761.864	9.850	13.331	11.677	-1.827	-3.481	1.654							
761.866	9.833	13.349	11.692	-1.859	-3.516	1.657							
761.866	9.843	13.349	11.692	-1.859	-3.516	1.657							
761.867	9.845	13.322	11.650	-1.802	-3.474	1.672							
761.868	9.850	13.373	11.628	-1.778	-3.523	1.745							
761.870	9.856	13.279	11.663	-1.807	-3.423	1.616							
761.871	9.831	13.351	11.671	-1.840	-3.520	1.680							
761.873	9.832	13.264	11.687	-1.855	-3.432	1.577							
761.874	9.831	13.272	11.661	-1.830	-3.441	1.611							
761.875	9.843	13.377	11.667	-1.824	-3.498	1.710							
761.877	9.784	13.538	11.583	-1.799	-3.754	1.955							
761.877	9.784	13.538	11.583	-1.799	-3.754	1.955							

Focusing problems often left the stellar images with a slightly distorted shape. A small flare, consistently from one side of the images, was often seen. In the case of the very bright HR 4646, this flare could extend up to 10 pixels from the centroid of the star image as focus drifted throughout the night. This required photometric apertures to be larger than optimal sizes. In the case of the present images, the stellar FWHM was about 4 pixels. This would correspond to an optimal aperture of approximately 7 pixels (see § 2.1.3.b). The apertures necessary were generally about twice this size, at 14-16 pixels. The effect of the flare is to involve more pixels under the stellar profile. Judging from the ruled-surface plot in Figure 9,  $n$  could be underestimated in equation (21) by  $\sim 20$  pixels. Inserting  $n = 130$  into equation (21), one finds that this increases the  $S/N$  by approximately 8%. That is, the presence of the flare increases the uncertainty in the observations by  $\sim 0.^m0006$ .

The idealized analysis of CCD photometry in § 2.1.3.b did not include the noise due to atmospheric scintillation. An estimate of the contribution to noise due to scintillation per star,  $\sigma_{\text{scint}}$ , (in mag (min) $^{-1}$ ) was estimated using an expression found in Kjeldsen and Frandsen (1992).

$$\sigma_{\text{scint}} = 0.^m0058 \left( \frac{\Delta t + t_d}{\Delta t^{-1}} \right)^{1/2} D^{-2/3} \chi^{3/2} \exp(-h/8\text{km}), \quad (43)$$

where  $D$  is the telescope diameter in meters,  $\Delta t$  is the integration time in minutes,  $t_d$  is the observational deadtime (including readout, etc.)  $h$  is the telescope elevation in km, and  $\chi$  is the airmass. The elevation at Devon is approximately 0.8 km. The aperture of the telescope is 0.5 m. For the present work integrations were approximately 0.0083 min. The deadtime was 1-2 minutes. Assuming an airmass  $\sim 1$ , the above expression gives a value of  $\sigma_{\text{scint}}$  per star per observation of  $\approx 0.^m013$  ( $0.^m0016$  for the telescope stopped down to  $D = 0.35$  m).

An illustrative result follows from the noise analysis. Two limitations to the system are the dark current and readout noise. It is instructive to consider what would be the  $S/N$  for the deepest possible integration. Consider a three minute exposure of a  $17^{th}$  magnitude star. This gives a dark count of

$$30 \times 4.9 \text{ e}^- \text{ s}^{-1} \times 180 \text{ s} = 4.4 \times 10^4 \text{ e}^-.$$

The sky count rate is

$$480 \text{ e}^- \times 1/0.5 \text{ s}^{-1} = 9.6 \times 10^2 \text{ e}^- \text{ s}^{-1}.$$

The star count rate (for 0.5 s) can be found from Pogson's equation,

$$\epsilon_5/\epsilon_{20} = 2.512^{17-5} = 2.512^{12} \approx 6.3 \times 10^4,$$

giving a count rate of approximately  $170 \text{ e}^- \text{ s}^{-1}$ . Thus, equation (21) yields (including the  $\sim 4.4 \times 10^4 \text{ e}^-$  noise due to the dark current) a value of  $S/N \approx 5$  for a  $17^{th}$  magnitude star.

### 3.4 The Light Curve for HR 4646

A systematic difference in the differential magnitudes between the January and February observing runs was discovered and calculated as follows. The mean values of  $v_{2-3}$  (check - comparison), and  $v_{1-3}$  (program - comparison) were calculated for sections of the January and February data. For  $v_{2-3}$ , the January data have an average of  $1.^m776$  while the February data have an average of  $1.^m724$ . The difference is  $0.^m052$ . This is consistent with the calculations of average values for  $v_2$  (check) and  $v_3$  (comparison). The average value of  $v_2$  increases by  $13.^m562 - 13.^m541 = 0.^m021$  and the average value for  $v_3$  decreases by  $11.^m786 - 11.^m817 = -0.^m031$ . For the mean of  $v_{1-3}$  between phases 0.40 and 0.60 (unbroken redundant coverage), the January data have an average of  $-1.^m776$ , while the February data have an average of  $-1.^m828$ . The difference is again  $0.^m052$ . Thus to correct for this

difference, the first set of data was lowered  $0.^m052$  relative to the second. Unfortunately, there was no other star in the field bright enough to serve as a second check star. The shift may be due to variation in the comparison and check star. One would not suspect that the changes made in the system between the two runs, that is, the increasing of exposure length and the rotation of the camera, had a significant effect. The increase in exposure lengths from 0.35 seconds to 0.50 seconds decreased the effect of slow shutter speed. Rotating the camera between the two runs placed the stars in different positions on the detector. The combination of these two changes might account for some small difference in magnitudes between runs, but a more reasonable explanation is that one or both of the comparison stars is a photometric variable.

The data of three nights, January 20/21, January 22/23, and February 11/12 were rejected due to poor quality, ie. an abnormally high degree of scatter ( $\sim 2\times$ ) in comparison with the rest. Poor sky conditions and occasional weak auroral activity were factors throughout these runs. A plot of the remaining data for magnitude differences between program and comparison, in the sense  $v_1 - v_3$ , is presented in Figure 16. The data points were phased with respect to the period given by Abt (1961) of  $1.^d2709334$  and computed from his epoch of maximum radial velocity  $T_0 = \text{JD } 2436758.245$ . Finally, the observations were averaged in 100 phase bins. The 99 normal flux points are presented in Table 4 and are plotted in Figure 17. The highest value for flux was arbitrarily set to 1.000. Note that the data, as presented, have not been transformed from the local to the standard UBV system.

An analysis of the internal errors in magnitudes was carried out in § 3.2. This included the effects of both processing noise (readout noise, truncation, averaging correction frames, zero-level correction, bias subtraction, and flat-fielding) and observational noise (scintillation noise and stochastic

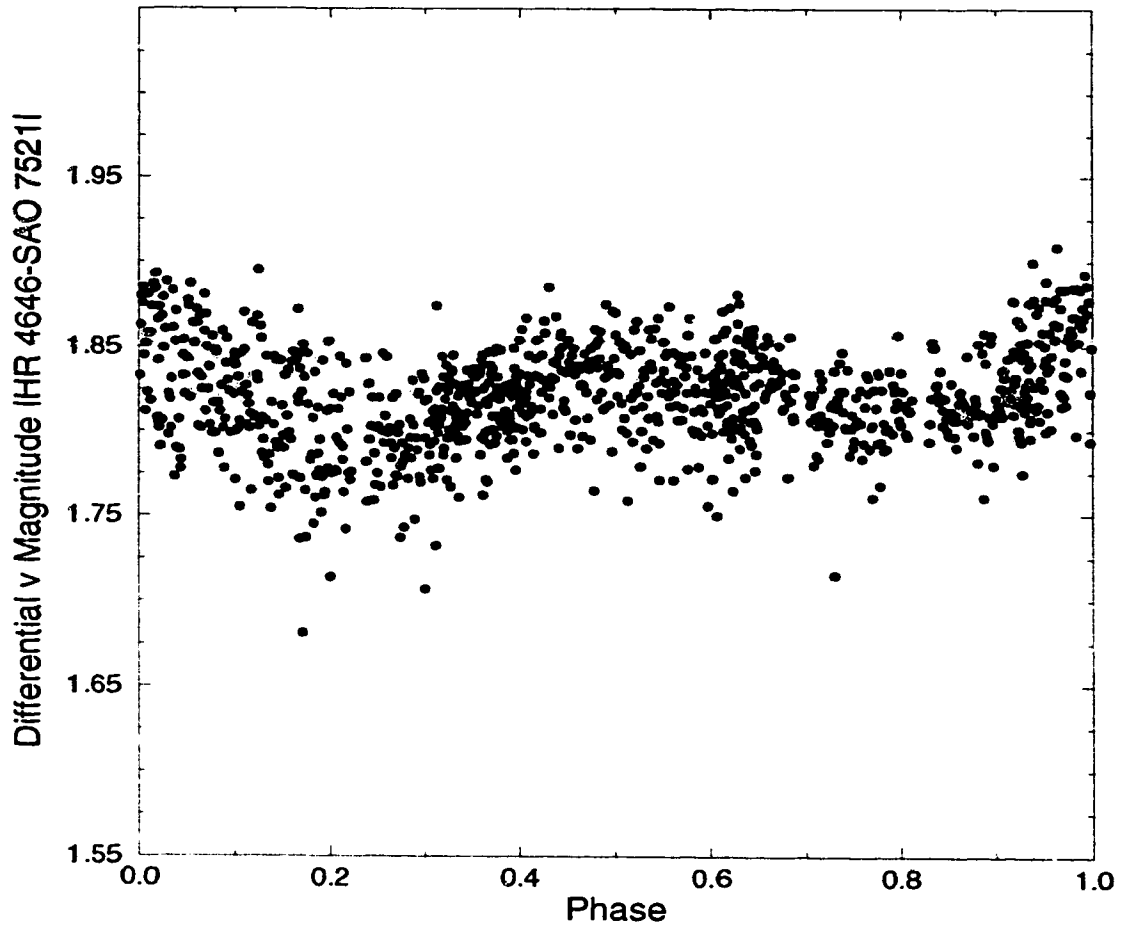


Fig. 16 - Plot of the differential magnitudes  $v_1 - v_3$  for the remaining 1030 data points. The data have been phased using Abt's period of 1.<sup>d</sup>2709334.

TABLE 4  
Photometric Data for HR 4646 Phased in 0.01 Phase Bins

Phase	$v_{1-3}$	$\sigma_{s.d.}$	Flux	$\sigma_{s.d.}$	N	Phase	$v_{1-3}$	$\sigma_{s.d.}$	Flux	$\sigma_{s.d.}$	N
0.000	1.855	0.024	0.995	0.022	11	0.500	1.831	0.019	0.974	0.017	9
0.010	1.854	0.032	0.994	0.029	10	0.510	1.817	0.029	0.961	0.026	9
0.020	1.841	0.036	0.983	0.033	10	0.520	1.827	0.025	0.970	0.023	10
0.030	1.831	0.034	0.974	0.031	10	0.530	1.831	0.022	0.974	0.020	8
0.040	1.814	0.027	0.959	0.025	8	0.540	1.818	0.029	0.962	0.026	10
0.050	1.861	0.020	1.000	0.018	8	0.550	1.838	0.018	0.980	0.016	9
0.060	1.841	0.027	0.983	0.025	11	0.560	1.821	0.022	0.965	0.020	10
0.070	1.826	0.021	0.969	0.019	9	0.570	1.833	0.025	0.975	0.023	9
0.080	1.821	0.028	0.965	0.025	9	0.580	1.810	0.016	0.955	0.015	9
0.090	1.822	0.019	0.966	0.017	8	0.590	1.812	0.026	0.957	0.024	8
0.100	1.816	0.029	0.960	0.026	13	0.600	1.819	0.024	0.963	0.022	18
0.110	1.819	0.029	0.963	0.026	10	0.610	1.829	0.024	0.972	0.022	18
0.120	1.831	0.033	0.974	0.030	11	0.620	1.827	0.030	0.970	0.027	18
0.130	1.793	0.027	0.940	0.025	8	0.630	1.827	0.025	0.970	0.023	18
0.140	1.805	0.029	0.951	0.026	9	0.640	1.819	0.025	0.963	0.023	18
0.150	1.808	0.022	0.953	0.020	10	0.650	1.836	0.010	0.978	0.009	8
0.160	1.819	0.038	0.963	0.034	12	0.660	1.838	0.011	0.980	0.010	8
0.170	1.788	0.052	0.936	0.047	9	0.670	1.829	0.011	0.972	0.010	9
0.180	1.788	0.025	0.936	0.023	10	0.680	1.820	0.022	0.964	0.020	9
0.190	1.792	0.036	0.939	0.033	8	0.690	-	-	-	-	-
0.200	1.779	0.036	0.928	0.033	10	0.700	1.811	0.015	0.956	0.014	6
0.210	1.796	0.032	0.943	0.029	9	0.710	1.810	0.017	0.955	0.016	9
0.220	1.790	0.023	0.938	0.021	3	0.720	1.806	0.007	0.951	0.006	8
0.230	1.794	0.036	0.941	0.033	3	0.730	1.815	0.035	0.959	0.032	10
0.240	1.793	0.022	0.940	0.020	9	0.740	1.804	0.014	0.950	0.013	8
0.250	1.810	0.025	0.955	0.023	8	0.750	1.806	0.012	0.951	0.011	9
0.260	1.797	0.017	0.944	0.016	8	0.760	1.810	0.017	0.955	0.016	8
0.270	1.777	0.021	0.926	0.019	10	0.770	1.805	0.025	0.951	0.023	10
0.280	1.791	0.023	0.938	0.021	8	0.780	1.806	0.015	0.951	0.014	8
0.290	1.805	0.024	0.951	0.022	8	0.790	1.822	0.016	0.966	0.015	8
0.300	1.790	0.029	0.938	0.026	12	0.800	1.813	0.011	0.958	0.010	10
0.310	1.807	0.027	0.952	0.025	20	0.810	1.819	0.000	0.963	0.000	1
0.320	1.809	0.022	0.954	0.020	15	0.820	1.794	0.000	0.941	0.000	1
0.330	1.808	0.018	0.953	0.016	20	0.830	1.830	0.016	0.973	0.015	9
0.340	1.816	0.011	0.960	0.010	12	0.840	1.813	0.011	0.958	0.010	8
0.350	1.823	0.015	0.966	0.014	10	0.850	1.807	0.011	0.952	0.010	9
0.360	1.812	0.024	0.957	0.022	21	0.860	1.819	0.010	0.963	0.009	10
0.370	1.820	0.018	0.964	0.016	17	0.870	1.810	0.007	0.955	0.006	7
0.380	1.810	0.013	0.955	0.012	17	0.880	1.818	0.032	0.962	0.029	9
0.390	1.817	0.019	0.961	0.017	17	0.890	1.814	0.024	0.959	0.022	9
0.400	1.825	0.018	0.968	0.016	20	0.900	1.819	0.010	0.963	0.009	8
0.410	1.820	0.018	0.964	0.016	13	0.910	1.813	0.018	0.974	0.016	12
0.420	1.832	0.021	0.975	0.019	8	0.920	1.823	0.023	0.966	0.021	19
0.430	1.840	0.021	0.982	0.019	10	0.930	1.836	0.027	0.978	0.025	18
0.440	1.833	0.021	0.975	0.019	11	0.940	1.840	0.022	0.982	0.020	11
0.450	1.833	0.018	0.975	0.016	9	0.950	1.845	0.028	0.986	0.025	12
0.460	1.824	0.018	0.967	0.016	9	0.960	1.858	0.031	0.998	0.028	9
0.470	1.830	0.027	0.973	0.025	11	0.970	1.851	0.018	0.992	0.016	11
0.480	1.833	0.017	0.975	0.016	8	0.980	1.859	0.027	0.999	0.025	9
0.490	1.841	0.025	0.982	0.023	10	0.990	1.859	0.027	0.999	0.025	9

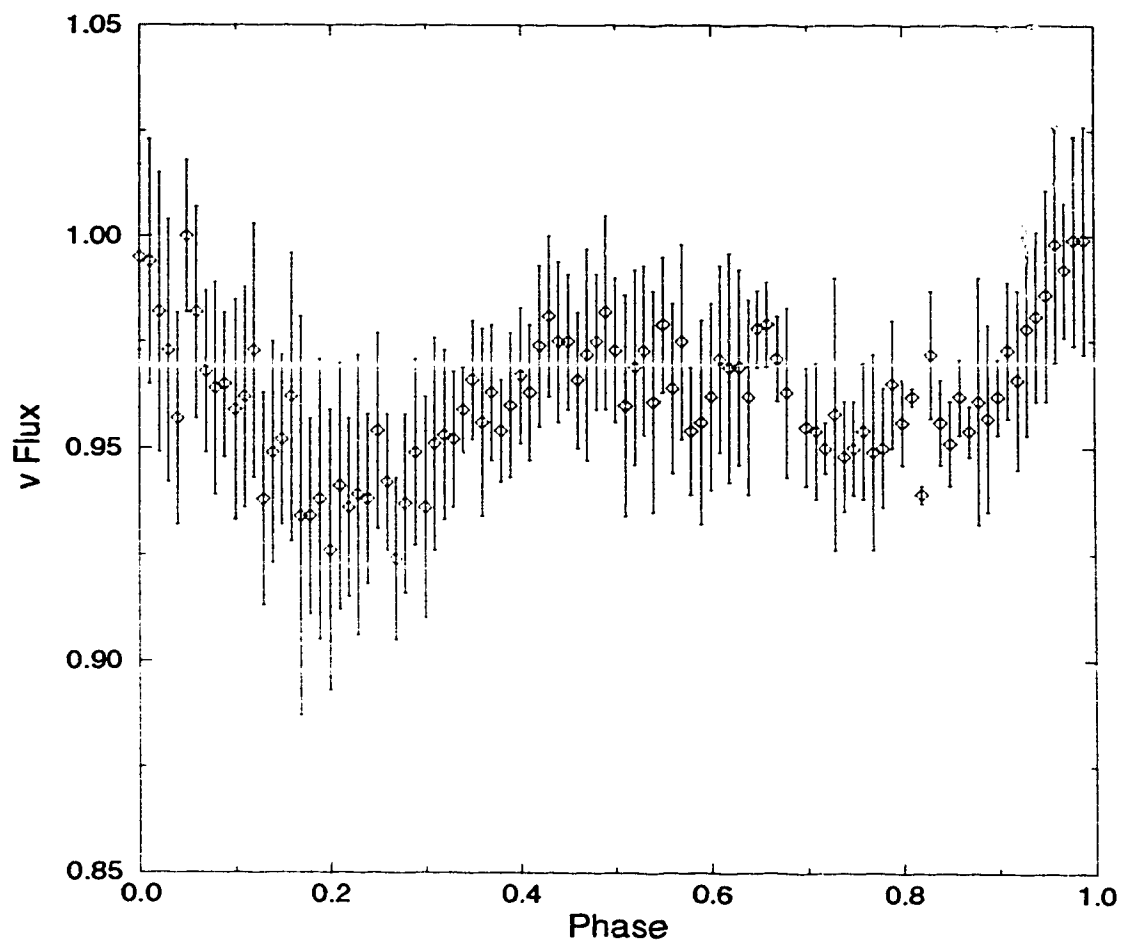


Fig. 17 - Plot of normal points in 100 phase bins. Phasing is with respect to a period of  $1.^{\text{d}}2709334$ .

noise due to sky and source photons). Estimates of the internal errors in magnitudes were calculated. The uncertainty in the differential magnitude  $v_1 - v_3$ , was found to be  $\sigma_{1-3}$ , was  $0.^m007$ . The scintillation for one star per observation was estimated to be  $\sigma_{\text{scint}} \approx 0.^m013$ . That is, the contribution of scintillation to the errors in observations should be  $\sim 0.^m02$ . The sum of these sources is then between  $0.^m02$  and  $0.^m03$ , which is consistent with the scatter in observations. Values for  $\sigma_{\text{s.d.}}$  for the data averaged in 0.01 phase bins (approximately 20 minute intervals) are tabulated in Table 4. A typical value is  $0.^m025$ .

No attempt was made to optimize the photometry carried out on the frames other than to omit dark-corrections during processing. As a final test to see if the scatter in the final light curve could be reduced, aperture photometry as per § 3.2.2 was carried out on groups of unprocessed frames. As expected, this did not decrease scatter. For example, the average of  $v_1 - v_3$  for the 10 observations starting with the one depicted in Figure 11 yields a value of  $\sigma_{\text{s.d.}} = 0.^m045$ .



## 4. MODELING OF HR 4646

### 4.1 A Simple Model

#### 4.1.1 Purely Ellipsoidal Variability

In order to create an approximate model of HR 4646 one can start by assuming that the observed photometric variability is due entirely to ellipsoidal distortion of the primary star. Since the two maxima of the light curve are not obviously asymmetric, reflection effects are neglected and the situation can be illustrated by a simple result due to Binnendijk (1960). The observed intensity  $I_{obs}$  is given by the following expression:

$$I_{obs} = I_{max} - I_0 \cos(2\theta), \quad (44)$$

where

$$I_0 = \frac{1}{2} \frac{15 + u}{15 - 5u} (1 + \tau) \varepsilon \sin^2 i, \quad (45)$$

and where  $I_{max}$  is maximum light,  $u$  and  $\tau$  are the limb and gravity darkening coefficients,  $\varepsilon$  is the ellipticity of the star and  $i$  is the orbital inclination. Thus, from the form of this expression one would expect the light curve of an ellipsoidal variable to vary predominantly as  $\cos(2\theta)$ .

#### 4.1.2 Analysis of the Model

To test the model, that is, to see if the light curve varies predominantly as  $\cos(2\theta)$ , a Fourier series of the form

$$I = \alpha_0 + \sum_{i=1,2} (\alpha_i \cos i\theta + \beta_i \sin i\theta), \quad (46)$$

where  $\theta$  is the orbital phase measured from the time of maximum velocity, was fitted to the data. Linear regression analysis was used to perform a Fourier least-squares fit for the first 4 terms. The coefficients along with standard errors are presented in Table 5. The residual error in the fit is

roughly 0.010 in flux. The dominance of the  $\cos 2\theta$  term supports the suggestion that HR 4646 is an ellipsoidal binary system. The Fourier series is plotted with the observations in Figure 18. Also note that the value of the Fourier fit at phase 0.0 and 1.0 is approximately 0.985 flux. Due to the high degree of scatter in the data this was taken as an estimate of the flux at maximum light. Thus, after this analysis 0.015 was added to the flux of each datum.

## 4.2 Spectroscopic Data

The most recent radial velocity data for HR 4646 are due to Abt (1961). HR 4646 was included in a campaign to determine the frequency of binaries among Am stars. Observations were made with the McDonald spectrograph in 1960 and yielded 9 radial velocities which are presented in Table 6 and are plotted with respect to phase in Figure 19. Abt states the errors in velocity to be on the order of a few  $\text{km s}^{-1}$ . Abt determined the spectral type for HR 4646 as A5 (Ca II K), F2 (Hydrogen), and F5 IV (metals). The elements from Abt's orbital solution are also used in the present analysis and are presented in Table 7.

## 4.3 A More Sophisticated Model

### 4.3.1 Estimation of System Parameters

Typical values listed for the mass and radius of A5 stars from tables can be used to estimate for the primary star:  $M_1 \approx 2.1M_\odot$  and  $R_1 \approx 1.7R_\odot$  (Popper 1980, Wolff 1983) These can be used to constrain the values for the secondary via the mass function

$$f(M) = \frac{M_2^3 \sin^3 i}{(M_1 + M_2)^2}. \quad (47)$$

Now,  $\sin i \leq 1$  which implies

$$f(M) \leq \frac{M_2^3}{(M_1 + M_2)^2}. \quad (48)$$

TABLE 5

Fourier Coefficients for Photometric Variation of HR 4646

$\alpha_0$	$\alpha_1$	$\alpha_2$	$\beta_1$	$\beta_2$
0.963	0.002	0.017	-0.006	-0.001

standard error of coefficients =  $\pm 0.001$

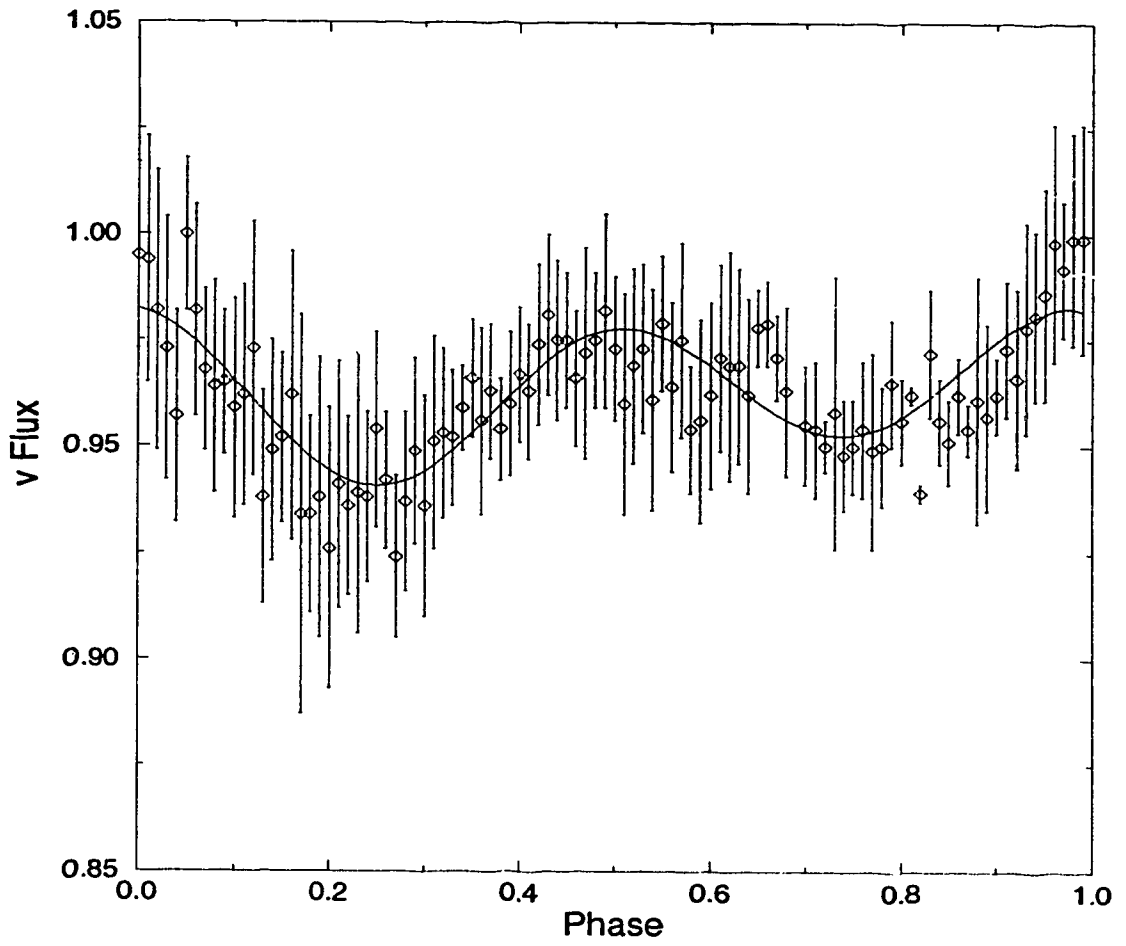


Fig. 18 - v flux observations of HR 4646 phased in bins of width 0.01. Phasing is with respect to a period of  $1^d.2709334$  and from epoch date  $T_0 = \text{JD } 2436758.245$ . The solid line represents a least-squares, fourth-order Fourier fit to the data.

TABLE 6  
Radial Velocities for HR 4646

JD	Phase	$v$ (km s <sup>-1</sup> )
744.783	0.408	-62.4
745.712	0.139	+44.3
746.612	0.847	+41.2
746.691	0.910	+54.1
747.639	0.655	-42.1
764.672	0.057	+63.2
765.636	0.815	+23.2
766.663	0.623	-51.4
771.650	0.547	-67.2

epoch=JD+2436000.000

TABLE 7  
Spectroscopic Orbital Elements of HR 4646

Element	Value
$P$	$1.^d2709334 \pm 0.0000007$
$T_0$	JD 2436758.245
$\gamma$	-2.2 km s <sup>-1</sup>
$K$	69.8 km s <sup>-1</sup>
$e$	0.00 (assumed)
$a_1 \sin i$	$1.220 \times 10^6$ km
$f(M)$	$0.0449 M_\odot$

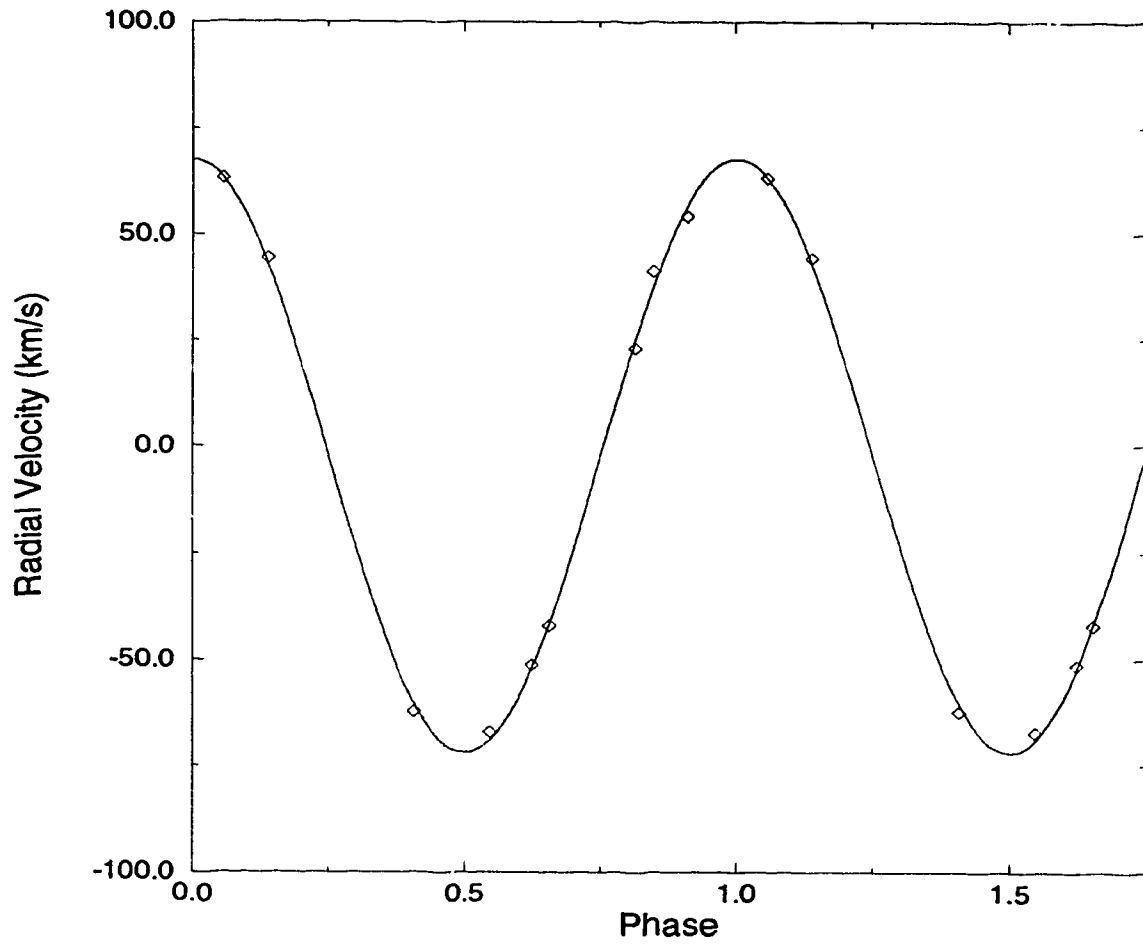


Fig. 19 - Radial velocities for HR 4646 plotted against phase. Phasing is with respect to a period of  $1.^d2709934$ . A sine-wave approximation to the radial velocity curve with an amplitude of  $69.8 \text{ km s}^{-1}$  is plotted along with the data (valid in the case of approximately circular orbits).

mainly varying, say, inclination  $i$  and secondary temperature  $T_2$ , until an adequate fit is achieved.

#### 4.3.2 Wilson-Devinney Code Applied to HR 4646

A version of the Wilson-Devinney (1971) DC light curve fitting routine, capable of simultaneously fitting both photometric fluxes and radial velocities, was applied to the data (see Martin, Hube, and Lyder 1990 and references therein for a discussion of this package). It was chosen due to its availability to the author and its commonly accepted use for modeling close binary systems. A solution is obtained by comparing the observed data to a set of synthetic light and radial velocity curves. DC then returns differential corrections to the preselected variable parameter set. Convergence is signalled by parameter corrections becoming smaller than their internal errors. The method followed was guided to a certain extent by that outlined in Martin, Hube, and Lyder (1990). There, the two stars of the ellipsoidal variable 42 Per are assumed to be tidally locked with synchronized rotational and orbital motion. In the present case the high degree of scatter in the photometric data and only small amount of radial velocity data made it difficult to constrain the variable parameters. Although convergence was not possible, a rough fit was obtained. The quality of the fit was judged by the output value for residual error. A typical value of 0.005 or less suggests that the DC code is converging to a solution.

##### 4.3.2.a *The Operation of LC*

Binary Maker (Bradstreet 1993), which operates the LC, or light curve component of the Wilson-Devinney code, was used to generate several initial synthetic light curves to compare to the data. Some intuition was gained as to the appropriate range of values to use in an attempt to find a solution by a more quantitative method. Of particular interest were parameters which

could not be estimated easily by other means, such as the potentials and the inclination. Typical curves that roughly fit the data had values for surface potential between approximately 3.0 and 4.0 and inclinations between  $60^\circ$  and  $75^\circ$ .

#### 4.3.2.b *The Operation of DC*

The method adopted was as follows. The value for secondary temperature  $T_2$  was set initially to 8500 K, the same value as the primary. Both of the potentials,  $\Omega_1$  and  $\Omega_2$ , were set initially to 3.5. The value of  $q$  was set to 0.34, both values for limb darkening to  $u = 0.50$ , and both values of gravity darkening to  $\tau = 0.80$ . At first, all the parameters were varied independently by  $\pm \sim 20\%$ . The inclination  $i$  was set initially at  $75^\circ$  and variation of this parameter returned corrections which centered on  $65^\circ$ . The changes in secondary temperature  $T_2$  and the potentials  $\Omega_1$ ,  $\Omega_2$  reduced the returned value of residual error the most (from  $\approx 0.09$  to  $\approx 0.07$ ). It was decided that the values for  $T_2$ ,  $\Omega_1$ , and  $\Omega_2$  would mainly be the parameters that would be varied. The values from parameter set (51), as well as the inclination, were fixed. The values for  $T_2$ ,  $\Omega_1$ , and  $\Omega_2$  were varied in turn, each independently. At first they were varied by  $\approx \pm 10\%$  (the amount and in the sense suggested by DC). Later, the changes decreased to  $\approx \pm 5\%$ . Periodically, one of the fixed parameters was varied by  $\approx 10\%$  in order to see if this would change the situation. The returned residual errors did not increase drastically ( $\leq \pm 0.01$ ). By this method, the residual error values dropped to approximately 0.025 after 25 iterations. The residual error values could not be reduced beyond this.

The final results are presented in Table 8. The uncertainties in each of the values are taken to be  $\approx \pm 5\%$  since this was the amount the parameters were varied before iterations stopped. It should be noted that following the DC code, even if a solution is found, does not guarantee uniqueness.



Furthermore, it is a path-dependent process. The initial choices for variable parameters and their initial values will preclude a wide class of solutions. In this case, there may be many choices of values for any of the above parameters which could give a slightly lower value for the residual error.

#### 4.3.3 Results / Analysis

Binary Maker was used to generate several light curves to illustrate the fit of the WD model to the data, As an example, the basic model in Table 8 is plotted for a few different choices of the parameters  $T_1$ ,  $T_2$ , and  $i$ . In Figure 20, the data are plotted along with models with ranges of  $6000K \leq T_1 \leq 10000K$  and  $5000K \leq T_2 \leq 6000K$ . Also, models with  $60^\circ \leq i \leq 70^\circ$ , are plotted in Figure 21. These suggest ranges of model parameter values which will fit the data within their scatter. Also, one can see the possibility of partial eclipses (deeper as inclination increases) being hidden by the large uncertainties in the data. In all typical models the secondary component has a diameter about half that of the primary and the photometric variation is principally due to ellipsoidal distortion of the primary component. A plot of the radial velocity data along with the WD synthetic radial-velocity curve (for the model described by the parameters in Table 8) is given in Figure 22. The preliminary model is then described by

$$\begin{aligned}
 i &= 65 \pm 3^\circ \\
 q &= 0.34 \pm 0.02 \\
 T_1 &= 8.5 \pm 0.4 \times 10^3 K \\
 T_2 &= 5.0 \pm 0.3 \times 10^3 K \\
 R_1 &= 2.6 \pm 0.1 R_\odot \\
 R_2 &= 1.0 \pm 0.1 R_\odot \\
 a &= 6.97 R_\odot
 \end{aligned} \tag{52}$$

where the quoted errors in  $i$ ,  $q$ , and  $T$  are the estimated 5% uncertainties from the application of the DC code. Judging from the fit of the resulting

TABLE 8  
DC Output for HR 4646

Element	Value
$i$	$65 \pm 3^\circ$
$q$	$0.34 \pm 0.02$
$T_1$	$8500 \pm 400$ K
$T_2$	$4500 \pm 200$ K
$\Omega_1$	$3.1 \pm 0.2$
$\Omega_2$	$3.6 \pm 0.2$
$r_1(\text{pole})$	$0.36 \pm 0.02$ $a$
$r_1(\text{point})$	$0.39 \pm 0.02$ $a$
$r_1(\text{side})$	$0.37 \pm 0.02$ $a$
$r_1(\text{back})$	$0.38 \pm 0.02$ $a$
$r_2(\text{pole})$	$0.15 \pm 0.01$ $a$
$r_2(\text{point})$	$0.15 \pm 0.01$ $a$
$r_2(\text{side})$	$0.15 \pm 0.01$ $a$
$r_2(\text{back})$	$0.15 \pm 0.01$ $a$

light curves to the data, however, one would suspect that these formal errors underestimate to a great extent the actual range of uncertainty in the parameters. For example, the values of  $T$  are more likely to have uncertainties  $\sim 2000$  K while the uncertainties in the values of  $i$ ,  $q$ , and  $\Omega$  are more likely  $\sim 10\%$ . The range of values for primary radius corresponding to these uncertainties is  $2.1R_{\odot} \leq R_1 \leq 2.6R_{\odot}$ .

It should be again stressed that this model is only very weakly constrained. This is due to the availability of only a small amount of radial velocity data and the high degree of scatter in the photometric data. The model could be improved by higher quality multi-colour photometry, a greater amount of radial velocity data, and the possible detection of short eclipses. The latter, if present, would facilitate the modeling of the system by providing a geometric constraint on the radius of the secondary.

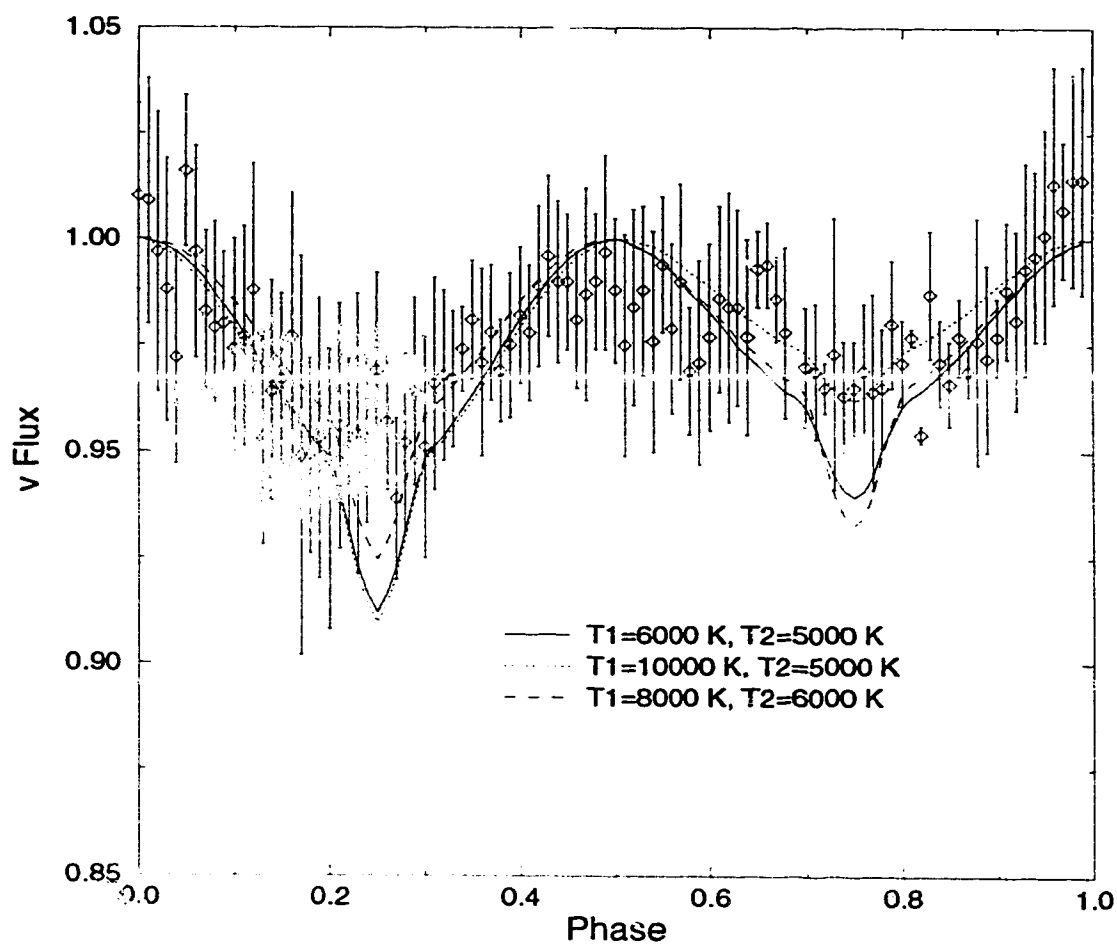


Fig 20 - The data are plotted along with synthetic light curves for models with ranges for parameters:  $6000\text{K} \leq T_1 \leq 10000\text{K}$  and  $5000\text{K} \leq T_2 \leq 6000\text{K}$ . All the other parameters are as listed in Table 8.

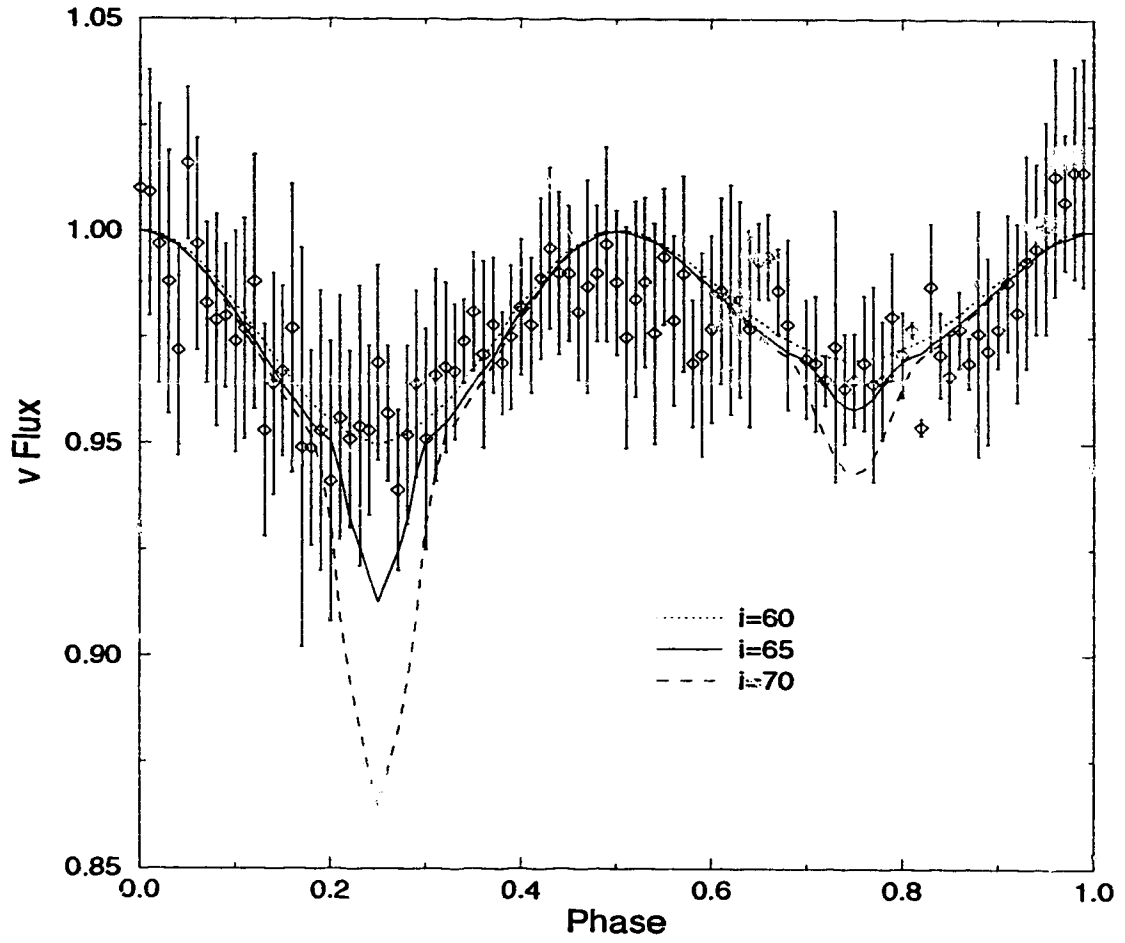


Fig 21 - Light curves for models with  $60^\circ \leq i \leq 70^\circ$  are plotted together with the data to illustrate the possibility of partial eclipses (deeper as inclination increases) being hidden in the scatter. All the other parameters are as listed in Table 8.

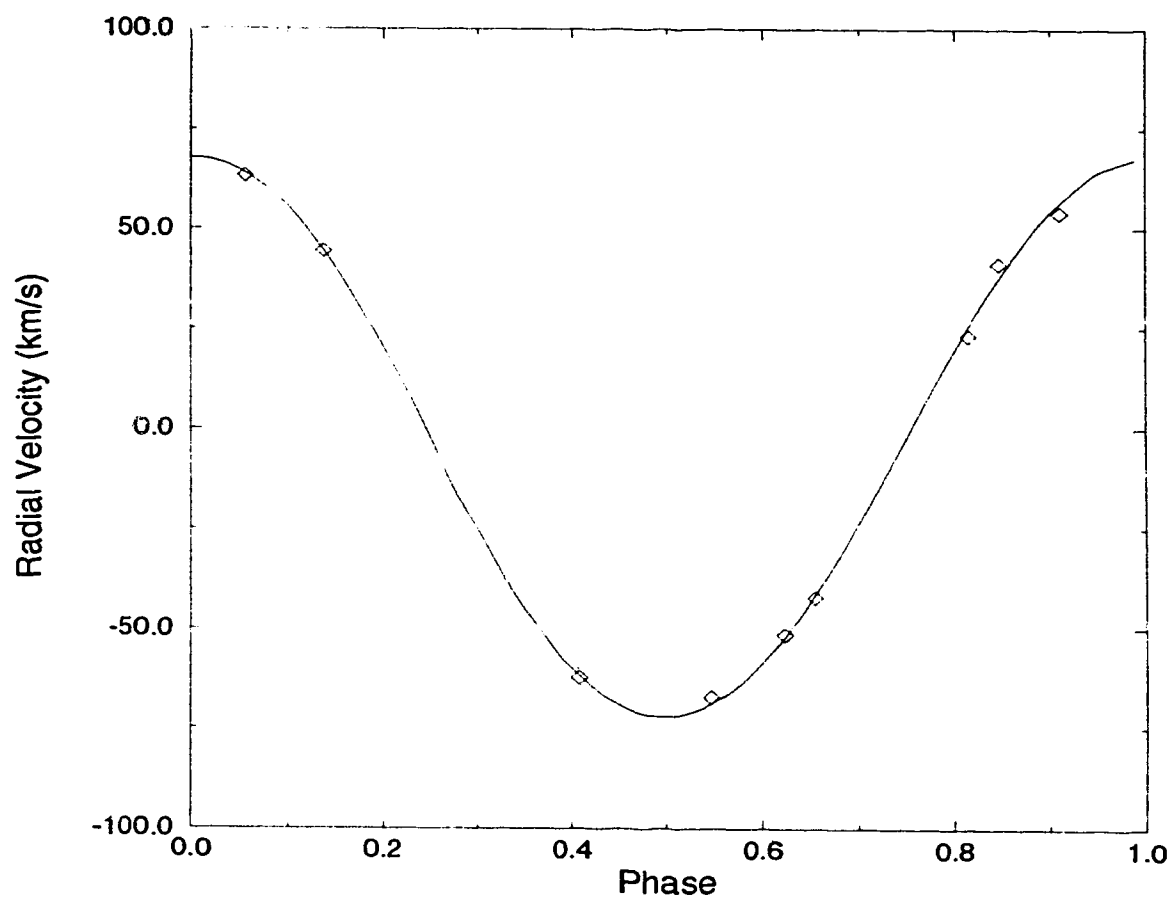


Fig 22.- Fit between the radial-velocity data for HR 4646 and the synthetic radial-velocity curve produced by the WD-code.

## 5. CONCLUSIONS

### 5.1 The Devon CCD Imaging System/Stellar Photometer

The final result of the present work is a basic overview of the characteristics of the CCD camera and the completion of the first step in developing an effective operating procedure for a future CCD photometer. The protocols developed for data handling and processing provide for relatively fast and, in the case of reductions, largely automated operation. The basic parameters of the CCD system are listed in Table 9. Where the values differ from manufacturer specifications, the latter are shown in brackets. The complete system, including observing procedures, data transfer protocols, and data processing, demonstrated some utility in the collection and reduction of observations for HR 4646.

A theoretical limit on photometry with the present system was discussed. The dark current of  $\sim 50 \text{ ADU pix}^{-1} \text{ s}^{-1}$  and readout noise of  $\sim 80 \text{ e}^-$  yields an estimate of the limiting magnitude of the system ( $S/N \approx 5$ ) of  $V \approx 17^m$  for a 180 second exposure. The work done so far has obtained photometry with a photometric precision of approximately  $0.^m025$  at  $V \approx 5^m$ . Much of this error is attributable to atmospheric scintillation, source photon noise and sky-noise, as well as noise associated with processing the frames. This is worse than the  $0.^m003$  precision which is possible with the photoelectric system at Devon. It is also worse than the potential  $0.^m002$  precision which is commonly quoted for CCD imaging systems. The primary problem of obtaining high precision flat-fields will have to be addressed, as well as issues involving high readout noise and dark counts. The regime of short exposure times may need to be avoided by a greater margin (exposures limited to longer than 1 second) to avoid the problem of slow shutter speed. It is therefore possible that high precision photometry cannot be obtained

**TABLE 9**  
**Devon Observatory CCD Imaging System Parameters**

	<b>Telescope</b>	
Aperture		0.5 m
Focal Ratio		$f/8$
Scale at Focus		51.1 arcsec mm <sup>-1</sup>
	<b>CCD</b>	
Pixels		$27 \times 27 \mu\text{m}^2 = 1.38 \times 1.38 \text{ arcsec}^2$
Full Frame		$512 \times 512 \text{ pix}^2 = 11.8 \times 11.8 \text{ arcmin}^2$
Operating Temperature		-27 °C (-30 °C)
CCD Gain		$4.9 \pm 0.2 \text{ e}^- \text{ ADU}^{-1}$
Readout Noise		$79 \pm 2 \text{ e}^- (< 10 \text{ e}^-)$
Signal Maximum		$320,000 \text{ e}^- \text{ pix}^{-1} = 65,535 \text{ ADU pix}^{-1}$
Dynamic Range		4100
Dark Current		$245 \text{ e}^- \text{ pix}^{-1} \text{ s}^{-1} (\sim 5 \text{ e}^- \text{ pix}^{-1} \text{ s}^{-1} @ -30^\circ\text{C})$
Dark Current Rate		$108 \pm 5 \text{ e}^- \text{ pix}^{-1} \text{ s}^{-1} \text{ K}^{-1}$
Peak Quantum Efficiency		$\sim 80\% (\lambda \approx 400\text{-}800 \text{ nm})$
	<b>Data Storage</b>	
Full Frames in RAM		Maximum 20
Full Frames on Hard-Disk		Maximum 450
Full Frames on Tape-Cartridge		Maximum 250



with the present system for apparently very bright stars such as the  $V \approx 5^m$  HR 4646. In this case, stars such as the  $V \approx 9^m$  magnitude B 1413 and B 1414 may provide future workers with a better means of testing the CCD photometer and assessing its noise characteristics. It is hoped that future workers will benefit from the present discussion while making improvements to both the camera and its operating procedures.

## 5.2 The Ellipsoidal Variable HR 4646

The results of the Wilson-Devinney code seem to confirm the results of the simple model. They are strongly indicative of tidal distortion in the primary component of HR 4646 leading to its principally ellipsoidal photometric variability. The best models have a primary component large enough to reproduce the length and depth of both primary and secondary minima while not so large as to require deep eclipses.

An observed value for projected rotational velocity of the primary component of HR 4646 was published after the present analysis was completed. Abt and Morrell (1995) quote a value of  $78 \pm 10 \text{ km s}^{-1}$  determined from fitting line profiles to the spectra. Line half widths were determined by fitting Gaussian profiles to the lines  $\lambda 4481 \text{ Mg II}$  and  $\lambda 4476 \text{ Fe I}$ . This can provide a check of the internal consistency of the model by assuming tidal synchronization of rotational and orbital velocities (valid for this case of close proximity of primary and secondary components). Under these conditions the following relation between the projected equatorial rotational velocity  $v \sin i$  (measured in  $\text{km s}^{-1}$ ), the radius  $R_1$  (in solar units), and period  $P$  (in days) can be applied (Martin, Hube, and Lyder 1990):

$$v \sin i = \frac{50.6 R_1 \sin i}{P}. \quad (53)$$

Using the quoted value of  $v \sin i = 78 \pm 10 \text{ km s}^{-1}$ , the adopted value for period of  $1.^d2709934$ , and the range of values for primary radius of  $2.1 R_\odot \leq$

$R_1 \leq 2.6R_\odot$ , equation (53) yields an inclination of  $49^\circ \leq i \leq 69^\circ$ . This is consistent with the preliminary model value for orbital inclination:  $i = 65 \pm 5^\circ$  (see Figure 22).

It is hoped that the preliminary result discussed here will generate interest for a follow-up study of this system.

## REFERENCES

1. Abt, Helmut J., 1961, *Astr. J. Suppl. Ser.*, **6**, 37.
2. Al-Naimiy, H.M., 1978, *Ap. & S. S.*, **53**, 181.
3. Batten, A. H., Fletcher, J. M., and MacCarthy, D. G., 1989, *Eighth Catalogue of the Orbital Elements of Spectroscopic Binary Systems*, Victoria, Publ. of the Dom. Astr. Obs..
4. Binnendijk, L., 1960, *Properties of Double Stars*, London, W & J Mackay & Co. Ltd..
5. Bowers, R. L., Deeming, T., 1984, *Astrophysics*, Vol. 1, Boston, Jones and Bartlett Publishers.
6. Bradstreet, D. H., 1993, *Binary Maker 2.0, Users Manual*, Contact Software.
7. Frandsen, S., Dreyer, P., Kjeldsen, H., 1989, *Astron. Astrophys.*, **215**, 287.
8. Gilliland, R. L., Brown, T. M., 1988, *P. A. S. P.*, **100**, 754.
9. Gilliland, R. L., Brown, T. M., Duncan, D. K., Suntzeff, N. B., Lockwood, G. W., Thompson, D. T., Schild, R. E., Jeffrey, W. A., Penprase, B. E., 1991, *A.J.*, **101**, 541.
10. Harris, W. E., 1990, *P. A. S. P.*, **102**, 949.
11. Kjeldsen H., Frandsen, S., 1992, *P.A.S.P.*, **104**, 413.
12. Kopal, Z., 1959, *Close Contact Binary Systems*, New York, John Wiley and Sons.
13. Martin, B. E., Hube, D. P., Lyder, D. A., 1990, *P.A.S.P.*, **102**, 1153.
14. Martin, B. E., Hube, D. P., Brown, C., 1991, *P. A. S. P.*, **103**, 424.
15. Martin, B. E., Hube, D. P., Steinbring, E., Cartledge, S., 1994, *I. B. V. S.*, Number 4093.

## APPENDIX

### A Manual for the Operation of the Devon Observatory CCD Stellar Photometer

#### Introduction

At the time of writing, the Devon Observatory 0.5 m telescope is configured with its CCD camera temporarily installed at the eyepiece mount with a single V filter. In the near future, however, the camera will be installed at prime focus in a new telescope front-end complete with a filter wheel assembly offering U.B.V.R.I. and  $H_{\alpha}$  as well as  $[O_I]$ ,  $[O_{III}]$ , and  $[S_{II}]$  line filters. One goal of this appendix is to outline the set of observing procedures that have been applied to date and provide a guide to the development of an operating procedure for the telescope in its final form. The main purpose, however, is to develop tested methods and routines for data transfer and reduction procedures applicable for its use as a stellar photometer.

The appendix is in two parts and is intended to guide the user from initial set-up and observation to final light-curve. Section 1 deals with the taking of program and reduction frames and subsequent data transfer protocols, while Section 2 addresses processing steps appropriate for reducing large volumes of photometric data on the available computing platforms.

#### 1. CCD Observations

##### 1.1 Getting Started

The telescope driving/tracking software which runs the 2 channel photometer is adequate for telescope pointing in its present form. This software runs on the IBM PC, hereafter referred to as the Drive Computer, in the Observatory "trailer". After starting up this machine, the drive clock, and the electronics bin in the warm room, run `C:/ oldmain`. Choose a bright

standard star from the menu and set the telescope origin by first centering the 5" telescope on the star and hitting <enter>. The drive software can be used by typing in the star name or coordinates, hitting <enter>, and then <esc>. Then simply use <m> for move telescope, hitting the <data> button on the drive paddle to confirm star position. Next, turn on the PC which runs the camera (hereafter referred to as the Camera Computer), the coolant pump, and the TEC unit.

## 1.2 Camera Start-up

The camera operation software runs in a typical Windows environment, and is adequate for control of all camera functions. It is, unfortunately, not well adapted for taking a long series of exposures. A few simple tricks, however, can serve to alleviate this problem. Start by double-clicking on the HPC-1 icon. The HPC-1 application will automatically perform the initialization procedures necessary for system operation. It will initialize the camera head, close the shutter, and turn on the thermoelectric cooler.

The user is then presented with a set of operations. These are **File**, **View**, **Process**, **Analyze**, **Expose**, and **Initialize**. **File** controls all the data storage operations, including saving and opening of images. The display scale can be controlled by **View**, and simple tasks like false colour mapping and histograms can be obtained through **Analyze**. The image reduction tasks in **Process** are crude at best, and will not be used. The main operations of interest are **Expose** and **Initialize**, which controls the overscan region, integration times, and the taking of reduction frames.

First, go to the **Initialize** option and click on the **Configure** command. Make sure the **Enable** camera switch is on for **Camera 1**. Also, the on/off switch for the TEC is located here, as well as the paths for image and reduction frames. The best choice for the paths is into a single directory, called

for instance **C:/data**. This means that when the frames are transferred to tape, only one directory need be selected for saving.

Next, select the **Expose** option. A dialog box is displayed when the **Exposure Control** function is selected. The controls for overscan and exposure length are really the only functions used here. The **Sub-frame** command allows for a smaller frame size when the focus command is used. This will speed the refresh rate somewhat. As in the case of the TEC, there is an **Enable** switch for the overscan. Make sure this is on. The overscan region is a mean bias level digitized onto the right edge of the frame. IRAF will need this region to set a zero intensity level for all the frames. A good choice for overscan width is 20-30 pixels. There is also an option of enabling an overscan along the top of the image as well as the right hand side. This will probably not be useful, and can be shut off.

Almost all other options can be shut off as well. The **Delay Time** is just a measured pause before the shutter is opened and can be set to 0.000 seconds. **DOS-based focus**, and **Low Gain** are not active with the present set-up. The options **Antibloom** and **Auto Stretch** are intended to control image bleeding and automatically perform reduction adjustments on images. Neither works well enough to be used effectively. Both should be shut off. The **Binning** option enables the pixels to be binned in groups of size say,  $2 \times 2$  and might prove useful in reducing noise under very poor seeing conditions. Otherwise, this option can be disabled.

The integration length is controlled by the command **Exposure Time** and is in seconds. The shortest supported integration length is 0.001 seconds, although anything shorter than 0.1 seconds is not advised due to the slow mechanical shutter speed. The longest possible controlled integration is 7200 seconds, but very high dark current will limit viable exposures to less than approximately 700 seconds.

### 1.3 Focus

After you have selected a bright star on the Drive Computer and centered it in the finder-scope, call up the **Expose** option and select the **Exposure Control** function. Set the integration time to perhaps 0.05 seconds and select **Sub Frame Focus**. If you set the sub-frame size to say,  $100 \times 100$  pixels, the refresh rate is about 15 seconds. Next, turn the Camera Computer monitor towards the warm room window and go into the dome. The screen should be easily visible from the dome. Notice that in the present setup, the E-W and N-S paddle directions for the finder-scope have the same directions in the HPC-1 display. Locate the second mirror focus-motor control buttons at the back end of the telescope. If the focus is not very good, the best method is to adjust the telescope right out of focus in order to know which direction to turn the motor. Then, adjust the telescope into focus with short pulses on the control button. Make sure you wait long enough for the screen to refresh before you hit the focus button again. When the telescope is in focus hit the <esc> key on the Camera Computer.

### 1.4 System Monitoring

It is a good idea to familiarize yourself with the functions available in the **Analyze** option. The preset colour schemes for the **False Color** function are useful for determining the quality of telescope focus. Good focus should be accompanied by concentric rings in the stellar images. There is a sometimes useful **Histogram** option. As well, there is a function for integrating counts along a line or column or in a user defined box. Note that for this 16-bit system, the highest pixel ADU readout is 65,535.

The **Coordinate Window** function will bring up a small display of cursor location as well as a readout of the sensor temperature. However, at present the temperature readout does not function properly. It will rise

when the TEC box becomes too warm, and does not give the proper temperature of the CCD. In future, the temperature will be monitored via a voltmeter at the TEC output jack. If this reading were to fluctuate by more than approximately  $\pm 0.1$  K (0.001 Volts), the TEC would not be operating properly.

First, check the control box. If it feels warm to the touch it has overheated. Make sure the cooling-fan vents are not blocked and that the warm room is not too warm. If this does not work, check in the *CCD Imaging Systems Installation and User's Guide* (1994) for the proper method to re-adjust the TEC set-point temperature.

The other potential source of trouble is that the coolant pump can stop working. Air cavities can form in the catacombs in the camera head. The only way these bubbles can be large enough to stop the pump is if the reservoir bottle has been tipped over while the pump is operating. The best method to remove cavitation is to shut off the pump (and camera) for an hour or so to let air collect at the highest point in the system. Then remove the camera head and rotate it in all directions until the bubbles rise out of the camera head towards the pump intake hose (marked with a white plastic ring). Start the pump. The air will simply bubble out into the reservoir.

## 1.5 Obtaining and Storing Images

You can store up to about 20 images in HPC-1's available memory. These are automatically stored as untitled\*.fts. This should probably be avoided, however, because if HPC-1 hangs before you have a chance to save, you cannot retrieve these images. The best method is to decide on a consistent labelling scheme and immediately save each frame. After you select **Full Frame Exposure**, HPC-1 will automatically operate the shutter, digitize the image, and display it on the screen. Go to the **File** option and select the



**Save As** function. You will find later that saving all program images with labels prefixed by a letter, say `v`, and then a 3 or 4 digit increment will save time when it comes to post-processing the data. You should also check that the camera computer system clock is accurate and thus encoding the correct time to the images. This will also ensure smooth post-processing. The lack of a means for creating macros with HPC-1 will probably soon demonstrate the need for a good labelling scheme. Thankfully, HPC-1 will warn you if you attempt to overwrite.

## 1.6 Reduction Images

Before program observations, and to account for systematic variations preferably during and after observing, you need to take at least 10 to 20 bias frames. These are automatically taken using the function **Bias Field** in the option **Initialize**. Depending on how you have set up your image paths, these will be saved as C:/data/bias.fts. You need to manually relabel these to avoid overwriting and should label them conveniently by, say, a prefix `z` followed by a three digit increment.

For each exposure length you want to be sure to obtain dark frames. Dark counts with this system are very high and for any integration greater than about a second a set of 10 to 20 dark frames is probably advisable if not necessary. There is also an automatic function for this. Use the function **Dark Field** in the option **Initialize**. These will need to be relabelled as well. Use perhaps the prefix `d` followed by a three digit increment.

The automatic function for taking flat frames is not useful. It will automatically use the bias frame saved as C:/data/bias.fts to perform a bias correction on each new flat. You will do all reductions later using IRAF. It is assumed that the user is working with the V filter fixed in the camera mount. Of course, flats would need to be taken in all of the filters used. You can

take acceptable dome flats using the dome lights and the white plastic square fixed to the dome opposite the shutter. Close the shutter, turn the dome so that the square is on the meridian, and carefully point the telescope so that it is centered on the square. Turn the dome lights down low and make sure that there are no shadows falling on the square. You will probably need at least 10-20 flat frames. Take these as you do program images but be sure that exposures are not shorter than about 0.4 seconds. Check the ADU readout levels using the **Analyze** option. You want to try for integrations that are around the 4 to 10 thousand mark. The goal is to have enough counts to incorporate the pixel-to-pixel gain variations. The spectral response of the chip to incandescent light sources is unknown and, of course, the telescope is pointed at a possibly non uniformly illuminated near field object (badly out of focus). This makes dome flats undesirable and one should try to obtain good twilight-sky and/or blank-sky flats. For sky flats taken at twilight, try to obtain flats in a few different telescope positions. The secondary mirror support structure does stick out of the front end and sunlight reflecting off this for a single position might create hot spots. Experiments with blank sky exposures suggest that you can leave the tracking motor off and average a large number of frames in order to eliminate at least faint star streaks. Save each of the dome, twilight-sky, and blank-sky frames with the prefixes `fd`, `ft`, `fb` and three digit increments. Each set can be averaged later and compared.

## 1.7 Data Transfer

At the end of the observing run you will have perhaps a few hundred images. The Camera Computer can hold approximately 400-500 images on hard disk. Although it is now possible to use a network connection to the University in order to transfer files directly, if you have any doubts you can,

and should, copy all images onto 120 Mbyte mini-cartridges. You will have to save some data to tape anyway, because the Sparc-station used to perform data reductions (hereafter referred to as the Processing Computer) usually has only enough available memory to hold 1-3 hundred frames at a time.

Exit HPC-1, shut off the TEC but leave the pump running for a while. Locate the Conner tape drive application icon for **Backup Exec** and double-click on it. If you choose the **Backup** option, everything is automatically set to transfer the contents of C:/data to tape. Simply select the **Select Files** function, highlight the C:/data directory and hit <spacebar>. Select the **Start Backup** command. Conner Backup will automatically create a directory of transferred files and write this to the tape. All that is left is to read the Universal Time code from the WWVB clock in the trailer and note the local time on the Camera Computer. The post-processing software will need this in order to encode the data points with a Julian Date.

If you only save to tape, you will of course have to transfer the data from tapes to the Processing Computer. This can be accomplished by transferring the data from tape to the PC in office P501 (hereafter referred to as the Transfer Computer). This too is pre-set. Start up the Conner Backup software here using the command C:/cbackup. Make sure drive D:/ is empty, which leaves about 60 Mbytes of available space (approximately 100 frames). When you select the **Start Restore** function in the option **Restore**, Conner Backup will prompt you for a destination drive for the files. Type in D:/. Conner Backup will automatically recreate the directory C:/data on drive D:/. Now, all that remains is to use an **ftp** command to transfer files to the Processing Computer as they are needed.

## 2. Image Processing/Data Reduction

The goal is to process all the data as efficiently as possible with the

available computing power. Since the Processing Computer has a somewhat limited available memory, the best method seems to be one which reduces the amount of space used on the disk. The idea is to process the \*.fts files as they come in from the Transfer Computer. Then, photometry can be carried out on the processed frames in one step, greatly reducing the amount of work. The following steps are geared towards the processing of a set of observations in one filter. It should be readily apparent, however, where the labelling scheme v\*.imh could be replaced with, say, b\*.imh or u\*.imh, etc.. It would only be necessary to have flat fields for these other filters.

## 2.1 Processing the Frames

It is assumed here that you are at least familiar with IRAF and know how to edit parameter files using **epar**. Also, you need to call up images on the display software **SAOIMAGE**. The processing steps outlined here are basically “stock” commands outlined in IRAF documentation such as *IRAF User Handbook Volume 1A: IRAF System* (Valdes 1987) and you should familiarize yourself with these manuals.

The best way to start is to import your reduction images to the Processing Computer into the IRAF directory. You can, for the present discussion, use the following set-up. Open an **xterm** window on the Processing Computer in room P504 (called stellar, with address 129.128.7.50). The **xterm** tool is located in /usr/openwin/demo. Logon again to stellar as **iraf**, run **saoimage** in background by entering **saoimage &**, and then type **cl**. IRAF is now running from directory /kepler/users/iraf/local. You can put your data into a sub-directory set aside for \*.fts files, called, say, /.../iraf/local/pixel. Then use the command **rfits** in order to convert these \*.fts files to IRAF files with an image-header. You can erase all of the \*.fts files once they are transferred to IRAF format.

Open the package **ccdred** in **imred**. The next step is to display one of

the flat fields to determine the regions of good overscan information as well as the region to trim. The package **ccdred** will need to know these regions, known as **biassec** and **trimsec** with the notation **\*.imh [x1:x2,y1:y2]**. You can display this by typing in **disp** and entering **f0001.imh**. Also, you should get an intensity readout along a column by typing in **implot f001.imh 1**. Take only perhaps the outside 15 columns of the overscan (some of the columns closer to the image area are usually corrupted). Trim as much as possible in the image, but make sure to leave a margin of 40 to 50 pixels around the coordinates of stars used in the analysis. Process the bias frames first. Use the package **zerocombine** with the default values at start-up. This will have **combine=average** and **reject=minmax**. For the most part the default settings in all the following commands will also be used. The advantages of some of the more sophisticated options are usually fairly modest, but where appropriate, changes will be outlined. If you are following the suggestions for labels, your value for **input** will be **z\*.imh** and a good choice for **output** would be **Zero**. This output is a nightly averaged bias frame and all the input bias frames can be erased. Now you can zero level and bias correct the rest of the reduction frames. First, set up the the parameters for **ccdproc**. The settings are all default values with the following exceptions. For now, you only want to correct for the overscan and bias, and trim the images. Thus, **oversca=yes**, **trim=yes**, and **zerocor=yes**, but all other corrections are set to **no**. Set the **biassec** and **trimsec** to the values determined in the last step. If you leave the value of **ccdtype** unset, **ccdproc** will automatically correct the rest of the images. Check the darks. If the counts are significant you can easily combine them as a super dark-field called say, **Dark**. This can be accomplished with **darkcombine** with the default setup, with **input=d\*.imh** and **output=Dark**. You will have to use **ccdproc** to dark correct the flat-fields before you go on to the

next step.

In this discussion, only one set of the flat-fields is used, preferably good twilight sky-flats. It has been noticed that with sufficiently exposed dome (and sky) flats, there is a central bright patch in the field. You will notice that this appears (after proper bias and dark corrections, of course) in images as well. It is probably due to the telescope optics. In any case, with the present analysis, it should be possible to remove all large scale variations down to  $\sim 2\%$  variation in background intensity across the fields. Combine the flat-fields with **flatcombine**. Good results can be obtained using the settings **combine=average** and **reject=avsigclip**. Here, the **input** would be **f\*.imh** and the **output** perhaps **Flat**. Erase all of the input flats (and darks).

Now, you should be left with only two super-fields (three if you have significant dark counts) to reduce all of the data. Start importing program images. The best choice is 100 at a time, as this is the maximum number that can be stored in the Transfer Computer. Once a batch of 100 \*.fts files are imported to the pixel directory, convert them to IRAF image header files and erase the input. Then use **ccdproc** to process the IRAF images. You only need to change the setting for **images** to **v\*.imh** and make sure **flatcor** (and possibly **darkcor**) is set to **on**. If you trim significantly it should be possible to get the images of an entire night ( $\sim 300$ ) onto the Processing Computer hard-drive. The final result should be only the set of, say, 300 image header files labelled **v\*.imh** (with, obviously, IRAF image pixel files stored somewhere else).

## 2.2 Stellar Photometry

Open the package **daophot** in **digiphot**. This package can be run successfully in mostly default settings. It performs aperture photometry, and

in the present analysis will use a single size for aperture and sky annuli on each individual star. The approach will be to use the initial frame, probably labelled `v0001.imh`, to act as a template for all the subsequent frames. Thus, you will determine the star coordinates on the first frame and shift the rest of the frames so that those stars are in the same positions. You can make one coordinate file for the first frame and use this to run the aperture photometry program on all the frames.

There are really only two values which need to be estimated and input. You need an estimate of the mean sky counts and a value for stellar FWHM. These values are needed for the search program **daofind**. The mean sky level can be found quickly by using **imstat** on a small region of blank sky in the image. The FWHM can be found using a stellar profile plot with the command **imexamine**; a typical value is 4.5 pix. All of the settings are defaults except for these parameters and user chosen values for aperture sizes. In **daopars** set **fitrad** to the stellar FWHM. In **datapars** set **fw hm p s f** to the stellar FWHM, **sigma** to the standard deviation of the average image background, and **thresho** to at least 10 times the standard deviation. In **photpars** set **apertur** to a sufficiently large aperture radius, say 10 arcseconds. Also, in **fitskypars** set the annulus using **annulus**, and the sky annulus using **dannulu**. The sky annulus should also be about 10 arcseconds. That is, we have a circular aperture of 20 arcseconds with a 10 arcsecond sky annulus on the perimeter. The average background value is set by **skyvalue**.

Next, run **daofind** on the first image. Look in the output coordinate file, default-labelled `v0001.imh.coo.1`, for the coordinates of the program, comparison, and check stars. Write these coordinates in a coordinate file called, say, `'coord'`. Now you can set up **imalign** to adjust the rest of the images. If you are following the suggested notation, set **images** to `v*.imh`,

the list and opens each of the corresponding files `v*.imh.mag.1`, and `v*.imh`. The program then reads the magnitude entries for `program`, `comparison`, and `check` stars from `v*.imh.mag.1`, as well as the exposure time from `v*.imh`. It does a standard calculation with the time to get the Julian Date and takes the differences in magnitudes between `program` and `comparison` stars, and between `comparison` and `check` stars, to get the differential magnitudes. It then writes all of the values to a single file, called `mag.dat`. The code is set up for calculating Julian Date, `t`, for February, 1995. The last term in the calculation of `t` is the correction between HPC-1 and WWVB clock times. A copy of `mcpdrv`, is located in `/kepler/users/iraf/local` and is run by using the command `mcpdrv.out`. After being appended by the subsequent observing runs, all post-processing, including calculation of fluxes and phase, and the binning of the data can be carried out on a single file. Copies of the author's programs for this purpose, called `mpdrv` and `mdbdrv`, are also located in `/kepler/users/iraf/local`. These programs are modified by altering the source-code files labelled `m*drv.for`, and reformatting. The number of observations is controlled by the parameter `n`, and the number of phase bins by the parameter `m`. The values of `x` are the magnitudes of the stars, the values of `d` are the differential magnitudes, `phs` and `bin` are the phase and phase-bin size, and the variables `t` are the components of the Julian Date read from the HPC-1 header file (hours, minutes, and seconds). The programs are run using the commands `m*drv.out` and the final output is phased and binned differential magnitudes or fluxes for the star combinations `program-comparison`, `program-check`, and `comparison-check`.

Overall, one can see that with a consistent labelling scheme, a simple and straightforward analysis, and wise choices concerning the amount of data handled at one time, the processing should be very smooth. In practice, none of the labels and, given that the same program star is observed, none of the



settings need be changed from night to night. Once all the switches are set, really all that is required of the user is to input the frames and type in each of the above listed processing commands in sequence. When one considers that in this method, the frames will already be properly sequenced and time encoded as they are stored and transferred to the Processing Computer, the entire process, observation to final light-curve, becomes very efficient.

```

PROGRAM mcpdrv
C Driver for copying data-files and calculating drift-mags
implicit none
integer n,i
integer t1,t2,t3,t4,x1,x2,x3,d1,d2,d3
parameter (n=225)
character*17 mag(n)
character*11 frm(n)
character*68 tme(n)
real t,t1,t2,t3,t4,x1,x2,x3,d1,d2,d3
open(8,file='mag.dat',status='new')
open(9,file='maglist',status='old')
do 10 i=1,n
  read(9,'(a)') mag(i)
  read(mag(i),'(a)') frm(i)
10 continue
  close(9)
  do 11 i=1,n
    open(10,file=frm(i),status='old')
    read(10,'(//////////,a)') tme(i)
    close(10)
    read(tme(i),'(37x,i1,x,i1,3x,i1,x,i1,3x,i1,x,i1,3x,i1,x,i1)')
    * t1,t2,t3,t4
    t1=10.000000*float(t11)+float(t12)
    t2=10.000000*float(t21)+float(t22)
    t3=10.000000*float(t31)+float(t32)
    t4=10.000000*float(t41)+float(t42)
    t=-0.023611+717.500000*float(t1)+0.041667*float(t2)
    * +0.000694*float(t3)+0.000012*float(t4)
    * +0.291667
    open(11,file=mag(i),status='old')
    read(11,'(//////////,38x,f12.3)') x1
    * read(11,'(////,38x,f12.3)') x2
    read(11,'(////,38x,f12.3)') x3
    close(11)
    d1=x1-x3
    d2=x1-x2
    d3=x2-x3
    write(8,'(f12.6,6f12.3)') t,x1,x2,x3,d1,d2,d3
11 continue
  close(8)
END

```

```

C      PROGRAM mdbcpdrv
      Driver for binning diff-mags
      implicit none
      integer n,m,i,j,tot
      parameter (n=1567,m=100)
      integer jtot(m)
      real t,x1,x2,x3,x4,eps,bin
      real phs,dd1,dd2,dd3,jj
      real xx1(m),xx2(m),xx3(m),xx4(m)
      open(8,file='vb.dat',status='old')
      open(9,file='vl.dat',status='new')
      eps=1.271000/float(m)
      do 11 i=1,n
        read(8,'(f12.6,4f12.3)') t,x1,x2,x3,x4
        j=1
        do 12 while(j.lt.m+1)
          bin=eps*float(j)
          j=j+1
          if(t.gt.bin) goto 12
          xx1(j-1)=xx1(j-1)+x1
          xx2(j-1)=xx2(j-1)+x2
          xx3(j-1)=xx3(j-1)+x3
          xx4(j-1)=xx4(j-1)+x4
          jtot(j-1)=jtot(j-1)+1
        goto 11
      12  continue
      11  continue
      tot=0
      do 13 i=1,m
        tot=tot+jtot(i)
        phs=float(i-1)/float(m)
        jj=float(jtot(i))
        dd1=(xx1(i)-xx4(i))/jj
        dd2=(xx1(i)-xx2(i))/jj
        dd3=(xx2(i)-xx4(i))/jj
        write(9,'(f12.3,3f12.3)')
      *   phs,-1.000000*dd1
      13  continue
      close(8)
      close(9)
      END

```

```

C      PROGRAM fixdrv
      Driver for copying data-files and fixing time
      implicit none
      integer n,i,m
      parameter (n=99)
      real t,d1,d1f
      open(8,file='v100.dat',status='old')
      open(9,file='hr4646lss.dat',status='new')
      do 12 i=1,n
        read(8,'(2f12.3,i12)')
      *      t,d1,m
        d1f=10**(-0.4*(1.830-d1))
        write(9,'(2f12.3,i12)')
      *      t,d1f,m
12     continue
      close(8)
      close(9)
      END

```